Improving the simulation of small-scale variability in radiation and land-surface parameterizations in a mesoscale numerical weather prediction model

Dissertation
zur
Erlangung des Doktorgrades (Dr. rer. nat.)
der
Mathematisch-Naturwissenschaftlichen Fakultät
der
Rheinischen Friedrich-Wilhelms-Universität Bonn

vorgelegt von
Annika Schomburg
aus
Braunschweig

Bonn, Februar 2011

Angefertigt mit Genehmigung der Mathematisch-Naturwissenschaftlichen Fakultät der Rheinischen Friedrich-Wilhelms-Universität Bonn

1. Gutachter: Prof. Dr. Clemens Simmer

2. Gutachter: Prof. Dr. Andreas Bott

Tag der Promotion: 26. Juli 2011

Erscheinungsjahr: 2011

Zusammenfassung

Zur Simulation von subskaligen physikalischen Prozessen in numerischen Wettervorhersagemodellen werden eine Reihe von Vereinfachungen und Annahmen angewandt, um Rechenzeit zu sparen. Dies gilt zum einen für die Simulation der Prozesse innerhalb der physikalischen Parametrisierungen, aber auch für die räumliche und zeitliche Frequenz der Aufrufe dieser Parametrisierungen. Die so verursachte Vernachlässigung von kleinskaliger Variabilität kann zu systematischen Fehlern aufgrund der Nichtlinearitäten in den physikalischen Prozessen und zu Inkonsistenzen zwischen den Variablen aus den unterschiedlichen Parametrisierungen führen.

In dieser Arbeit werden zwei Methoden vorgestellt, die eine effizientere Berücksichtigung von Heterogenitäten in Atmosphärenmodellen ermöglichen, zum einen innerhalb der Atmosphäre selbst, zum anderen an der Erdoberfläche als untere Randbedingung für die Atmosphäre. Die erste Methode, die *adaptive Strahlungstransportparametrisierung*, ist eine effektive Methode zur Berechnung der Strahlungseffekte in der Atmosphäre und an der Landoberfläche und führt zu einer Verbesserung der Erfassung von kurzfristigen kleinskaligen Änderungen im Wolkenfeld in Bezug auf Strahlungseffekte. Die zweite Methode hat das Ziel einer *skalenkonsistenten Kopplung von Atmosphären- und Landoberflächenmodellen* durch die Kopplung eines hochaufgelösten Boden-Vegetations-Transfermodells an das gröbere atmosphärische Modell, wobei der atmosphärische Antrieb mit Hilfe eines in dieser Arbeit entwickelten Downscalings auf die kleine Skala disaggregiert wird. Beide Methoden führen zu einer verbesserten Berechnung der Energiebilanz an der Landoberfläche; erstere durch eine realistischere Simulation der Strahlungsflüsse, zweitere durch Verbesserung der turbulenten Flüsse sensibler und latenter Wärme. Beide Ansätze wurden in das numerische Wettervorhersagemodell implementiert und in der COSMO-DE Modellkonfiguration auf einem Gitter mit 2.8 km horizontalem Gitterabstand getestet.

Das Konzept der adaptiven Strahlungstransportparametrisierung macht sich die räumlichen und zeitlichen Korrelationen in den optischen Eigenschaften der Atmosphäre zunutze, wodurch eine effizientere Ausnutzung der verfügbaren Rechenzeit möglich ist. Aktuelle Strahlungsrechnungen basierend auf dem COSMO-internen komplexen Strahlungscode (basierend auf einem δ-Zweistromverfahren), die jeweils in einem Teil der Gitterpunkte vorliegen, werden ausgenutzt, um möglichst realistische Strahlungsinformationen an den restlichen Gitterpunkten zu erhalten. Zur Validierung dieses Schemas wurden drei Fallstudien mit unterschiedlichen synoptischen Bedingungen gerechnet, und die Ergebnisse des adaptiven Schemas mit Ergebnissen für das COSMO-DE-Standardschema verglichen, in welches komplexe Strahlungsrechnungen viertelstündlich auf einem vergröberten Gitter aufgerufen werden. Als Referenz wurden häufige Strahlungsrechnungen auf dem kompletten dreidimensionalen Gitter durchgeführt. Die Ergebnisse zeigen, dass das adaptive Schema in der Lage ist, die Sampling-Fehler des Standard-Verfahrens in den Netto-Strahlungsflüssen an der Landoberfläche deutlich zu reduzieren, und im Gegensatz zum operationellen COSMO-DE-Verfahren die räumliche Variabilität in den Strahlungseffekten

korrekt zu simulieren. Fehler in den dreidimensionalen Heizraten werden auf größere Mittelungsskalen verringert. Auch physikalische Zusammenhänge zwischen den Strahlungsgrößen und Wolkenwasser oder Regenraten werden besser erfasst als mit dem Standardschema. Es wird gezeigt, dass diese Verbesserungen auch einen positiven Einfluss auf die dynamische Modellentwicklung haben: Modellläufe, die mit adaptiver Strahlung gerechnet werden, weichen weit weniger von den Referenzläufen ab.

Eine Methode um subskalige Variabilität an der Erdoberfläche in atmosphärischen Modellen zu berücksichtigen, ist der so genannte Mosaik-Ansatz. Beim Mosaik-Ansatz wird der Boden und die Erdoberfläche auf einer explizit höheren Auflösung gerechnet als der atmosphärische Teil. In der vorliegenden Arbeit wurde ein statistisches Downscaling-Verfahren für die atmosphärischen Antriebsvariablen für dieses höher aufgelöste Boden-Vegetations-Atmosphären-Transfermodul entwickelt, um eine skalen-konsistente zwei-Wege Kopplung zwischen den beiden Sub-Systemen Atmosphäre und Erdboden/Landoberfläche unterschiedlicher Gitterweite im Mosaik-Ansatz zu ermöglichen. Dieses Disaggregationsschema kombiniert deterministische mit stochastischer Modellierung in einem schrittweisen Downscaling Verfahren. Im ersten Schritt werden bi-quadratische Splines zur Interpolation von der groben zur feinen Skala verwendet. Im zweiten Schritt werden Zusammenhänge zwischen atmosphärischen Variablen als Prädiktanden und Oberflächenparametern as Prädiktoren, abhängig vom Atmosphärenzustand, ausgenutzt. Im letzten Schritt wird die realistische kleinskalige Varianz abgeschätzt, und die fehlende Variabilität als autoregressives Rauschen generiert und hinzugefügt. Dieses Disaggregationsverfahren wurde basierend auf hoch-aufgelöstem Modelloutput aus COSMO-Modellsimulationen mit 400 m horizontaler Gitterweite entwickelt und validiert, dazu wurde ein automatisches Regel-Such-System entwickelt. Das Verfahren wurde extensiv "offline" getestet, d.h. angewendet auf Modelloutput, aber auch "online", d.h. in das mesoskalige COSMO-Modell implementiert und eine Reihe von Fallstudien durchgeführt.

Angewendet auf die atmosphärischen Variablen der untersten COSMO-Modellschicht ist das Disaggregationsschema in der Lage, die Referenzfelder adäquat zu rekonstruieren. Durch die beiden deterministischen Downscaling-Schritte werden Fehler reduziert, der stochastische Downscaling-Schritt führt zu einer guten Rekonstruktion der subskaligen Varianz, jeweils in Bezug zu hochaufgelösten Referenz-Feldern.

Es wird gezeigt, dass der Mosaik-Ansatz an sich zu deutlichen Verbesserungen in der Simulation der turbulenten Austauschflüsse verglichen mit Simulationen ohne Parametrisierung der subskaligen Oberflächenvariabilität führt. Gemittelt über sechs Fallstudien wird eine Verbesserung in den sensiblen und latenten Wärmeflüssen von 9 W/m^2 bzw. 13 W/m^2 erreicht, wiederum mit hochaufgelösten COSMO-Modellläufen als Referenz. Die Anwendung des neuen Downscaling-Verfahrens jedoch führt zu einer nur geringen zusätzlichen Verbesserung, trotz eines deutlich positiven Einflusses auf die einzelnen Terme in den Fluss-Gleichungen. Die Ursache für dieses Verhalten liegt darin, dass sich im Standard-Mosaik-Ansatz ohne atmosphärische Disaggregation die Fehler in den einzelnen Termen besser gegenseitig eliminieren, so dass der Effekt der realistischeren Struktur der verschiedenen Variablen durch das Downscaling kaum deutlich wird.

Zusammenfassend kann, basierend auf den Ergebnissen in dieser Arbeit, die adaptive Strahlungsparametrisierung ohne Einschränkung für die operationelle Anwendung empfohlen werden, da sie einen deutlich positiven Einfluss hat und keine zusätzliche Rechenzeit

erfordert. Der Mosaik-Ansatz an sich hat einen deutlich positiven Effekt auf die Simulation der turbulenten Wärmeflüsse, wobei jedoch ein Anstieg der Rechenzeit, abhängig von der gewählten subskaligen Auflösung, in Kauf genommen werden muss. Die Effekte des neuen atmosphärischen Disaggregation in einer kombinierten Anwendung mit dem Mosaik sind vergleichsweise klein, weswegen trotz des minimalen zusätzlichen Rechenaufwands ein operationeller Einsatz in meteorologischen Modellen nicht empfohlen ist. Das Downscaling als solches stellt jedoch ein nützliches Verfahren zur Erzeugung hoch-aufgelöster atmosphärischer Antriebsdaten für hydrologische Modelle dar.

Abstract

For the simulation of subgrid-scale physical processes in mesoscale numerical weather prediction models various kinds of spatial and temporal sampling or averaging methods are employed to decrease their computational burden. These methods are applied both within the physical parameterizations, but also by restricting the number of calls to these parameterization schemes in time and space. This under-representation of small-scale variability can lead to systematic errors due to the nonlinearity of processes, and may cause inconsistencies between variables computed by the different parameterization schemes.

In this work two methods are presented, which provide an efficient spatial and/or temporal sampling of heterogeneities, in the atmosphere itself and at the earth's surface as lower boundary of atmospheric models. The first method, called adaptive radiative transfer parameterization, provides an efficient technique to compute the radiative effects in the atmosphere and at the soil surface. The second method allows for a scale-consistent coupling of atmospheric and soil-surface models, by running a high-resolution soil-vegetation-atmosphere transfer model coupled to the coarser atmospheric model, connected by a novel atmospheric disaggregation scheme. Both developments incorporate small-scale variability in radiative and soil/surface processes in an efficient and consistent way. Furthermore, both methods improve the representation of the energy budget at the earth's surface; the first by giving more accurate radiation surface net fluxes, the second by improving the turbulent exchange fluxes of sensible and latent heat. Both approaches have been implemented into the COSMO numerical weather prediction model, and tested in the COSMO-DE model configuration on a 2.8 km grid.

The adaptive radiative transfer scheme takes advantage of the spatial and temporal correlations in the radiation characteristics of the atmosphere, and thus makes the parameterization computationally more efficient. The adaptive scheme generalizes the accurate radiation computations made in a fraction of the spatial and temporal space to the rest of the field. For validation three case studies with different synoptic conditions were carried out and the performance of the adaptive scheme is compared to the currently operational COSMO-DE radiation configuration, with quarter-hourly radiation computations on 2x2 averaged atmospheric columns. The reference for both schemes are frequent radiation computations on the full grid. The results show that the adaptive scheme is able to reduce the sampling errors in the surface radiation fluxes considerably and to conserve the spatial variability better, than to the operational scheme. Errors in the three-dimensional heating rates are reduced for larger averaging scales. Physical relations between the radiative quantities and cloud water or rain rates are captured better than with the operational scheme. It is shown, that these refinements also lead to improvements with respect to the dynamical development of the model simulation: the adaptive model runs show a smaller divergence from the reference model run than the currently operational scheme.

One approach to deal with subgrid-scale variability at the surface in atmospheric models is the so-called mosaic approach, in which the soil and the surface are modelled on

an explicit higher horizontal grid resolution than the atmospheric part. In this work a statistical downscaling scheme for the atmospheric input variables needed to drive this higher resolved soil-vegetation-atmosphere-transfer model has been developed, ensuring a scale-consistent two-way coupling between the two sub-systems in the mosaic approach. The statistical downscaling combines deterministic with stochastic modeling in a stepwise approach. Downscaling rules between atmospheric variables as predictands and surface parameters as predictors, depending on the atmospheric state, have been developed. In order to model the small-scale variability correctly, the still missing variance is estimated, and added as autocorrelated noise. The disaggregation system has been built up and tested based on high-resolution model output (400 m horizontal grid spacing). A novel automatic search-algorithm has been developed for deriving the deterministic downscaling rules. The approach has been extensively tested in an offline testbed by applying it to model output, but also "online" in the mesoscale COSMO model.

When applied to the atmospheric variables of the lowest layer of the atmospheric COSMO-model, the disaggregation is able to adequately reconstruct the reference fields. Applying the deterministic steps, root mean square errors are reduced. The stochastic step finally leads to a close match of the subgrid variability and temporal autocorrelation with the reference fields. These "offline" tests and also the "online" application in fully coupled COSMO simulations in combination with the mosaic approach indicate that the mosaic approach is able to improve the performance of the turbulent surface exchange fluxes notably compared to simulations without any surface variability representation. Averaged over six case studies root mean square errors of sensible and latent heat fluxes were reduced by about 9 W/m^2 and 13 W/m^2, respectively, in the COSMO simulations using the 400 m high-resolution COSMO model runs as reference. The application of the new downscaling scheme for the disaggregation of atmospheric forcing variables for the soil module, however, leads to only marginal improvements, despite the positive impact of the downscaling for the single terms in the flux equations. The explanation lies in a cancelling of errors for the computation of the fluxes in the standard mosaic approach, due to which the effect of the overall more realistic structure of the surface variables achieved by the distributed atmospheric forcing is mitigated.

In summary, the results indicate that for operational purposes the adaptive radiation parameterization can be recommended without restriction, because it has a large positive impact and does not lead to a significant increase in computation time. The effects of the novel atmospheric disaggregation scheme are small, both with respect to the improvement for the turbulent fluxes but also with respect to computational demands. Given the additional algorithmic complexity an operational application of this downscaling algorithm can currently not be advocated. An operational application of the mosaic approach itself, however, would be beneficial due to its considerable improvement for the representation of the turbulent heat fluxes and the dynamical model development. An increase in computation time would have to be accepted, however, depending on the chosen subgrid resolution.

Contents

1. Introduction

Mesoscale atmospheric models are used by meteorological centres throughout the world. They have become an indispensable tool, primarily for the daily numerical weather prediction, but also for regional climate scenario simulations. With increasing computer capabilities, grid size resolutions have increased in the last decade, such that short range operational weather forecast model runs can be carried out on the meso-γ-scale, i.e. on mesh-sizes of just a few kilometres (see e.g. *Baldauf* et al., 2009). Many atmospheric processes take place, however, at much smaller scales, not resolved by these high-resolution grids. Hence, physical parameterizations, which estimate the effects of these processes on grid-scale processes, are and will be essential. This holds for example for radiative transfer, cloud microphysics, soil/surface processes and small-scale turbulent motions. The concepts and assumptions behind these parameterizations, however, have been developed for the application on larger scales. Often they are the same as applied in large-scale global models. The development of new ideas and concepts is required, to make these parameterizations applicable to small scales. One challenge that needs to be met is the computational cost, because these parameterizations need a considerable fraction of the total computer time. If the spatial and temporal resolution of an atmospheric model is increased, this also leads to a substantial increase of computation time due to the parameterizations, which also need to be carried out on higher temporal and spatial resolutions. A further pressure towards more economical models is the trend towards running model ensembles instead of one deterministic simulation, in order to estimate the uncertainty of a prediction (see e.g. *Molteni* et al., 1996; *Marsigli* et al., 2005).

For these reasons it is common practise to apply different kinds of spatial and temporal sampling or averaging methods within these parameterizations or to their update frequency, to decrease their overall computational burden. This, however, can lead to systematic errors due to the nonlinearity of the processes, and may cause inconsistencies between quantities computed by the different parameterization schemes.

To simulate non-linear processes adequately, not only mean values but also higher moments, especially the variability, need to be represented adequately. The recently emerging field of stochastic modeling (*Palmer and Williams*, 2009) aims at taking into account processes which are too small or too fast to be explicitly modeled by injecting stochastic noise into the near-grid scale. The methods introduced in this work aim also at incorporating variability in radiative and soil/surface processes at all scales in an efficient, consistent way. Two methods are presented, which provide a better spatial and/or temporal sampling of heterogeneities, in the atmosphere itself and at the earth's surface as lower boundary of atmospheric models, without leading to a large increase in computational costs. The first method provides an efficient technique for radiation updates, the second allows a scale-consistent coupling of atmospheric and soil-surface models.

Cloud fields show very heterogeneous structures, especially in convective situations with rapidly developing and advecting cloud clusters. The representation of such complex cloud

cover patterns becomes more and more realistic with increasing model resolutions. This leads to the necessity to update the radiative effects of the atmosphere at high temporal and spatial resolution, to keep track of cloud processes and ensure consistency between the different variables and parameterizations. The nonlinearity inherent in radiative processes of clouds hamper the computation of radiative effects on averaged quantities (see e.g. *Barker* et al., 1999; *Venema* et al., 2010). Radiative surface fluxes and atmospheric heating rates strongly influence the surface heat energy budget and the temperature tendencies in the atmosphere, respectively. Therefore these fundamental energy sources and sinks need to be considered adequately in numerical weather prediction and climate models. As radiative transfer parameterizations are, however, very computationally demanding, all operational numerical weather prediction and climate models employ some kind of temporal and spatial sampling techniques to save computation time. The standard approaches are to carry out the radiation computations at large temporal intervals and/or on a coarsened spatial grid. In this work an alternative approach is presented, called *adaptive radiative transfer parameterization*, which employs the available computer time in a more intelligent and efficient way, by exploiting spatial correlations in the radiative effects, according to a method first introduced by *Venema* et al. (2007). In this method a fraction of the atmospheric columns receives radiative transfer computation updates at a high temporal frequency, for the other columns a search for a nearby recently updated column is carried out. The radiative effects of the chosen column are then copied and corrected for local solar zenith angle, albedo and ground temperature. In this work the concept has been further extended, implemented into the mesoscale COSMO model, and compared with the performance of the operational radiation update method.

Not only atmospheric cloud fields, but also the earth's surface is characterized by heterogeneity, extending from microscopic to global scales, which has to be accounted for in atmospheric modeling (e.g. *Avissar and Pielke*, 1989; *Avissar*, 1992; *Giorgi and Avissar*, 1997; *Gao* et al., 2008). Surface heterogeneity is induced by land use, orography, and soil texture variability, and is additionally caused by spatial variability in atmospheric forcing, such as different micro climates or precipitation patterns. Even for atmospheric models running on grid resolutions of a few kilometres, most landscape patterns are still sub-grid scale. Moreover, most processes in the soil and at the interface between soil and atmosphere are also highly non-linear. Examples are threshold-dependent processes such as runoff production, snow melt and stomata control; or the turbulent exchange coefficients, which are non-linear functions of the near-surface atmospheric stability. For these reasons modeling of exchange processes either needs to be performed at high resolutions, or has to account for this sub-grid heterogeneity in some way. The use of averaged state variables or parameters instead leads to systematic errors (e.g. *Schlünzen and Katzfey*, 2003). One approach to deal with sub-grid scale variability at the surface in atmospheric models is the so-called mosaic approach (*Seth* et al., 1994; *Ament and Simmer*, 2006), in which the soil and the surface are modelled on an explicit higher horizontal grid resolution than the atmospheric part. The question then arises, how to couple these two different grids at the interface. Usually the high-resolution turbulent exchange fluxes, which constitute the lower boundary forcing for the atmospheric model, are averaged to the coarse atmospheric grid. In general the atmospheric forcing is assumed to be homogeneous for all soil/surface sub-pixels of one atmospheric pixel. In this work the latter

assumption is abandoned, instead a statistic downscaling scheme for all atmospheric input variables needed to drive a Soil-Vegetation-Atmosphere Transfer (SVAT) model has been developed. This ensures a scale-consistent two-way coupling between the two sub-systems soil/surface and atmosphere. The statistical downscaling combines deterministic with stochastic modeling. Relations between atmospheric variables as predictands and surface parameters as predictors are exploited, dependent on the atmospheric state. Additionally the required small-scale variability is estimated, and if not explained by the predictors, added as autocorrelated noise. This approach has been extensively tested, in an offline testbed by applying it to model output, but also "online" implemented in a mesoscale atmospheric model.

Both methods, the adaptive radiation scheme and the atmospheric disaggregation, aim at improving the representation of the energy budget at the surface of the earth. The first by giving enhanced radiation surface net fluxes, the second by improving the turbulent fluxes of sensible and latent heat. An adequate representation of the energy budget at the lower boundary of atmospheric models is crucial for most processes in the planetary boundary layer. Incoming and outgoing radiation and exchange fluxes determine the amount of available energy, which can be seen as the "driving" force for boundary layer buildup during the day, and crucial for the boundary layer structure. Atmospheric stability or instability depends directly on available energy, and thus also convective activity and cloud processes. Moreover, the related feedback processes between the atmosphere, e.g. clouds and precipitation on the one hand and soil moisture on the other hand, are crucial for the dynamics in atmospheric models. Especially the transition phases in the morning and afternoon are sensitive to small changes in net radiation and turbulent fluxes. The same holds for the generation of thermally forced flows such as slope winds or valley winds (e.g. *Weigel* et al., 2006). The available latent heat has a large impact on the atmospheric hydrological cycle. Also the prediction of the screen level parameters in 2 m height, one of the main tasks of an weather forecast model, depends on an accurate radiative forcing and turbulent fluxes at the lower boundary.

Both approaches have been developed based on COSMO model output. The COSMO model (*Steppeler* et al., 2003), is a mesoscale weather-forecast model and regional climate model. The COSMO-DE model configuration has been used, which is an operational setting of the German Meteorological Service, and has a horizontal grid resolution of 2.8 km.

The work is structured as follows: Firstly, a description of the COSMO model is given (chapter 2), because this is of relevance for both aspects of this work. Chapter 3 introduces the adaptive radiation parameterization and contains results of an application for three cases studies. The scale-consistent coupling of land-surface and atmospheric models is presented in chapter 4, starting with a literature review (section 4.1), the model setup (section 4.2) and a description of the new downscaling scheme (section 4.3). Results, for the variables themselves and for an offline and online application of the scheme in combination with the mosaic approach, are given in section 4.4. Both, chapter 3 and 4 contain a discussion of the respective results, a general conclusion and outlook is given in the final chapter 5. Parts of this work have been published in peer-reviewed articles, the novel disaggregation scheme in *Schomburg* et al. (2010) and the application of the adaptive radiative transfer scheme in *Schomburg* et al. (2011).

2. The COSMO-Model

2.1. Introduction

The COSMO-model is part of the numerical weather prediction system of the German Meteorological Service (DWD). It has been developed and is maintained by the *COnsortium of Small-scale MOdeling* which is an association of several European weather services. The German COSMO limited area forecast system consists of a two step model hierarchy, COSMO-EU and COSMO-DE. They both operate on the meso-γ-scale, the former with a horizontal grid spacing of 7 km and 40 vertical layers, the latter with a 2.8 km grid spacing and 50 vertical levels. In operational mode, COSMO-EU receives boundary information from the GME, the global general circulation model of DWD. COSMO-DE is nested into COSMO-EU (Figure 2.1).

In this work the standard COSMO-DE model configuration is adopted, hence this model description will concentrate on the COSMO-DE characteristics.

A model simulation is based on the integration of the set of primitive non-hydrostatic hydro-thermodynamic equations. The prognostic variables are the wind vector, the pressure perturbation p (which is the deviation from a time constant reference pressure field p_0), the air temperature T, the specific humidities for water vapour q^v, cloud liquid water q^c, cloud ice q^i and for rain water content q^r, specific snow water content q^s and specific graupel content q^g.

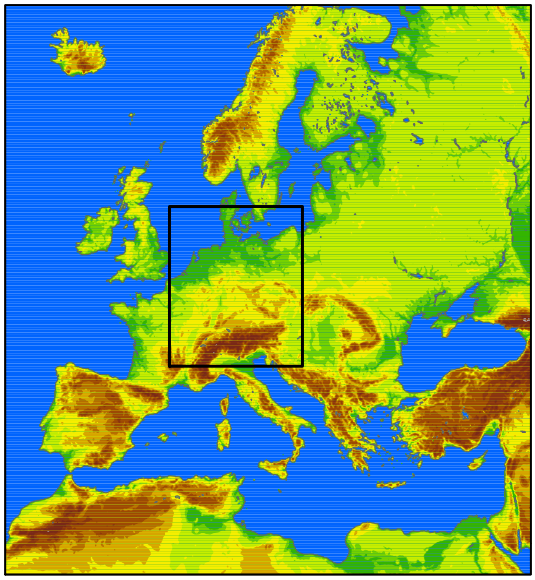

Figure 2.1.: COSMO-EU (outer) and COSMO-DE (inner) model domains.

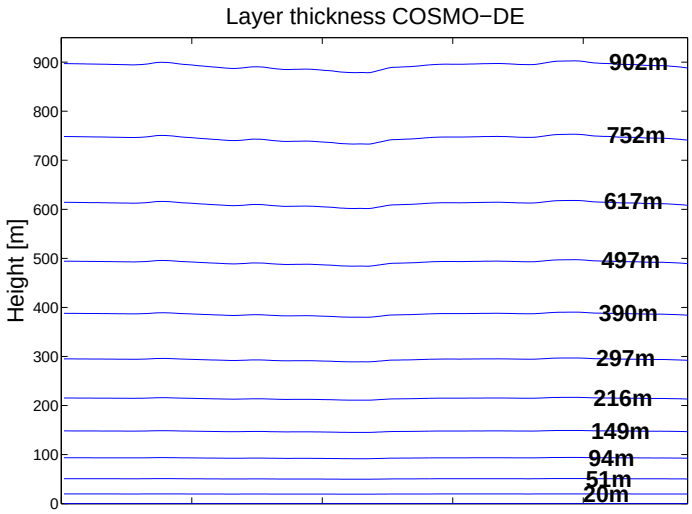

Figure 2.2.: Heights of lowest 11 model layer boundaries in COSMO-DE.

2.2. Coordinate system and grid structure

In COSMO, a spherical coordinate system is employed with geographical longitudes and latitudes as horizontal coordinates and the distance from the earth surface as vertical coordinate. The model grid is based on a rotated coordinate system with the model equator intersecting the centre of the model domain, to avoid the problem of converging coordinate lines towards the pole. The vertical coordinate ζ is a hybrid vertical coordinate which is parallel to the orography in the lower levels and horizontal in the upper part. The grid box boundaries are referred to as half-levels in contrast to the main levels, which intersect the grid box centre. The thickness of the layers decreases from top to bottom, thus, the vertical resolution near the surface is higher than in the upper atmosphere (see Figure 2.2). The model variables in COSMO are staggered on an *Arakawa-C* grid, i.e. temperature, pressure and the humidity variables are defined in the centre of the boxes, whereas the velocity components are defined at the respective grid box faces (*Schättler* et al., 2005). Using this configuration, a more exact representation of the differential operators is obtained in contrast to the Arakawa-A grid, where all variables are defined at the same point.

The model can be run in sequential or parallel mode. For parallel mode horizontal domain decomposition is applied.

As upper boundary condition the $\zeta = 1/2$ level acts as a rigid lid by setting the vertical velocity to zero. For avoiding a backscatter of waves at the upper boundary, an enhanced damping is implemented for the upper model layers.

2.3. System of equations

The model is based a complete set of unfiltered primitive equations with the consequence that processes at each scale have to be considered, including the fast moving sound and gravity waves. To achieve numerical stability, a small time step has to be used, which is computationally expensive. The *mode splitting* approach, proposed by *Klemp and*

Wilhelmson (1978), is chosen to handle this problem: the equations are split up in terms for the fast sound wave processes, and for the meteorological relevant processes on larger time scales such as advection and the tendencies from the physical parameterizations. The former are solved with a smaller time step than the slow processes (*Steppeler* et al., 2002). Thus we have

$$\frac{\partial \psi}{\partial t} = f_\psi + s_\psi \tag{2.1}$$

where ψ is any prognostic model variable, f_ψ is the forcing term for the slow modes and s_ψ is the source term describing sound- and gravity-waves. During the smaller time steps, the f_ψ-terms are kept constant.

The basic model equations provide a complete set of the relevant state-variables if all terms describing the impact of the subgrid-scale processes are known. These include the stress tensor, the turbulent fluxes of water vapour, liquid water and ice, the phase changes, the precipitation fluxes of rain, snow and graupel, the sensible heat flux and the radiation flux density. All these processes have to be calculated as functions of the model variables using the respective parameterizations (see chapter 2.5).

For solving the equations numerically, the spatial and temporal differential operators are replaced by the respective finite differences in space and time. In COSMO-DE the integration is based on a two-time-level Runge-Kutta integration scheme third order in time (*Baldauf* et al., 2009). Two other optional integration schemes are implemented in the model, a three-timelevel time-splitting Leapfrog scheme (used for COSMO-EU) and a threedimensional semi-implicit integration scheme.

2.4. Data assimilation

The model runs in this work are forced by COSMO analyses, therefore a brief description of the COSMO data assimilation methods used to produce the analysis is given in this section.

For operational data assimilation a *nudging* technique is implemented, which "pulls" the prognostic model variables into the direction of the observed data. For this purpose an additional forcing term, a so-called relaxation term, is introduced into the prognostic equations; the development of a variable ψ can thus be written as (*Schraff and Hess*, 2002):

$$\frac{\partial}{\partial t}\psi(x,t) = P_\psi(x,t) + G_\psi \cdot \sum_{k_{(obs)}} (W_k \cdot (\psi_k - \psi(x_k,t))). \tag{2.2}$$

P_ψ denotes the dynamics and parameterizations of the model, ψ_k is the k^{th} observation influencing grid point x at time t, x_k is the location of the observation and G_ψ is a constant so-called *nudging-coefficient* and W_k a weight between 0 and 1, determining to what degree a grid point should be influenced by a given observation.

The characteristic time scale for the relaxation process is determined by the coefficient G_ψ, such that that the deviation of the model value from the observed value decreases in about half an hour to 1/e. In practise, the nudging term is kept smaller than the largest dynamic and physical terms, in order not to disturb the internal equilibrium of the model. Fields for which the nudging technique is applied, are horizontal wind, potential

temperature and relative humidity on all layers and pressure at the lowest model level. The analysis increments are hydrostatically balanced thus avoiding direct sources of vertical wind.

Newly implemented is a method for the incorporation of radar precipitation observations of the DWD radar composite into the COSMO-DE, the so-called *latent heat nudging*. Temperature increments are determined proportional to the ratio between observed and simulated values and to the available latent heat in the model. For this procedure the relative humidity is kept constant which leads to a change in specific humidity. As a consequence, simulated precipitation is adjusted into the direction of the observation (*Baldauf* et al., 2009).

The assimilation system is completed by an analysis of sea surface temperatures once a day, and a snow depth analysis every 6 hours. No soil moisture assimilation is carried out in COSMO-DE. In COSMO-EU, however, an adjustment of soil moisture is applied such that the 2 m-temperatures corresponds well to the observed temperatures. This is done by minimizing a cost function (*Hess*, 2001).

2.5. Parameterizations

In the following a short overview of the different parameterizations of the COSMO model is given. The radiation scheme, the turbulence parameterization options and the soil module TERRA are described in some more detail, because they are of special importance for this work.

2.5.1. Grid scale clouds and precipitation

Clouds arise from condensation of cloud water by saturation adjustment. The treatment of grid scale precipitation is based on a Kessler-type 1-moment-bulk approach (*Kessler*, 1969), which has been expanded to consider five prognostic water categories: water vapour and hydrometeors of cloud water, cloud ice, rain water, snow, and graupel. The particles of these classes interact through the parameterization of several microphysical processes (*Baldauf* et al., 2009).

2.5.2. Partial cloudiness

Clouds produced by the grid scale scheme always cover the whole grid box, i.e. the cloud cover is 100%. For radiative transfer calculations and post-processing applications additional knowledge of the subgrid cloudiness is required. Subgrid cloudiness is considered by means of an empirical function depending on relative humidity, height, and convective activity.

2.5.3. Moist convection

It is assumed that deep convection (showers and thunderstorms) is a grid scale process at the COSMO-DE scale of 2.8 km. Only shallow convection is parameterized by a mass flux scheme of *Tiedtke* (1989) with a closure based on moisture convergence. However,

no convective precipitation is produced by this scheme, because precipitation forming for shallow convection is excluded. In COSMO-EU also deep convection is parameterized by the Tiedtke-scheme.

2.5.4. Radiation

The radiation scheme in the COSMO models was developed by *Ritter and Geleyn* (1992) and is based on the one-dimensional *δ-two-stream approximation* of the radiative transfer equation. The spectrum is divided into broad spectral intervals, for which the radiative transfer calculations are carried out. Absorption, emission and scattering by cloud particles, aerosols and gas molecules is accounted for. For subgrid-scale clouds in a vertical column the maximum-random overlap assumption is applied. The cloud optical properties are parameterized based on a fit of the optical properties of eight cloud types following *Stephens* (1984). Aerosols are given by a constant climatology. Effects of three gases are considered: water vapour, carbon dioxide, which has a constant value of 330 ppm, and ozone, the temporal variability of which is described by a climatological annual cycle. The radiation scheme provides net fluxes at the surface in the solar and thermal regime and three-dimensional heating rates for every vertical layer in a column.

In COSMO-DE radiation computations are carried out every 15 minutes; these calculations are applied to 2x2 columns of averaged atmospheric properties with a correction for the local albedo for the solar radiation surface flux and for ground temperature for the thermal radiation flux (*Baldauf* et al., 2009). In COSMO-EU, radiation effects are calculated hourly and fluxes and heating rates are kept constant in between. The solar zenith angle used in the radiation computations is the zenith angle valid for the middle of the interval between two radiation updates.

2.5.5. Subgrid-scale turbulence

Even for high horizontal resolutions on the order of 10^2 or 10^3 meters, a parameterization of subgrid-scale turbulence is required. At small scales, the boundary layer approximation of neglecting horizontal turbulent exchange becomes questionable, therefore a three-dimensional approach is recommended for scales below 1 km.

The turbulence parameterization estimates influence of subgrid scale turbulent diffusion on the gridscale variables in the primitive equations. The formulation is based on K-theory, which relates the subgrid-scale flux to the gradient of a variable ψ and a diffusion coefficient K, in three-dimensional form:

$$\mathbf{F}_\psi = -\underline{\mathbf{K}}_\psi \cdot \nabla\psi. \tag{2.3}$$

The mixing coefficients K_m and K_h for momentum and heat have to be determined in the parameterization scheme. In COSMO several options for turbulence schemes are implemented. Two are used for this work:

Prognostic TKE[1] scheme: This is the operational scheme developed by M. Raschendorfer, which is based on a closure of order 2.5. The exchange coefficients are calculated depending on the thermal stratification and vertical wind shear (*Doms* et al., 2007). The

[1] Turbulent Kinetic Energy

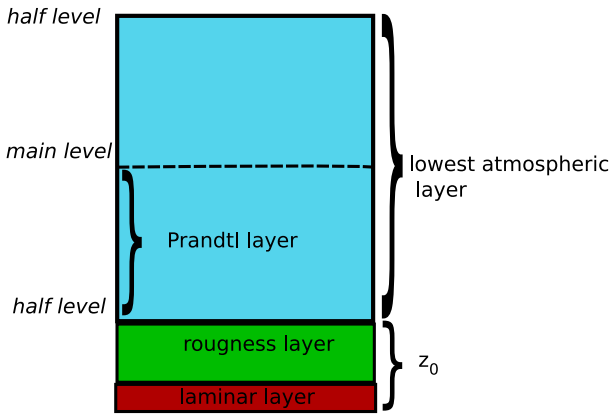

Figure 2.3.: Sublayers of the transfer scheme.

scheme has been extended by an additional TKE source term, which avoids the TKE getting unrealistically close to zero under stable conditions.

LLM[2]-Scheme: This scheme has been developed in the framework of the LITFASS[3]-project for the use in a modified model version of the COSMO model on the 100 m scale (*Herzog* et al., 2002). Here the turbulence coefficients are specified by a more simple Prandtl/Kolmogorov approach based on a first-order closure assumption. The coefficients are parameterized based on stability functions depending on a model developed by *Smagorinsky* (1963) and a length scale which is a function of the grid spacing to take the numerical resolution into account. Hence the scheme adapts to the chosen resolution. In contrast to a one-dimensional scheme, the gradients in three-dimensional space are considered. The horizontal turbulent exchange coefficients are simple functions of the vertical coefficients.

2.5.6. Surface fluxes

The surface flux transfer scheme computes the flux density of model variables at the lower model boundary where only turbulent and molecular processes are of importance, i.e. it acts as the interface between surface and atmosphere. The operational COSMO transfer scheme is based on the diagnostic TKE equation, which provides the stability functions, employing the vertical gradients of the model variables, which is needed for calculating the turbulent length scale. The transfer layer is divided into three sublayers, as depicted in Figure 2.3. The transport resistance (which is proportional to the reciprocal of the transfer coefficient) is the sum of the three respective resistances. The lowest layer just above the rigid earth surface is the laminar sublayer. In the laminar sublayer resistance due to molecular diffusion is a linear function of height. Above the laminar layer up to the height of the roughness length z_0, lies the turbulent roughness layer. Here the resistance is an exponential function of height and dependent on roughness elements. The turbulent Prandtl layer constitutes the upper part of the transfer layer, which covers half of the lowest atmospheric model layer, with constant vertical turbulent flux densities and

[2]LITFASS-Lokal-Modell
[3]Lindenberg Inhomogeneous Terrain - Fluxes between Atmosphere and Surface - a long term Study

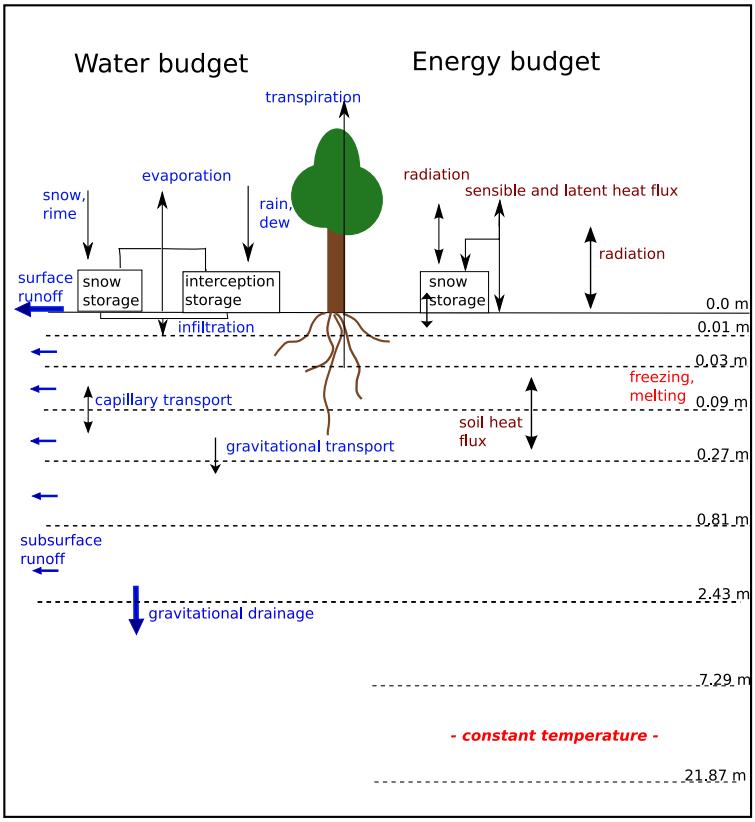

Figure 2.4.: Processes and structure of the SVAT module TERRA.

is characterized by a stability dependent resistance which is a logarithmic function of height.

2.5.7. Soil processes

The lower boundary condition is modelled by the soil and vegetation model TERRA (*Doms* et al., 2007). Two implementations of TERRA are available: the two-layer soil model following *Jacobsen and Heise* (1982) and the extended multi-layer version TERRA-ML. Only the latter option is employed in this work and described in the following.

TERRA calculates the temperature and humidity at the land surface, i.e. at the interface between atmosphere and soil. Those quantities are needed for the computation of the surface fluxes of energy and water, which are responsible for the exchange of heat, moisture and momentum between the surface and atmosphere. In TERRA all processes are modeled strictly one-dimensionally, thus no interactions between adjacent soil columns are considered. An overview of the processes and the structure of TERRA is provided in Figure 2.4.

The atmospheric driving variables for TERRA are:

- Temperature (of lowest atmospheric model layer)
- Humidity (of lowest atmospheric model layer)

- Horizontal wind (of lowest atmospheric model layer)
- Radiation fluxes (shortwave and longwave, at surface)
- Pressure (at surface)
- Precipitation (at surface)

Hydrological processes: In the hydrological part of the soil module the water content of the water storages at the surface and in the soil are calculated. Water storages are the interception store, which contains surface water (including rain water and dew on the vegetation), the snow store (contains snow, frozen surface water and rime) and all soil layers. For computing the water budgets in these storages a number of processes are considered (Figure 2.4). Coupling of soil and atmosphere takes place via precipitation and formation of dew and rime as sources, and evaporation, transpiration and runoff as sinks of water.

The water budget at the surface can be written as

$$E_b + E_i + E_{snow} + \sum_{k=1}^{ke_{soil,hy}} Tr_k = -(F_{q^v})_{sfc} \tag{2.4}$$

with E_b evaporation of bare soil, Tr_k water extraction by roots, and E_i, E_{snow} evaporation from interception and snow store in $kg\ m^{-2}s^{-1}$, respectively (a list of all symbols used can be found in appendix B). $ke_{soil,hy}$ is the number of active layers of the hydrological part of TERRA. Starting point for all evaporation components is the potential evaporation E_{pot}:

$$E_{pot}(T_{sfc}) = \rho K_h |\mathbf{v}_h|(q^v - Q^v(T_{sfc})) \tag{2.5}$$

where T_{sfc} denotes the temperature at the surface and Q^v the specific humidity at saturation, K_h is again the transfer coefficient for heat. Then the bare soil evapotranspiration can be written as

$$E_b = (1 - f_{snow}) \cdot (1 - f_i) \cdot (1 - f_{plnt}) \cdot Min[-E_{pot}(T_{sfc}); F_m] \tag{2.6}$$

where f_{snow}, f_i and f_{plnt} are the fractional coverages of the soil by interception water and plants, respectively. F_m is the maximum moisture flux through the surface that the soil surface can sustain by diffusion after *Dickinson* (1984), depending on soil type. Evaporation from interception and snow storage are parameterized as the potential evaporation at the respective temperatures:

$$E_i = E_{pot}(T_{sfc}) \qquad \text{and} \qquad E_{snow} = E_{pot}(T_{snow,sfc}) \tag{2.7}$$

Plant transpiration is parameterized according to *Dickinson* (1984) as a function of potential evaporation and a parameterized resistance. A part of this resistance is the stomatal resistance, which varies between a minimum value, if conditions are at an optimum for photosynthesis and transpiration, and a maximum value if the stress for plants due to low insolation, low soil moisture, and unfavourable ambient temperature and humidity is high.

Thus, after evaluation of Equation 2.4, the surface flux of water vapour is known, and hence the virtual specific humidity q^v_{sfc} at the surface can be estimated by a parametric drag-law formulation:

$$(F_{q^v})_{sfc} = -\rho K_h L |\mathbf{v}_h|(q^v - q^v_{sfc}). \tag{2.8}$$

Here, q^v is the specific humidity at the lowest atmospheric layer above the surface, K_h is the transfer coefficient of heat calculated in the transfer scheme in section 2.5.6, L is the latent heat of vapourization and $|\mathbf{v}_h|$ the horizontal wind velocity in the lowest atmospheric layer.

Vertical water transport in the soil occurs due to gravity and capillary forces and is described by the Richards equation:

$$F_{w_l} = -\rho_w[-D_w(w_l)\frac{\partial w_l}{\partial z} + K_w(w_l)] \tag{2.9}$$

with F_{w_l} soil water flux, ρ_w water density, D_w hydraulic diffusivity and K_w hydraulic conductivity, which are dependent on water content w_l and soil texture. At the upper boundary the flux is replaced by infiltration, which is inherently limited by the maximum infiltration rate, which is again a function of soil type and wetness of the soil. If the potential infiltration rate is higher than this limit; the surplus is converted into surface runoff and eliminated from the hydrological cycle of the model. Runoff from a soil layer is generated, if the water content of the layer exceeds the field capacity w_{FC}. Soil water can drain from the lowest soil model layer, but the diffusion flux upwards into layer six is neglected, i.e. the soil can not be moistened due to moisture gradients by the ground water. This can lead to dry soils, because the drainage can not be compensated by diffusion fluxes.

Thermal processes: The basic equation for temperature computations is the heat conduction equation:

$$\frac{\partial T_{so}}{\partial t} = \frac{1}{(\rho c)}\frac{\partial}{\partial z}(\lambda\frac{\partial T_{soil}}{\partial z}) \tag{2.10}$$

with ρc heat capacity and λ heat conductivity. There are seven active layers for heat processes, see Figure 2.4. In the eighth layer a constant temperature is assumed, given by the annual average air temperature at 2 m height above the surface (*Baldauf* et al., 2009).

At the upper boundary of TERRA the heat flux $\lambda\partial T/\partial z$ is replaced by G_{sfc}, the sum of radiation budget and heat fluxes. This forcing at the surface can be written as

$$G_{sfc} = (F_h)_{sfc} + L(F_{q^v})_{sfc} + Q_{rad,net} + G_P + G_{snow,melt} \tag{2.11}$$

consisting of the sum of sensible heat flux $(F_h)_{sfc}$, latent heat flux $L(F_{q^v})_{sfc}$, net radiation $Q_{rad,net}$, which stems from the radiation parameterization, G_P which considers effects of freezing rain and melting snowfall, and $G_{snow,melt}$ models influence of melting processes on soil temperature. As the energy budget is explicitly used for determining the soil heat flux G_{sfc}, energy is conserved at the earth surface.

The effective surface temperature T_G is an area-weighted average over snow temperature T_{snow} and the snow-free temperature surface temperature T_{sfc}. For water bodies the temperature is kept constant throughout the model run. For operational use its value is interpolated from the sea surface temperature (SST) of the nearest sea point. This has

been altered for the current work, see section 4.2.

External Parameters: An atmospheric model requires information on the state of the earth's surface. Two different types of information can be distinguished: primary data, which are directly extracted from an external data set, and secondary data, which are transformed primary data. Some of the external data sets are freely available, but some, such as information on high-resolution soil type, have to be purchased. The primary data sets are (*Doms* et al., 2007):

- **Orography:** For operational applications, the GLOBE data set, which is a Digital Elevation Model (DEM) provided by the National Oceanic and Atmospheric Administration (NOAA), with a resolution of 30 arc seconds is employed. For deriving information on coarser scales, the subgrid elevations are averaged, and the subgrid-scale variance is used for the derivation of the roughness length. Moreover a filtering of steep orography is applied in order to avoid large elevation difference in adjacent grid boxes in mountainous areas.

- **Dominant land cover:** Operationally the CORINE (CoORdination of INformation on the Environment) data set, an European initiative with 250 m resolution is used. The vegetation classes in this data set are grouped into more general categories with similar characteristics for application in the model.

- **Dominant soil type:** The data used by DWD are based on the FAO/UNESCO Soil Map of the World from 1974, with a very coarse resolution of 5 arc minutes ($\sim$ 10 km). Hence, the resolution of the data set is more than 3 times coarser than the COSMO-DE resolution of 2.8 km. For the soil texture eight classes are distinguished: 'ice', 'rock', 'sand', 'sandy loam', 'loam', 'loamy clay', 'clay' and 'peat'. All thermal and hydraulic parameters (e.g. heat capacity, heat conductivity, field capacity, etc.) are derived from these eight classes by lookup-tables.

- **Mean surface temperature** is needed for TERRA as constant lower boundary condition for the deepest soil level, as described above. These data are made available by the University of East Anglia with a 0.5° resolution.

Refined new primary data sets have been processed for this work, details are given in section 4.2.

The secondary data sets are determined mainly by lookup-tables:

- **Land mask:** is primarily determined on the basis of the land cover data. All pixels which have a land fraction larger than 50% are treated as land point, otherwise as water pixel.

- **Roughness length:** depends on subgrid scale orography and land use, the influence of the latter one is determined via lookup-tables. Over water surfaces the roughness length is not an external parameter but a variable calculated internally as a function of wind velocity using the Charnock formula.

- **Plant cover, leaf area index, rootdepth:** These vegetation quantities are not constant over the year. The maximum and minimum values are determined via

lookup tables from land cover information. The final values are parameterized on the basis of an interpolation between these maximum and minimum values as function of Julian day, latitude and elevation.

- **Forests:** Recently, field masks for deciduous and evergreen forests have been introduced to account for the effects of forests on albedo and transpiration.

3. Adaptive radiative transfer parameterization

3.1. Overview: Radiation codes in numerical weather prediction models

The increasing resolutions of current weather forecast models of a few kilometres in principle require three-dimensional radiative transfer computations. Accurate radiative transfer (RT) computations based on the three-dimensional spectral radiative transfer equation are, however, extremely complex and computationally demanding. Consequently various parameterizations, with different degrees of simplifications, have been developed. In particular for the application in operational weather prediction models or for long period climate simulations large simplifications are inevitable to reduce computational costs. Common simplifications are the computation of radiative transfer reduced to flux densities on broad spectral bands for one-dimensional vertical atmospheric columns, assuming horizontal homogeneity within the model column. Also the treatment of clouds in the RT parameterization requires a number of assumptions, e.g. for the overlap of partial cloud cover in the vertical. Many input parameters required for atmospheric radiative transfer, especially cloud characteristics, are highly uncertain and also parameterized in operational models. Despite reductions in complexity, radiation transfer parameterizations are for most applications still too demanding to be computed for each model timestep and the full spatial grid. Different approaches have been implemented by the national weather services and climate centres to overcome this limitation by sampling in time and space. The most common strategy is temporal sampling, i.e. the radiation scheme is called at time intervals of more than one model time step. The fluxes and heating rates are kept constant in between, either based on a medium solar zenith angle, or adjusted in each timestep according to the current solar zenith angle. Spatial sampling strategies interpolate between sparse computations or average atmospheric properties over multiple columns before passing the data to the RT parameterization.

The Integrated Forecasting System (IFS) of the European Centre for Medium-Range Weather Forecasts (ECMWF) for example employs a comparatively sophisticated radiative transfer scheme since June 2007, making use of the two-stream approximation in the Rapid Radiative Transfer Model (RRTM) for shortwave (*Clough* et al., 2005) and longwave (*Mlawer* et al., 1997) radiation, while treating cloud variability by the Monte Carlo Independent Column Approximation (McICA, *Pincus* et al. (2003)). To save computation time the radiation scheme is called only at large temporal intervals (once per hour or once per three hours, depending on model resolution) and on a coarsened grid, where the radiative effects are interpolated to the finer grid by a cubic interpolation scheme. The temporal interpolation for each dynamic model timestep is done by accounting for

the correct solar zenith angle for shortwave flux and for changing surface temperatures for the upward longwave flux in each timestep (*Morcrette*, 2000; *Morcrette* et al., 2008).

In the COSMO model (*Steppeler* et al., 2003) also the two-stream approximation is employed based on code by *Ritter and Geleyn* (1992); however, as described in section 2.5.4 calls to this scheme are also restricted in time and space. The scheme is called either once per forecast hour or quarter-hourly, in the configurations COSMO-EU and COSMO-DE, respectively. In the latter configuration the atmospheric input parameters are first averaged over four columns, before carrying out the radiation calculations. The obtained surface radiation fluxes are adjusted taking the local albedo and surface temperature into account (*Baldauf* et al., 2009).

Temporal and spatial sampling methods in radiation transfer code can lead to errors: temporally sampling neglects the varying local insolation due to changes in solar zenith angle and advection and evolution of clouds; spatial averaging reduces spatial variability of radiative effects which is problematic due to the nonlinear characteristics of radiative transfer. Inconsistent situations may occur, when the radiative properties are not allowed to react to the changing atmosphere over several timesteps, thus raining clouds and strong solar fluxes are allowed to coexist in rapidly changing convective atmospheres. *Morcrette* (2000) studied the sampling effects on operational simulations and analyses for the IFS global model. He found a larger sensitivity with respect to temporal sampling, than to spatial sampling followed by subsequent interpolation. In 10-day forecasts he found temperature errors depending on the temporal frequency of radiation computations. This error increased with height, due to feedbacks between convective clouds and radiation, especially in the tropics. For longer, e.g. seasonal, predictions these errors grow, thus a higher temporal sampling is beneficial.

Several approaches have been developed in recent years to bypass the conflict between the need of frequent radiation computations and computational limits. Computation time can be reduced by training an artificial neural network (ANN) with a detailed radiation scheme offline (*Chevallier* et al., 1998, 2000; *Krasnopolski* et al., 2005). *Krasnopolski* et al. (2010) tested such ANNs in the National Center for Environmental Prediction (NCEP) Climate Forecast system (CFS) by comparing simulations with the original inherent radiation code (RRTMG) with simulations employing the ANN emulating the complex radiation code. The differences were small and comparable to internal model variability, compiler changes etc. while a considerable speedup was achieved for the climate simulations. A drawback of this method is the need to re-train the ANN for any configurational changes such as the vertical resolution. *Pielke* et al. (2005) proposed an approach based on look-up-tables. Radiative effects for all possible inputs are pre-calculated and stored to disk. As for the ANN, look-up-tables need to be recomputed for every change in the model setup, making the model inflexible. Furthermore, given the expected increase in the number of model levels, the number of possible combinations may soon become prohibitive.

In *Venema* et al. (2007) (from now on VSAS07) two adaptive radiative transfer parameterizations are presented, which exploit temporal and spatial correlations in the 3D optical property fields. Radiation calculations by the implemented RT scheme are performed in only a fraction of time and space. The so-called *temporal adaptive scheme* identifies the grid points in the model domain where the largest changes since the last radiation update

have occurred and targets these columns for the next RT computations. In that way it is guaranteed, that always the grid boxes where the cloud characteristics have changed most strongly, get an update in radiative effects. These grid cells are chosen employing a simplified radiation scheme, based on multiple linear regression which uses vertically integrated atmospheric variables as predictors, estimating the changes in the radiative effects since the last update. The rest of the field is updated by computing the change in the radiative tendencies by the same simplified radiation scheme and adding them to the radiation effects from the last timestep. In the second proposed scheme, the *spatial adaptive scheme*, only a small, but fixed part of the field is updated by the internal radiation scheme at high temporal frequency. For the other columns a search for a nearby similar atmospheric column is carried out and the radiative effects of the most similar column are applied with a correction for solar angle and albedo.

Manners et al. (2009) adopted this idea and developed two adaptive RT schemes in spectral space, and employ a reduced RT calculation at timesteps between calls to the full complex radiation scheme. Their *split time-stepping* approach divides the RT computation in bands with strong gaseous absorption terms, which are optically thick and hardly dependent on cloud characteristics, and in bands which are optically thin, where clouds have a strong influence. The latter RT calculations are updated with a higher temporal frequency to keep track of changes due to developing and advecting clouds. Their second method, the *incremental time-stepping* method, uses a simple radiation scheme to compute temporal changes for the window region, i.e. the optically thin part of the atmospheric spectrum, where variability is mainly caused by variations in cloud properties. These increments are added to the results of the full complex scheme, which is computed at a lower temporal frequency.

The adaptive schemes in VSAS07 were introduced and, as a proof of principle, tested in an offline environment and only for the radiative net fluxes at the surface. In a case study it was shown that such schemes are able to predict the surface fluxes much more accurately, using the same computational resources as used for the standard temporal and spatial sampling methods. In addition, the spatial error fields of the adaptive approaches were characterized by notably smaller correlation lengths. The reduction in the number of calls to the complex scheme leads to only a small reduction in accuracy. The spatial adaptive scheme gave overall better results than the temporal adaptive scheme. Therefore, in this work results from the implementation of the spatial scheme in the operational weather forecast model COSMO are presented. The spatial adaptive radiation parameterization has been extended to be applied also to the vertical heating rates. The performance of this enhanced scheme is compared to the standard operational radiation update scheme. In the next section, the adaptive scheme is introduced, whereas in section 3.3 the performed simulations and experiments are outlined. Section 3.4 contains the results of the adaptive scheme as applied in the COSMO model, these results are discussed in section 3.5. This chapter on the adaptive radiation scheme has been published in *Schomburg* et al. (2011).

3.2. Enhanced adaptive radiation scheme

VSAS07 presented two adaptive radiative transfer schemes, termed temporal and spatial adaptive scheme, respectively. Both schemes apply so-called *intrinsic calculations*, i.e.

Table 3.1.: Cost function for finding a nearby radiatively similar atmospheric column. The weights are optimized for minimal heating rate errors.

Cost function	$\delta = w_1\Delta CCL + w_2\Delta CCT + w_3\Delta LLWP + w_4\Delta IWV + w_5\Delta\alpha + w_6\Delta t + w_7 dist$
Weights	$w_1 = 0.37$; $w_2 = 7.85$; $w_3 = 2.1734\,(kg\,m^{-2})^{-1}$; $w_4 = 2.0801\,(kg\,m^{-2})^{-1}$; $w_5 = 13.69$; $w_6 = 0.0018 s^{-1}$; $w_7 = 0.744$;

CCL: low level clouds (below 800 hPa) [1]; CCT: total cloud cover [1]; $LLWP$: logarithm of liquid water path [$\mathrm{kg\,m^{-2}}$]; IWV: integrated water vapour [$\mathrm{kg\,m^{-2}}$]; α: surface albedo [1]; t: time since last update [s]; $dist$: distance between grid points [1].

calculations made by the atmospheric models own complex radiation scheme, and *extrinsic calculations*, which apply a simple generalization algorithm to the intrinsic calculations for grid points not updated by a call to the complex scheme. The number of intrinsic radiation computations is kept comparable to that for the operational configuration, but distributed in a more efficient way. This work is restricted to the spatial adaptive scheme, because it gave overall better results according to VSAS07, i.e. the correlation in the fields could be exploited more efficiently with the spatial scheme than with the temporal scheme. In this work the scheme has been extended to atmospheric heating rates and some further small improvements have been introduced. Furthermore, the scheme has been implemented and tested in the COSMO model for investigating impacts for numerical weather forecasts on the meso-γ scale.

The spatial search scheme exploits spatial correlations in the radiative effects in the following way: Only in the first timestep of the model simulation the radiation routine is called once for the whole field. For all following timesteps, the model domain is divided into small subdomains. At a high frequency the radiation effects at only one of the subdomain columns is updated by a call to the intrinsic radiation scheme. For grid points not updated a search is performed for a nearby similar, recently updated column. Similarity is evaluated by comparing a weighted sum of absolute differences in low cloud cover, total cloud cover, liquid water path, integrated water vapour, surface albedo, time since the last update of the respective column and distance between the two columns (see Table 3.1). This weighted search sum has been extended by the spatial distance between the columns and the integrated water vapour compared to the version introduced in VSAS07. Having found the most similar column, the shortwave (SW), longwave (LW) and photosynthetic active radiation (PAR) surface fluxes and atmospheric heating rate profiles are copied to the respective column. The solar fluxes and heating rates are corrected for solar zenith angle, and the surface fluxes also for the local albedo. For the longwave surface fluxes a correction, according to the local surface temperature, has been applied (see Table 3.2).

3.3. Implementation and experimental design

The adaptive scheme is compared with the operational radiation configuration of COSMO-DE, i.e. with radiation calculations carried out for 2x2 averaged columns every 15 minutes. For clarity of notation the scheme will be referred to as “2x2” scheme from now on. The

Table 3.2.: Adjustment of radiation effects after coping a nearby, recently updated column in the adaptive scheme.

Variable	Correction
Column of SW heating rate	$H_{SW} = H_{SW}\frac{cos(\Theta_x)}{cos(\Theta_c)}$
SW and PAR surface radiation flux	$F_{SW/PAR} = F_{SW/PAR}\frac{cos(\Theta_x)}{cos(\Theta_c)}\frac{1-\alpha_x}{1-\alpha_c}$
Column of LW heating rate	no correction
LW surface radiation flux	$F_{LW} = F_{LW} + (\sigma(1-\alpha_{IR})(T_{G,c}^4 - T_{G,x}^4)$

Θ: solar zenith angle, α: surface albedo, σ: Stefan Boltzmann constant, T_G: ground temperature, α_{IR}: infrared albedo; the indices c and x denote the value from the copied and the actual local grid point, respectively.

Table 3.3.: Overview of radiation configurations.

Radiation scheme	Call frequency [min]	Number of columns updated
Reference	2.5	all
Adaptive	2.5	1/25
COSMO-DE (2x2)	15	1/4 (averaging 2x2 columns)

adaptive scheme is called every 2.5 minutes, applying the intrinsic radiation scheme only for one out of 5x5 atmospheric columns, while the extrinsic generalization is applied to the other columns (see Fig. 3.1). This setup requires about the same computation time as the standard COSMO-DE setup. Update patterns for the adaptive approach, i.e. the sequence in which the pixels are updated, are given in VSAS07 for regions of different size: the ordering is such that subsequently updated columns have a large distance between them.

The most accurate results with respect to radiation would be obtained by radiation computations for the full domain on a high temporal frequency. This optimal but much too expensive setup has been taken as reference for testing our adaptive scheme and the standard COSMO-DE 2x2 configuration. Unless denoted otherwise, all comparisons shown in the following are based on intrinsic radiation computations carried out every 2.5 minutes on the full model domain. The radiation configurations compared are listed in Table 3.3.

For the comparisons a COSMO model version was developed in which the different radiation options are computed diagnostically, i.e. the dynamics are driven by one of the three radiation options, which is for most comparisons the reference setup. The radiation effects of the other two schemes are computed in addition and provided as additional model output.

The largest errors of radiation effects are expected for situations with heterogeneous atmospheric conditions, i.e. small-scale convective cloud patterns, where the atmospheric state changes rapidly and hence frequent radiation calculations are most important. Three days have been chosen for the comparison, which span a range from mainly convective to more stratiform clouds. The first day is a convective summer day, 21 June 2004, when instable air masses covered Central Europe under an elevated trough, and a large number

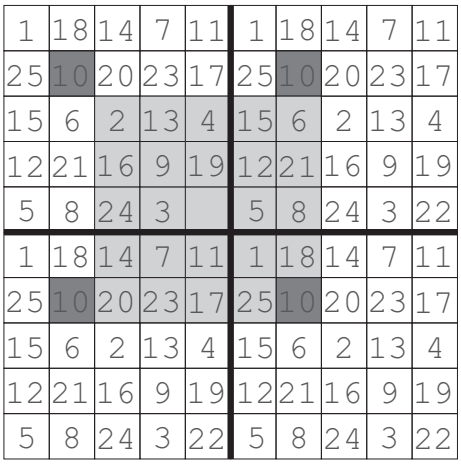

Figure 3.1.: Illustration of the spatial adaptive parameterisation setup tested in the COSMO-DE model configuration: Every 6 timesteps (i.e. 2.5 minutes) one out of 5x5 columns is updated by a call to the intrinsic radiation scheme (in this example the dark shaded grid boxes). The update sequence is indicated by the numbers 1-25 in the grid boxes. For the other grid boxes (for example the grid box without number) a search for a similar, recently updated atmospheric column is carried out, in a search region of 5x5 surrounding columns (light shaded pixels). The radiation fluxes and heating rates found are then copied and corrected, see text.

of showers and thunderstorms developed in the whole model domain. The second day is a slightly less heterogeneous autumn day, 19 September 2001, where a low-pressure system over the North Sea led to convective activity in parts of the model domain. As a third case a winter day (22 December 2005) with stratiform, very homogeneous and slowly changing cloud conditions has been chosen. Germany was under the influence of an occluded front belonging to a low pressure system centred over Scandinavia. During the day the front and its broad stratiform cloud band crossed the model domain from north-west to south-east and led to moderate rain in lower and snow in higher altitudes. The COSMO-DE runs were forced by COSMO-EU operational analyses obtained from the German Meteorological Service as initial and boundary values.

3.4. Results

3.4.1. Radiative fluxes and heating rates

For the three case studies, COSMO model runs were carried out, where frequent intrinsic radiation computations of the full domain served as reference and provided the radiative effects for driving the dynamics and the soil-surface parameterizations of the model. For the comparison the radiation properties resulting from the adaptive radiation computations and the operational 2x2 column-averaging quarter-hourly radiation updates were computed as well. Hence, the three different radiation computations are based on the same atmospheric fields and can be compared directly, disregarding effects which would

Table 3.4.: Daily mean root mean square differences and systematic deviations (bias) from the reference simulation for shortwave and longwave surface net fluxes.

	RMSD [W m^{-2}]				Bias [W m^{-2}]			
Day	SW		LW		SW		LW	
	2x2	adapt	2x2	adapt	2x2	adapt	2x2	adapt
21-06-2004	31.43	23.80	7.15	5.34	-2.01	-0.20	-0.09	0.07
19-09-2001	19.62	15.81	6.53	5.08	-0.60	-0.17	-0.05	0.08
22-12-2005	2.36	1.71	5.25	4.14	-0.08	-0.04	0.11	0.07

result from diverging dynamics in different model runs. The resulting radiative fluxes and heating rates were written to an output file every 2.5 minutes.

The adaptive scheme reduces the hourly averaged RMSD for the summer case by about 25% in both the shortwave and longwave regime; also the bias is largely decreased, see Figure 3.2. The instantaneous (2.5 min) errors of the COSMO-DE radiation scheme show a quarter-hourly cycle due to the 15-minute update cycle. Errors are low directly after a new computation of the full field and increase during the following 15 minutes. The instantaneous errors of the adaptive scheme are lower throughout the time. The errors of the COSMO-DE fluxes do not reach zero at a new calculation at a quarterly hour interval because of two reasons: Firstly, the solar zenith angle is taken as at the middle of the update interval, which leads to deviations from the reference values, and secondly errors arise due to the averaging over four columns.

The root mean square errors and biases for the surface fluxes for all three cases are listed in Table 3.4. The adaptive scheme almost always outperforms the 2x2 standard scheme. The errors are generally smaller for the more homogeneous cases, but about the same relative improvement compared to the 2x2 scheme is achieved by the adaptive scheme as for the summer day.

The daily cycle of the errors for the atmospheric heating rates is depicted in Figure 3.3. The RMSD for the shortwave heating rates hardly differ between the adaptive and the 2x2 scheme, whereas in the longwave regime the adaptive scheme has the higher RMSD. The systematic errors are small, but the adaptive scheme clearly outperforms the 2x2 scheme (lower panel in Fig. 3.3). Only during sunset the solar radiation shows high systematic errors, probably due to the fast changing path lengths of the sun through the atmosphere leading to very different transmissivities. The average vertical profile of RMSD and bias (see Figure 3.4) shows that the adaptive scheme leads to larger random errors for the cloud level, while the systematic errors are much smaller, especially the LW bias. This behaviour can be traced to the weighted difference function used to search for the most similar column, which is mainly based on vertically integrated atmospheric properties. Hence columns of heating rates may be copied which have the same integrated cloud properties, but differ in the vertical position of the clouds. Such errors are penalized twice in the root mean square difference, once in the level where radiation is overestimated and once in the level where it is underestimated. The systematic errors over the whole field, however, are small. In the 2x2 operational COSMO-DE radiation scheme systematic errors can occur due to the averaging of the atmospheric properties, which can lead to biases due to the nonlinearity of radiative transfer processes, especially in case of clouds.

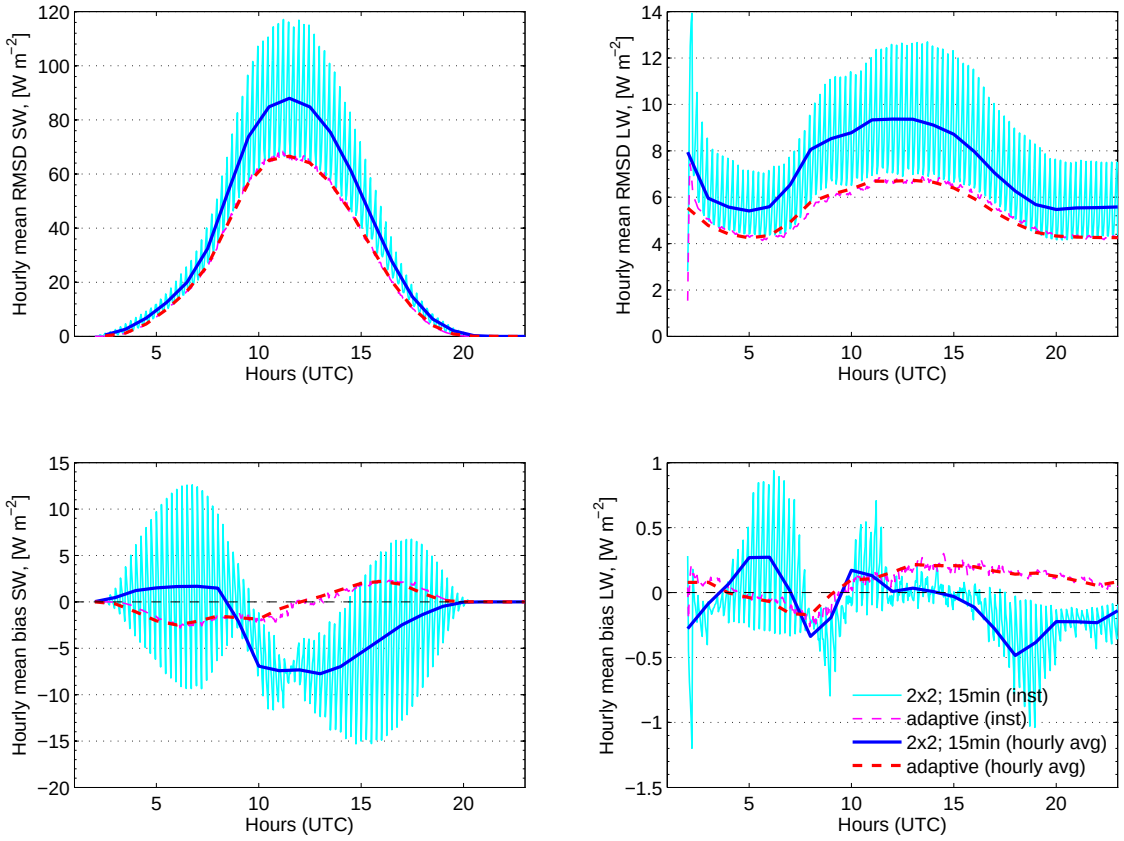

Figure 3.2.: Top: Instantaneous and hourly averaged root mean square differences in surface net radiation fluxes for shortwave (left) and longwave (right) for the 2x2 COSMO-DE scheme (solid) and for the adaptive scheme (dashed), for 21 June 2004. Bottom: The same for the biases. For the adaptive scheme the instantaneous and hourly averaged errors are almost identical.

Table 3.5 summarizes the daily mean values of the heating rate errors for the three case studies. Averaged over the day, the COSMO-DE radiation scheme performs better than the adaptive scheme for the longwave RMSD. The average bias over the day is small, although instantaneous biases can be much larger. The reason is the shape of the diurnal cycle of the bias, which shows an overestimation (underestimation) for the shortwave (longwave) heating rates in the morning and vice versa in the afternoon for all case studies, averaging to a small value close to zero over the day. The hourly biases of the 2x2 scheme are almost always higher than for the adaptive scheme (Fig. 3.3 bottom).

An interesting characteristic of the error fields is the temporal autocorrelation, i.e. the correlation of the errors with time lag. *Buizza* et al. (1999) showed that temporally persistent perturbations have a remarkable influence on model dynamic development (in their study model runs with temporally correlated perturbations increased the divergence of the model runs in an ensemble), while noise which varies randomly from timestep to timestep has no considerable influence. In this study the temporal correlations of the difference fields could be reduced by about 34% and 45% for the shortwave and longwave surface fluxes, respectively. The spatial autocorrelations of the difference fields have also

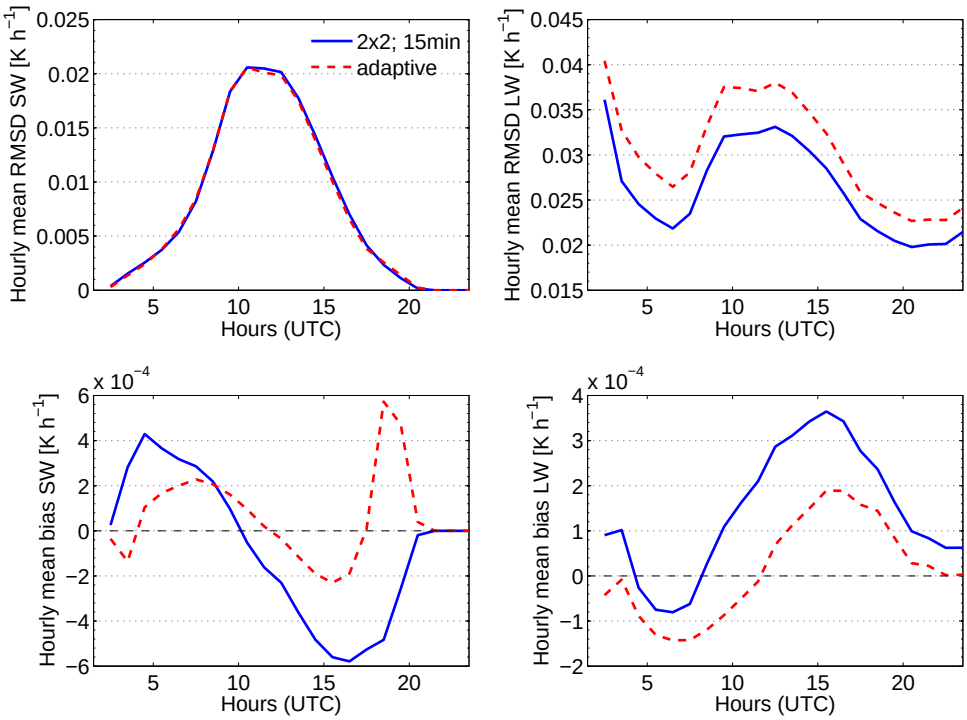

Figure 3.3.: Diurnal cycle of mean root mean square differences and bias for columns of atmospheric heating rates for the summer case 21 June 2004. Left: shortwave; right: longwave.

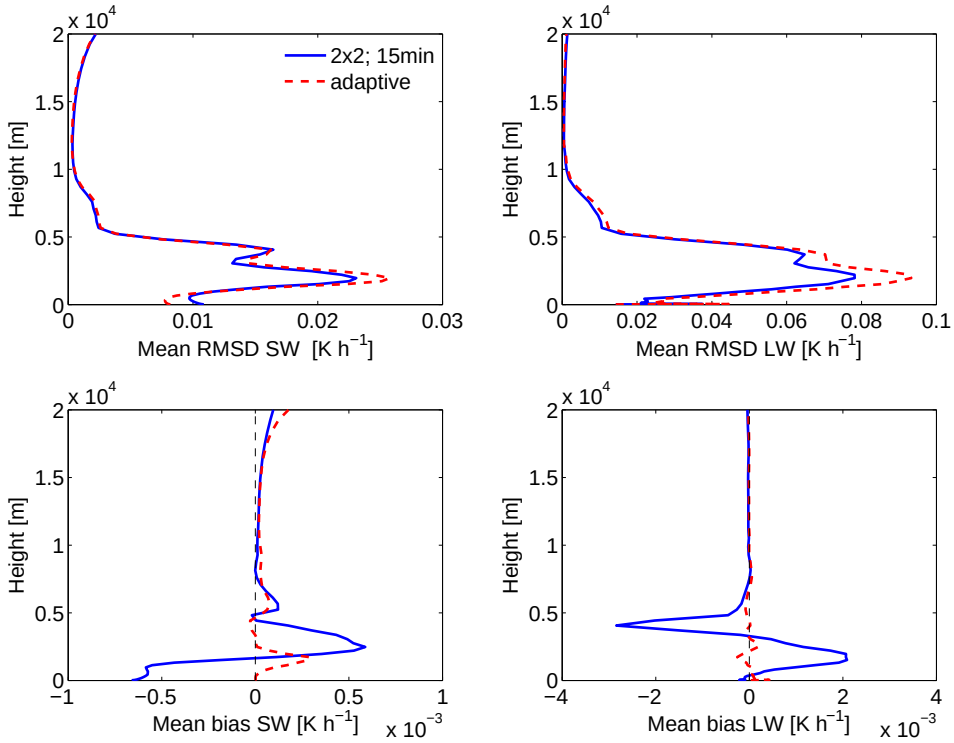

Figure 3.4.: Mean profile of root mean square differences and bias of atmospheric heating rates for the summer case 21 June 2004. Left: shortwave, Right: longwave.

Table 3.5.: As Table 3.4 but for the atmospheric heating rates.

	RMSD [10^{-3} K h^{-1}]				Bias [10^{-3} K h^{-1}]			
Day	SW		LW		SW		LW	
	2x2	adapt	2x2	adapt	2x2	adapt	2x2	adapt
21-06-2004	7.8	7.7	26.2	30.4	-0.008	0.006	0.014	0.002
19-09-2001	6.1	6.3	29.1	33.8	-0.007	0.009	0.008	-0.002
22-12-2005	1.3	1.2	29.0	32.9	-0.003	0.004	0.003	-0.004

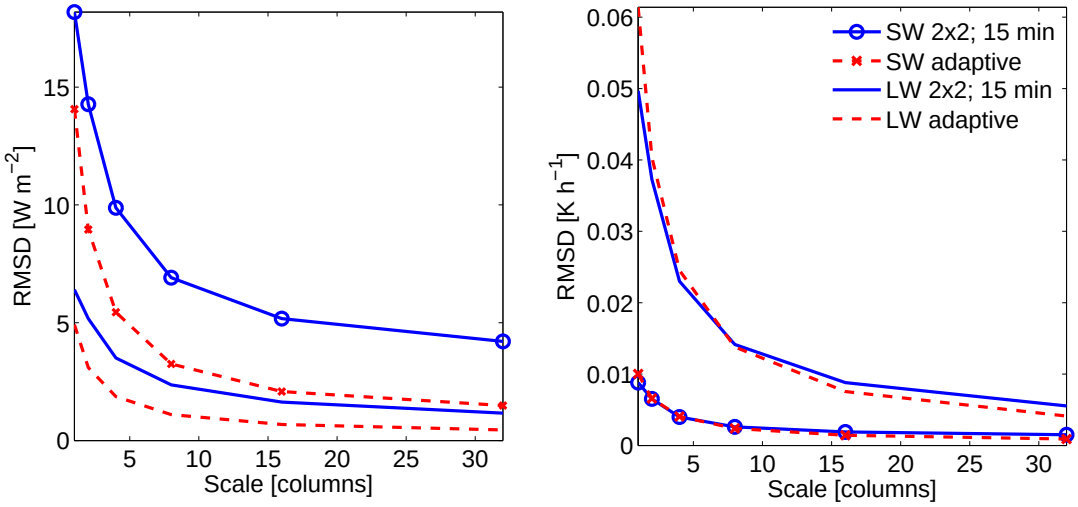

Figure 3.5.: Root mean square differences computed for different spatial scales, based on results for all three case studies. Left: surface fluxes; right: heating rates. The radiation fields were first averaged to larger scales and subsequently the root mean square differences have been computed on these larger scales.

been computed in this study, showing that the correlations in the difference fields are also slightly lower for the adaptive scheme than for the 2x2 scheme (not shown).

The errors of the adaptive scheme decrease more strongly with increasing scale than for the 2x2-averaged radiation, see Figure 3.5. This holds not only for the radiation fluxes at the surface, but in particular also for the atmospheric heating rates. Thus while on the smallest scale the results for the adaptive scheme are worse in terms of errors for the heating rates, on larger scales the adaptive scheme is more accurate.

The mean standard deviations, i.e. the spatial variability of the radiation fields, are underestimated by the 2x2 averaging scheme (Table 3.6). Due to the smoothing of the 4-column-filter especially small convective clouds are smoothed out (see also section 3.4.3).

3.4.2. Test case with 7 km resolution

Many mesoscale weather forecast models and some regional climate models operate on resolutions on the 10 km scale and above. As mentioned before, the COSMO-EU model configuration of the German weather service has a grid spacing of 7 km. On this resolution the cloud cover in the columns changes less rapidly in time than on the 2.8 km grid.

Table 3.6.: Mean standard deviation of radiation effects obtained from the different radiation update schemes.

	Flux [W m^{-2}]						Heating rate [K h^{-1}]					
Case	SW			LW			SW			LW		
	ref	adapt	2x2	ref	adapt	2x2	ref	adapt	2x2	ref	adapt	2x2
21-06-2004	143	142	135	30.9	31.1	30.1	0.056	0.056	0.053	0.090	0.090	0.082
19-09-2001	116	116	113	35.3	35.4	34.6	0.044	0.044	0.043	0.092	0.093	0.084
22-12-2005	49	49	49	39.1	39.2	38.9	0.028	0.028	0.027	0.127	0.127	0.120

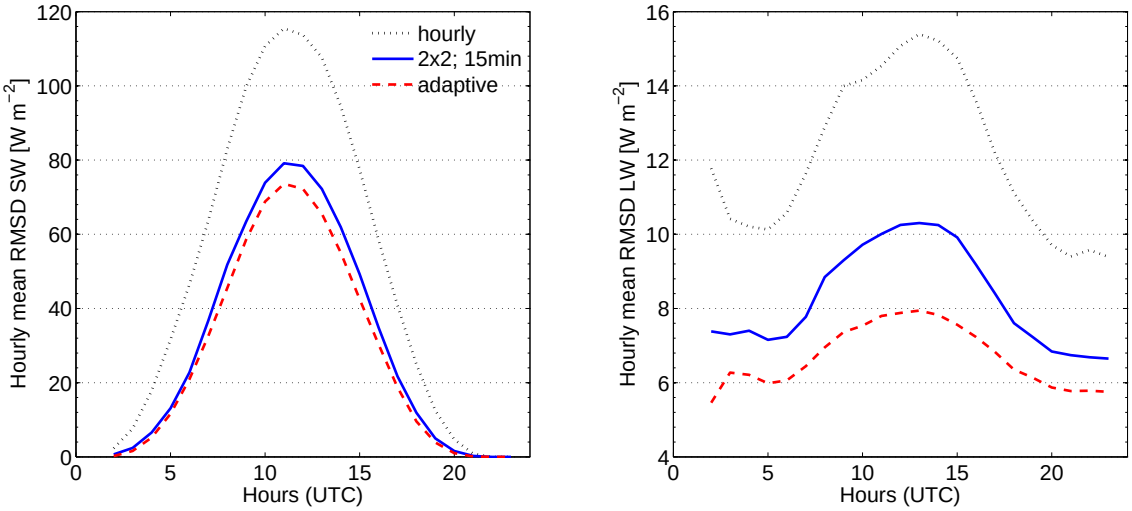

Figure 3.6.: RMSD for surface radiation net fluxes for a model run with 7 km resolution, again for the summer case. Left: shortwave; right: longwave. Additionally shown are the errors for hourly radiation updates for the whole field.

Hence, for lower resolutions the problems caused by infrequent radiation calculations are expected to be less important. The convective summer test case has been simulated on 7 km resolution with COSMO-EU settings. The operational COSMO-EU update practise (computing the radiation just once per forecast hour and keeping the radiation fields fixed in between) has been simulated and compared to the quarter-hourly 2x2 averaging option and the adaptive scheme. The reference radiation update interval and also the time step of the adaptive schemes were set to 6 minutes. The total number of radiation calculations in the four methods were again set to be equal.

The adaptive scheme still outperforms the 2x2 column-averaging scheme for the surface fluxes in terms of root mean square differences (Figure 3.6), although the relative improvement is smaller than on the smaller scale considered in the previous section. For the heating rates the 2x2 averaging scheme outperforms the adaptive approach as on the 2.8 km scale (not shown). The by far worst results for both fluxes and heating rates are obtained by the hourly update scheme, indicating that also for this scale one of the other two schemes should be chosen as standard setup.

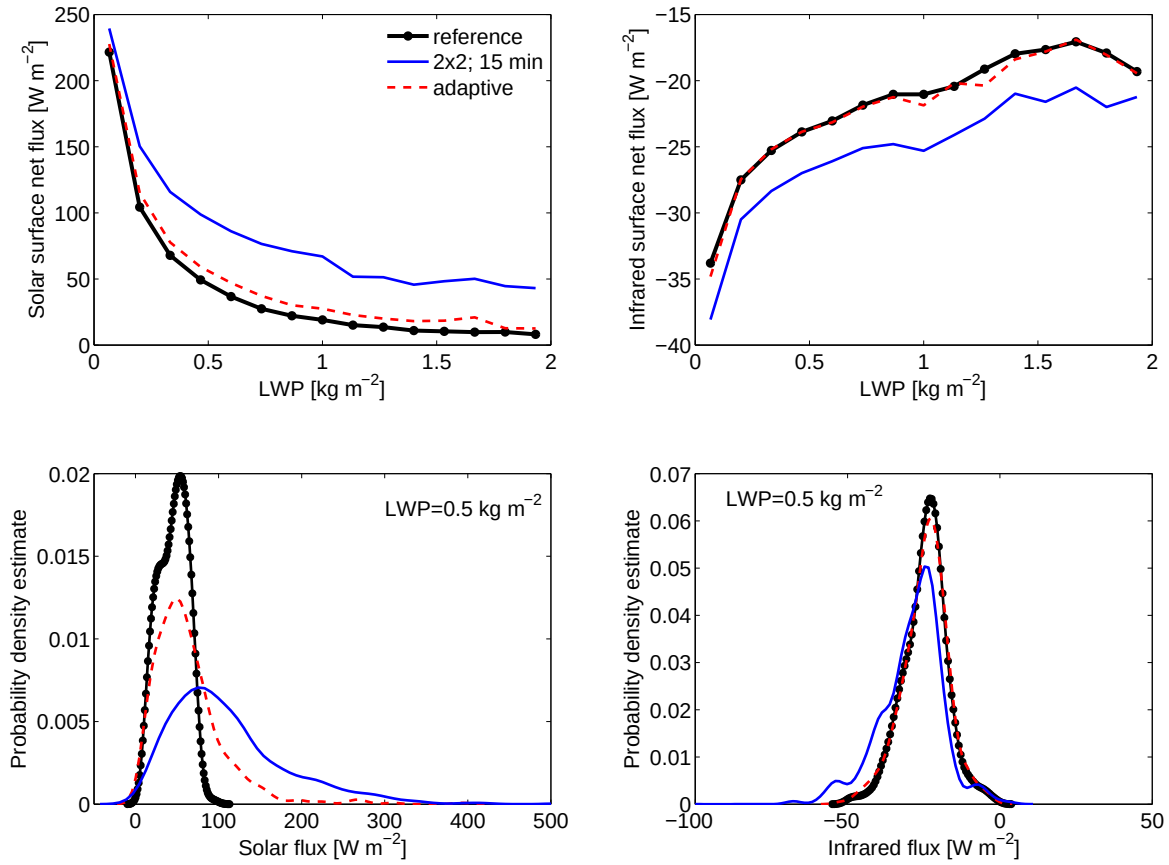

Figure 3.7.: Top: Mean shortwave (left) and longwave (right) surface net fluxes for different LWP values. For legability cloudfree columns have been omitted. Bottom: Estimated probability density function of radiation fluxes for a LWP value of 0.5 kg m^{-2}, based on a normal kernel function. Data taken from 1200 to 1700 UTC on 21 June 2004.

3.4.3. Physical consistency

In addition to the quantitative performance in terms of errors of the radiation fields also consistency of radiative effects within the model with other variables and other physical parameterizations is of importance. To illustrate physical relations between radiative effects and cloud characteristics, the mean solar and infrared surface fluxes as a function of the atmospheric liquid water content are depicted in Figure 3.7 (top). For increasing liquid water path (LWP) the solar (infrared) surface net flux decreases (increases) logarithmically for the reference and the adaptive radiation, whereas for the 2x2 averaging scheme this behaviour is less pronounced. Also the probability density function for a specific LWP value (Figure 3.7, bottom) is much wider, less peaked and shifted to higher values for the 2x2 scheme, illustrating that too high radiation fluxes may occur for thick clouds; this distinction is most pronounced for the shortwave flux (Fig. 3.7 lower left panel). Again this relation is much better captured by the adaptive scheme.

To study the physical consistency more quantitatively one could compute this probability density function for each LWP value, yielding a 2D histogram of LWP and solar surface

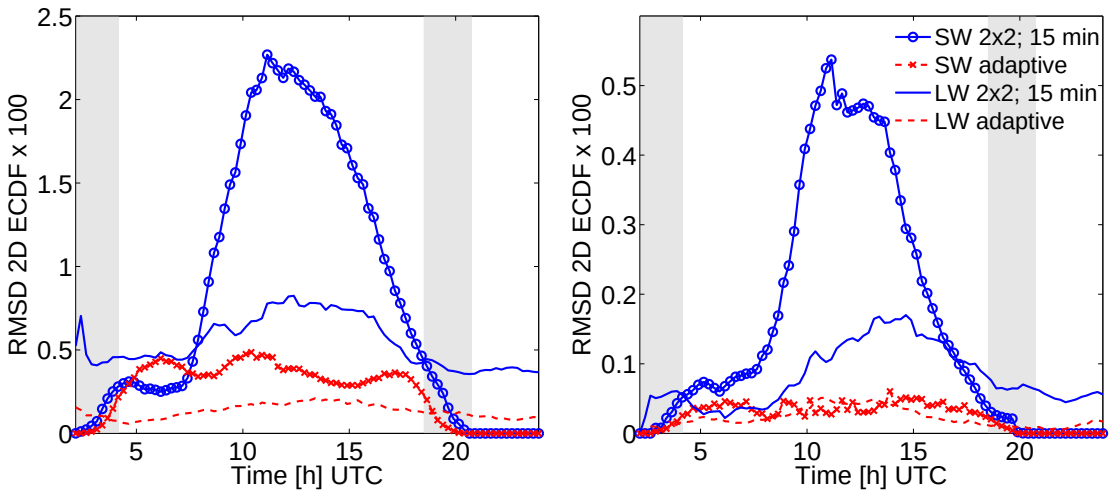

Figure 3.8.: Left: RMS difference between the ECDFs for logarithmic LWP (left) and rain rate (right) and surface radiation fluxes of the 2x2-column-averaging scheme and the adaptive scheme for the summer case study. The light grey bars denote sunrise and sunset, respectively. Right: The same for rain rates and radiation fluxes.

net flux and subsequently calculate the RMSD between this histogram for the reference radiation and one of the other schemes. The disadvantage of a histogram is, however, that the RMSD can depend on the bins widths chosen. Therefore, this error measure has been computed on the 2D empirical cumulative distribution functions (ECDF). The two-dimensional ECDF is obtained from a two-dimensional histogram by integrating in both directions. In this way, small random errors do not have a strong influence, but systematic deviations do.

In Figure 3.8 the root mean square differences of these ECDFs with respect to the ECDF of the reference radiation are depicted, for LWP and surface radiation net fluxes (left) and rain rate and surface net fluxes (right), respectively. Evidently, the differences between the 2x2-column averaging scheme and the reference is much larger, both for shortwave and longwave net fluxes, than for the adaptive scheme. This illustrates that the radiative variables computed by the adaptive radiation scheme are much more consistent with other model variables; as expected. For the 2x2 scheme the LW errors show a peak during the first hours of the model run; this peak is even more pronounced in the other two case studies (not shown). This can be explained by a spin-up effect, caused by the initialization with coarser scale analysis (7 km grid spacing). In the first hour of the model simulation the cloud cover changes rapidly, from the smooth coarse scale cloud field to a cloud field realistic for this scale. Thus, especially in the first hour an appropriate sampling of the radiative effects is important.

3.4.4. Effects on model dynamics

For the evaluation of different radiation parameterizations the overall effect on the model dynamics is very important. It is desirable that the errors inevitably caused by any radiation scheme, which samples in time and space, has negligible influence on the model

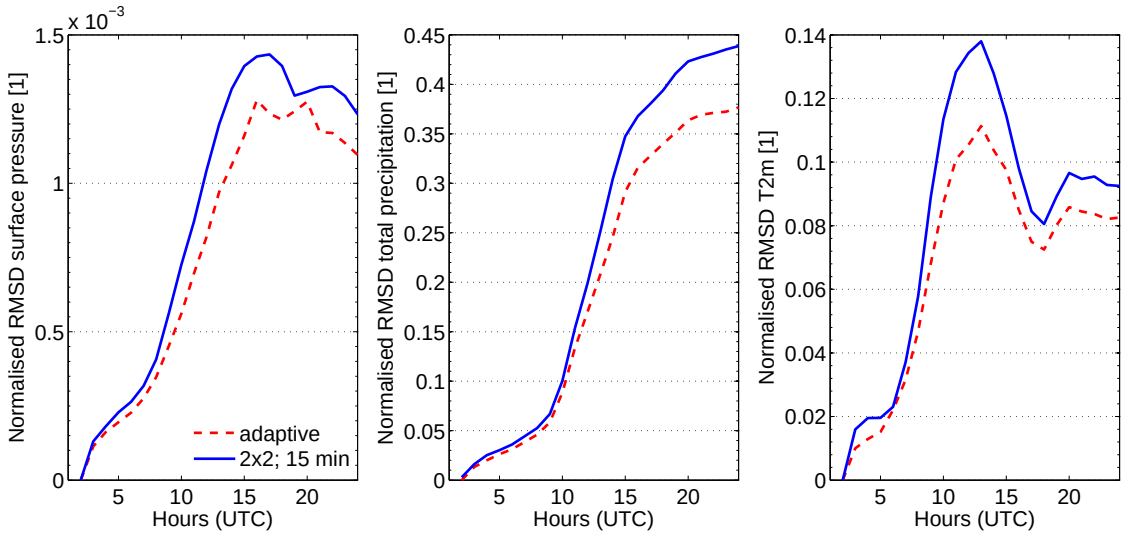

Figure 3.9.: Root mean square difference of surface pressure, total precipitation and 2 m temperature for model runs driven by different radiative forcing for 21 June 2004. The errors are normalized with the standard deviations of the reference field for the respective variable.

dynamics, i.e. the weather development. To investigate this effect, three single model runs have been carried out, one driven by the high-frequent reference radiation computations, one driven by the adaptive radiation computations and one with the quarter-hourly 2x2 averaging COSMO-DE scheme. For a numerical weather forecast model it is highly relevant how much the two computationally cheaper model runs diverge from the reference model run. In Figure 3.9 the RMS difference for three variables, which are important in daily weather forecasts and good indicators of the dynamical behaviour of the model, is displayed (for the summer case). These are the surface pressure, the total precipitation (sum since model initialization) and 2 m temperature, normalized with the standard deviations of the respective reference field to remove effects which are caused by the diurnal cycle alone. The differences in total precipitation and 2 m temperature are caused by differences in cloud formation and movement. The root mean squared differences are larger for the 2x2 radiation update configuration for all three variables, indicating that the model run with the adaptive radiation diverges less. These dynamical effects have been verified for a second convective day to ensure robustness of the results (Fig. 3.10).

3.5. Summary and discussion

The concept of adaptive parameterizations for radiative surface fluxes had been introduced first in VSAS07. Now, in this work, the spatial adaptive scheme has been improved and extended to heating rate profiles. The scheme has been implemented and tested in the COSMO-DE model with the same setup as used for daily weather forecast simulations by the German meteorological service on 2.8 km horizontal resolution. The results for case studies with different synoptic conditions were compared with radiative effects computed with the standard radiation setup based on four (2x2) averaged columns com-

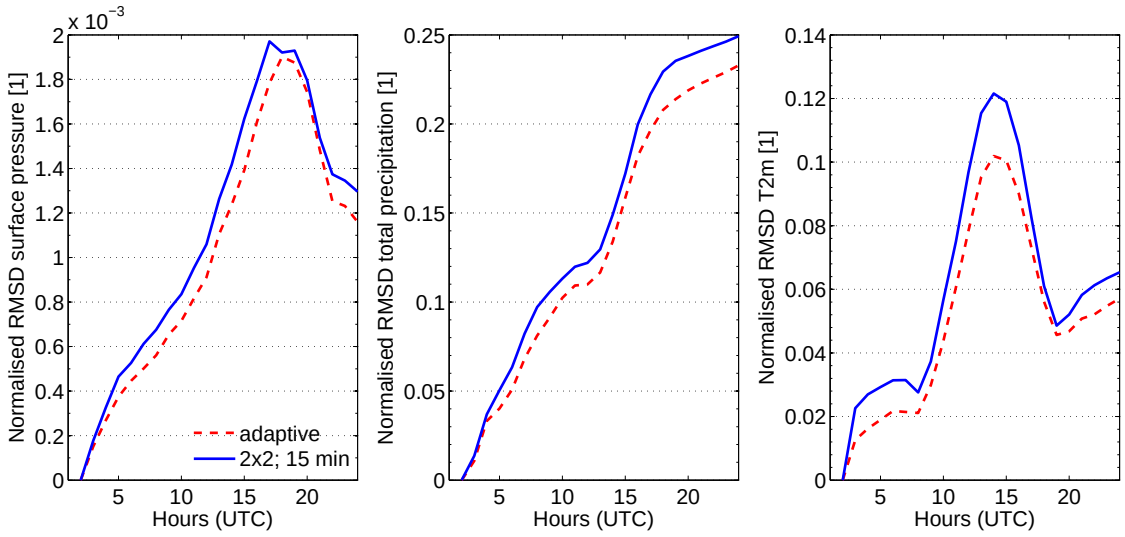

Figure 3.10.: Same as Figure 3.9, for 28 August 2010.

puted once per 15 minutes. Such spatial and temporal sampling strategies are common in operational atmospheric models due to computer time limits. This study shows that the adaptive concept provides the envisioned benefits in a real model implementation, which was also shown for a spectral adaptive RT parameterization by *Manners* et al. (2009). It is shown in this work that the adaptive scheme produces better results in terms of random and systematic errors for the surface fluxes. The errors for the longwave heating rate profiles did not show these improvements on the smallest scale, but for both, fluxes and heating rates, considerable improvement is achieved for larger averaging scales, which are dynamically more important. The 2x2 averaging scheme leads to too low variability of the radiation fields due to the smoothing, whereas the adaptive scheme matches the reference standard deviations well.

Model consistency has been evaluated analyzing relations between radiation surface fluxes and rain rates or cloud water content, leading to the conclusion that the adaptive scheme performs better in conserving these physical relations by capturing changes in cloud cover. For the 2x2 scheme the correlations are smoothed out due to averaging; fast moving and developing clouds can not be tracked. The adaptive scheme benefits from new calculations made at high frequency in each region and thus follows rapid developments. The search of similar, recently updated atmospheric columns assures that the heating rates and surface fluxes are taken from similar cloudy or cloudfree columns, leading to more consistent radiative and atmospheric characteristics.

Simulations with the different radiation options have also been carried out for the operational COSMO-EU model, which runs on a larger model domain with 7 km horizontal grid spacing. Operationally updates are computed only once per forecast hour and kept constant in between. This setup leads to the worst results, compared to the adaptive and the 2x2 quarter-hourly schemes, indicating that also for that scale either the adaptive or the 2x2 scheme would be more appropriate.

It is crucial for weather forecasts that the CPU-time saving configuration is chosen, which has the least deteriorating effect on the dynamical model development. Therefore,

single model runs were carried out where the different radiation quantities of the adaptive and 2x2 averaging schemes were not just computed diagnostically, but were actively used to force the model. We found that the model runs with the operational quarter-hourly 2x2 averaged radiation diverges more from the reference model run with highly frequent calls to radiation scheme than the model run employing the adaptive scheme. Thus, it can be concluded, that the lower errors for the surface fluxes, the better performance for the heating rates on larger averaging scales, and the more realistically captured physical relations have a highly positive impact. All this is achieved without an increase in computation time, but based on a more intelligent way of exploiting the available computation resources, and distributing the information from the complex radiation scheme to the rest of the field.

For training the scheme an optimization algorithm had to be applied to find the weights for the cost function used to search for nearby similar columns. In VSAS07 it was shown, that the scheme is not sensitive to the exact values of these weights. Hence an advantage compared to neural networks, which emulate complex radiation schemes (e.g. *Krasnopolski* et al., 2010) is that re-training is much less important for changes in the radiation scheme or the vertical resolution, the scheme can be applied as-is in other atmospheric models or in combination with other radiation codes. The obtained speedup, however, is potentially smaller than for neural networks because the complex radiation scheme is not emulated but only exploited more efficiently. If a neural network is employed for the radiative transfer, no online radiation computation with the complex radiation scheme are carried out at all.

As further improvement of the scheme a combination of the spatial adaptive scheme with the temporal adaptive scheme proposed in VSAS07 is planned. In that scheme the grid points for which a call to the complex radiation scheme is carried out are not fixed (see section 3.1), but a very simple radiation scheme based on a multiple linear regression is used to find the columns that have undergone the largest atmospheric changes since the last update. This gives even better information on the radiative quantities in regions where the clouds are developing and moving rapidly. Furthermore, remaining differences between the best matching nearby column and the true atmospheric profile can be corrected by the simple radiation scheme.

An improvement of the results for the heating rates should also be envisaged, potentially by better correction methods or a search algorithm which not only incorporates vertically lumped measures.

For high horizontal resolutions the problem of fast moving clouds is an important task; the persistence assumption made in many operational codes leads to highly inconsistent situations. For this reason, the adaptive approach has been tested on the meso-γ-scale. However, it has been shown, e.g. by *Morcrette* (2000) for longer, seasonal simulations, that errors due to sampling of radiation computations build up in time. They can have considerable impact on the dynamical development of the model, leading to a too cold stratosphere through cloud-radiation-convection interactions for simulations with the ECMWF model. Thus, also for larger scale models, especially for climate simulations where the heat budget is of particular importance, the use of adaptive radiation computations as a tool to provide better radiative fluxes and heating rates without increasing computational burden, should be considered.

The concept of adaptive parameterizations, i.e. the combination of complex computations and more simple generalizations, has been applied to radiative transfer, because it is one of the most expensive parameterization in terms of computation time. The general idea of combining complex parameterization with more simple schemes to spread the accurate information in time and space (or spectral space) to save computational resources can also be applied to other parts of the model physics or also model dynamics. The mode-splitting approach by *Klemp and Wilhelmson* (1978) for example, which computes the fast atmospheric waves on intermediate time steps between the coarse model time steps for advective and physical processes, is based on a similar idea.

4. Scale-consistent two-way coupling of land-surface and atmosphere

4.1. Motivation, strategy and literature review

The accurate representation of the turbulent surface exchange fluxes in atmospheric models is challenging, because these fluxes are the result of a long, interacting chain of parameterizations, above and below the earth's surface. The processes in the soil and at the interface between atmosphere and surface are generally modelled by Soil-Vegetation-Atmosphere-Transfer (SVAT) models, which in practise are column-models, without lateral exchange. The coupling of the soil to the the atmosphere is parameterized according to Monin-Obukhov similarity theory (*Stull*, 1988), which describes the near-surface layer above homogeneous terrain. Turbulent transport of a variable is parameterized proportional to the vertical gradient of this variable between surface and lower atmosphere, and a turbulent diffusion coefficient K.

Land cover characteristics can have a strong impact on lower boundary characteristics and the surface heat budget, thus accurate land-surface information in atmospheric models is important. As an example, large differences can be expected for forested areas versus bare soil areas, due to the larger roughness of forests, leading to a stronger coupling of the surface and air temperature. Moreover, trees can reach to deeper soil moisture reservoirs, and thus moisten the lower atmosphere by evaporation, even if bare soil moisture is limited due to near-surface soil moisture deficits. Furthermore, forested areas have a lower albedo under snow cover than bare soil. Thus, fluxes and surface temperatures can vary considerably for different surfaces. In an idealized experiment using a mesoscale model, *Avissar and Pielke* (1989) found the maximum sensible heat flux ranging between -10 $\mathrm{W/m^2}$ (for water bodies) and 450 $\mathrm{W/m^2}$ (for urban areas), the maximum latent heat flux between 0 $\mathrm{W/m^2}$ (built-up areas) and 610 $\mathrm{W/m^2}$ (agricultural crops) and the range of maximum surface temperature varied between 27°C (water bodies) and 50°C (built-up areas). *Avissar* (1992) analyzed the sensitivity of soil heat fluxes and soil temperature to the availability of soil water. The soil water availability is dependent on underlying soil texture and water content. He found differences of 18 K in surface temperature, 385 $\mathrm{W/m^2}$ in sensible heat flux and 515 $\mathrm{W/m^2}$ in latent heat flux in simulations with a dry bare soil surface versus simulations with a moist, vegetated surface, respectively, for a cloudless midsummer day in the subtropics. Over moist surfaces the available energy is mainly used for evaporation, and over vegetated surfaces with available water in the plant root zone, the plants extract this water by transpiration. Large differences in the turbulent fluxes over different land-use classes were also found in flux measurement campaigns, e.g. the LITFASS[1] campaign (*Beyrich and Mengelkamp*, 2006). *Beyrich* et al. (2006) e.g.

[1]Lindenberg Inhomogeneous Terrain - Fluxes between Atmosphere and Surface - a long-term study

found differences of a factor of four of the sensible heat flux over forest versus farmland. Considerable differences were also found between different types of farmland.

4.1.1. Strategy

The scale-consistent coupling of land-surface and atmosphere is the central aspect of the subproject C4 in the Transregional Collaborative Research Centre 32: "Patterns in Soil-Vegetation-Atmosphere Systems: monitoring, modeling and data assimilation", in which framework large parts of this work have been carried out.

A new downscaling system to disaggregate the atmospheric variables down to a finer grid in a mosaic approach, i.e. higher horizontal resolution of the land-surface, is introduced. Hence, the approach addresses the scale gap between high-resolution surface models and atmospheric models running on a coarser grid. The novelty of the approach is not only the much smaller scale compared to previous studies (2.8 km as coarse atmospheric scale and 400 m resolution at the soil surface), but also the explicit reconstruction of the small-scale statistics, i.e. the subgrid-scale variance. The reproduction of the correct variance is especially important if the downscaled variables are used as input data to model nonlinear processes.

A statistical approach, guided by physical considerations, is chosen. Output from high-resolution (400 m) coupled model simulations has been used to generate a dataset (see section 4.2), from which the downscaling rules were derived. The atmospheric disaggregation introduced here represents a further advancement of the work by *Ament and Simmer* (2006), who implemented and tested the mosaic approach in the COSMO model. The concept, however, can be easily adapted to generate input for other SVAT or hydrological models that need high-resolution atmospheric forcing input.

The downscaling system for atmospheric variables comprises three steps. In a first step a bi-quadratic spline interpolation is applied, which conserves the coarse pixel value as a mean (see section 4.3.1). In the second step high-resolution surface information is used to exploit relations between surface and atmospheric near-surface variables (section 4.3.2). A novel automatic rule-search algorithm has been set up to find relationships, which might act only under certain atmospheric conditions. In the final step autoregressive noise is added in order to replenish the variance in the high-resolution runs (section 4.3.3). The application of this disaggregation system to the different variables is shown in section 4.4, and summarized and discussed in 4.5. Large parts of this chapter have been published in *Schomburg* et al. (2010).

4.1.2. Relevance of subgrid-scale surface heterogeneities

Processes in the subsystems of the climate system, especially processes in the soil and vegetation on the one hand and in the atmosphere on the other hand, are acting on highly different spatial and temporal scales. In the atmosphere small-scale spatial heterogeneities are smoothed quickly due to turbulence, whereas the variability of the soil-vegetation subsystem is highly persistent due to the lack of fast turbulent motions. The different spatial scales of processes in the atmosphere and at the earth's surface make a consistent coupling of land-surface and atmosphere difficult; and they are not accounted for explicitly in most operational weather forecast and climate models.

Two kinds of surface heterogeneity effects on the atmosphere can be distinguished (*Giorgi and Avissar*, 1997): The first effect is the dynamical effect of circulations arising due to surface heterogeneity, which cannot be described explicitly by the model if the model resolution is too coarse. Secondly, if nonlinear processes are involved, the aggregation of subgrid-scale heterogeneity-effects up to the scale of the meteorological model is hampered, because:

$$\overline{F(x)} \neq F(\overline{x}) \tag{4.1}$$

which means that averaging of the subgrid-scale properties and computing the flux based on these mean parameters leads to errors. Instead, the turbulent fluxes themselves need to be averaged.

In SVAT models many processes are highly nonlinear. For example runoff generation is threshold dependent, since it occurs if soil moisture exceeds saturation. Stomatal- and aerodynamic resistances are nonlinear functions of local micro-climate variables such as temperature and water vapour. The exchange coefficients are nonlinearly dependent on the thermal near-surface stability. The saturated water vapour mixing ratio is an exponential function of temperature. Moreover, snow and ice processes are nonlinear since they depend on the melting temperature. Hence, subgrid-scale effects are particularly important during the cold seasons in regions with inhomogeneous terrain due to the dependence of snow formation and melting on a step function. Nonlinear effects also play a role in the relation between turbulent heat fluxes and mean vertical profiles: the vertical gradient of potential temperature may suggest an upward flux, while the true averaged flux can be directed downward if strong turbulence in small instable regions dominates the mean heat flux. As another example of nonlinearity, a small variation in surface conductance in a dry landscape leads to a large change of surface fluxes, while the same variation in a moist landscape has almost no effect (*Avissar*, 1992).

In many studies the effects of subgrid-scale surface heterogeneities on atmospheric quantities and on the overall model performance of numerical weather prediction and climate models have been investigated. However, most of these studies have been carried out on the basis of large scale models with horizontal resolutions on the order of 10-100 km (e.g. *Seth* et al. (1994), *Avissar and Schmidt* (1998), *Hu and Islam* (1998), *Giorgi* et al. (2003), *Molod* et al. (2003)). In large-scale models, both of the above mentioned effects of subgrid-scale variability, the dynamical effect and the effect of nonlinear aggregation, can not be resolved. In small scale models such as the COSMO-model used in this work, the dynamical effect can be modeled explicitly to some degree, because it is caused by surface pattern scales of at least 5-10 km (*Avissar*, 1998). The problem of nonlinear aggregation effects, however, remains relevant even at high horizontal resolutions, because the scale of surface heterogeneities is usually still much smaller.

In several studies effects of nonlinear processes on the simulation of the turbulent fluxes have been investigated. *Gao* et al. (2008) assessed the impact of the improvement in land-surface information data sets on atmospheric modeling by substituting land-surface information from coarse global data sets by high-resolution remote-sensing information in atmospheric simulations on a 3 km grid over the Heihe river basin in China. MODIS land-surface temperatures and station observations were used as validation data. Improved soil texture information led to large changes in lower atmosphere humidity and as a result in altered precipitation. Refined land use information had a large effect on the temperature of

the lower boundary. They also detected a large impact of soil and land use heterogeneity. Representing the heterogeneity more adequately by the new data sets decreased the local circulations and thus the simulated precipitation sums and helped to decrease a formerly existent wet bias considerably.

Land surface contrasts lead to differences in the amount of absorbed radiation and the partitioning of this incoming radiation into latent and sensible heat flux, i.e. the Bowen ratio. Errors in the Bowen ratio of about 20%, which can result from neglection of subgrid scale heterogeneity, can have a significant influence on climate simulations (*Seth* et al., 1994). *Avissar* (1998) found the latent heat flux to be the most sensitive term of the energy budget with respect to spatial land cover variability. He also found that the usage of averaged stomata conductance, leaf-area-index (LAI) and surface roughness instead of high-resolution values in SVAT modeling has a considerable impact on energy fluxes at the surface, whereas the use of an aggregated albedo has less impact. *Henderson-Sellers and Pitman* (1992) demonstrated that small changes in input parameters for a land-surface model can change the results considerably and in a nonlinear way for fractions of a rough surface in an otherwise smooth grid box. They proved the necessity of an adequate representation of subgrid effects for a realistic simulation of the surface energy budget by carrying out simulations with different fractions of subgrid-scale lake areas. For larger subgrid lake fraction within a grid box, one obtains higher evaporation rates, and consequently lower sensible heat fluxes. Moreover, a net reduction in the energy-flux was obtained due to lower roughness, partly compensated through a lower albedo of the water compared to the surroundings. *Bonan* et al. (1993) studied the effects of subgrid-scale variability in LAI, minimum and maximum stomatal resistance and soil moisture on the grid-scale fluxes by comparing energy fluxes computed based either on parameter-averaging or on flux-averaging. They found only small differences for reflected solar radiation and emitted infrared radiation, but large differences for sensible and latent heat flux. LAI was the most important parameter in this context, stomatal resistances were only important for moist soils, for dry soils the evapotranspiration was limited by the water deficit. Evapotranspiration and sensible heat exhibited very strong non-linear dependence on LAI, on some days even the sign of the flux was different for flux- or parameter-averaging. Interactions between the different parameters increased the errors due to parameter-averaging even more.

4.1.3. Subgrid variability in models

Surface heterogeneity

Due to the results from the studies cited in the previous section, which indicate the need of an adequate representation of subgrid-scale land-surface heterogeneities in atmospheric models, different methods have been developed. Different aggregation techniques are available, which model the effects of subgrid-scale variability on the grid box average of energy and water budgets and exchange of momentum, energy and water. A comprehensive overview on the representation of heterogeneity effects in atmospheric models is given in *Giorgi and Avissar* (1997). The initially available simple methods did not treat subgrid information explicitly. These are the *dominant type* approach and the *parameter averaging* approach (also called *effective parameter method* or *parameter aggregation*).

The former method models all processes and parameters as if the whole grid cell would be covered by the dominating vegetation type. In the latter, the parameters of the different existing vegetation classes are averaged before any soil calculations are carried out. This approach is problematic due to the nonlinearities in the processes, as mentioned before. Two more sophisticated approaches have been developed, which treat subgrid-scale land-surface heterogeneities explicitly. These are the so called discrete approaches including the *tile approach*, first described in *Avissar and Schmidt* (1998), and the *mosaic approach*, first presented by *Seth* et al. (1994), and continuous approaches describing heterogeneities by probability density functions (PDFs). A central issue of any PDF-based heterogeneity formulation is the choice of an appropriate PDF and the corresponding parameters. In literature a wide range of functions are described, e.g. Gauss-, Beta-, lognormal, exponential or Gamma-functions. The relevant processes are then integrated over the adequate PDFs.

In the literature, the nomenclature for the two discrete methods is ambiguous, in this study the definition also used in *Heinemann and Kerschgens* (2005) and *Ament and Simmer* (2006) will be used. In the tile approach, the soil processes are modelled separately for each of the different land use classes, which are available at the subgrid-scale, and subsequently the resulting fluxes are averaged according to the fractional coverage of these land use classes. In the mosaic approach, the coarse atmospheric column is subdivided into an explicit number of subpixels for which the soil processes are computed separately. Dependent on the number of subpixels this approach is usually more computationally demanding, but it has several advantages. Effects of different surface characteristics such as land use, orography, soil texture, soil moisture and soil temperature can be considered in a consistent way, as each subpixel has its own characteristics. Therefore this approach is sometimes also called "explicit subgrid approach". Calculating the fluxes on the small scale and forming an average in a second step leads to less biased results than averaging the soil characteristics and then calculate the fluxes, due to the nonlinearities. *Avissar and Schmidt* (1998) reasoned, that patterns in landscape having a characteristic length scale smaller than 5-10 km can be modelled by mosaic or tile methods, for larger patches also dynamical circulations may arise, which can not be modelled by these flux-aggregation techniques.

In the literature several studies applying one or more of these techniques can be found. *Avissar* (1991, 1992) combined the tile approach with the PDF-approach, describing the variability of the different parameters of the soil-vegetation atmosphere system by probability density functions. Such a land-surface parameterization simulates the whole distribution of surface energy, fluxes, temperatures and moistures within a grid box. This, however, is computationally expensive because the integration of these PDFs over the different land-surface characteristics is necessary. Thus, in his study mean values for all parameters are used as a start, only the stomatal conductance is represented by its PDF as a proof of concept. He also states that in principle two kinds of heterogeneities need to be considered in atmospheric models: landscape patchiness, i.e. different kinds of land cover such as forests, urban areas, water bodies etc., and intra-patch heterogeneity, such as different stomatal resistances within a vegetated area of a certain type.

Essery et al. (2003) compare simulations of a land-surface scheme with or without tiled subgrid heterogeneity representation, either uncoupled or coupled to a global circulation

model (GCM). They found larger differences between the tile representation and the aggregated approach, if coupled to the GCM, due to feedbacks to the atmosphere. Another application of the tile approach in a GCM is presented in *Koster and Suarez* (1992).

Schlünzen and Katzfey (2003) analyzed the performance of mesoscale models with respect to the parameterization of subgrid-scale land-surface processes for a meteorological situation strongly influenced by local effects. The flux aggregation in the tile approach was compared against parameter averaging and the dominant type approach. Flux aggregating achieved the best results, the worst were achieved by the parameter averaging method. *Heinemann and Kerschgens* (2005, 2006) tested three methods (parameter averaging, tile, mosaic) in an offline mode for a small-scale model on the meso-γ-scale and a high-resolution run as reference. The authors obtained the largest errors for parameter averaging and the best results for the mosaic method. They advised to use the mosaic or at least the tile approach in mesoscale models or regional climate models. They found differences for the approaches on different averaging scales between 20 down to 2 km and thus confirmed the necessity of taking subgrid-scale variability into account even on very small scales. The largest errors occurred if water bodies are part of the subgrid-scale heterogeneity.

Ament and Simmer (2006) implemented the mosaic and tile approaches into the COSMO-model. They compared model runs with 7 km resolution using the different averaging methods with measurements and also with high resolution runs on 1 km horizontal grid spacing. The best results again were obtained with the mosaic approach, the worst for the effective parameter method. They also found that using only a very small number of subpixels in the mosaic approach, namely the same number as tiles in the tile approach, yielded better results for the mosaic with an almost equal computing time.

Some of the established land-surface codes already comprise some kind of subgrid heterogeneity representation. The Community Land Model (CLM; *Oleson* et al., 2004) for example, allows for multiple land cover types within a grid cell via a tile approach and for multiple plant functional types in vegetated columns. The ECMWF integrated forecasting system (IFS) employs the TESSEL-model (Tiled ECMWF Scheme for Surface Exchanges over Land), where each grid-box is separated into fractions according to land cover. For each of these fractions the land-surface energy budget and skin temperature are computed separately. Also in the UK Met Office Unified Model a nine-tile surface-exchange scheme is implemented (*Cox* et al., 1999).

Atmospheric subgrid-variability in surface schemes

If the mosaic approach is employed in an atmospheric model, techniques are needed to realize the coupling between the two different scales in the atmosphere and at the surface. In the upward direction, from the soil to the atmosphere, the high-resolution turbulent fluxes at the interface are averaged to the coarser (atmospheric) scale, before passing them over to the atmospheric model. For the downward direction, i.e. for the coupling of the coarse atmosphere with the high-resolution surface, the standard approach is to assume a constant atmospheric forcing for all subpixels belonging to one atmospheric column to drive the SVAT model. However, especially over heterogeneous land-surfaces also the lower part of the atmospheric boundary layer is heterogeneous. This atmospheric heterogeneity to some degree induces (or reduces) surface heterogeneity; by assuming

homogeneous atmospheric forcing, this aspect is neglected. Moreover, the concept of blending height, as for example described in detail in *Claussen* (1991, 1995) as the height at which the flow becomes independent from variations in surface characteristics, leads to the conclusion that surface heterogeneities need to be considered in atmospheric models in which the lowest vertical model layer is below the blending height. This is usually the case for models on the meso-γ-scale, which have a lowest model level at 10 m or even below. Thus, from a physical point of view, the disaggregation of atmospheric quantities due to heterogeneities at the surface in the lowest atmospheric model layer(s) should be taken into account. A spatially distributed atmospheric forcing should lead to a more realistic input for the soil module and can thus lead to improvements for the fluxes, again especially due to the involvement of nonlinear processes.

An explicit distribution of atmospheric forcing was first tested by *Seth* et al. (1994). The authors disaggregated temperature, humidity, convective precipitation and clouds to the high surface resolution. Temperature and humidity were downscaled proportional to either soil temperature and soil moisture anomalies, or, in a second comparison, orographic height anomalies. The method was tested for a stand-alone version of the biosphere-atmosphere transfer scheme (BATS, *Dickinson* et al., 1993) and evaluated with respect to surface fluxes and hydrology (soil moisture and runoff). The horizontal resolution in their study was coarse (3.0° atmospheric resolution with 0.5° mosaic resolution); simulations were carried over a time period of 20 years. The authors found that due to the downscaling of atmospheric variables the heat fluxes changed by up to 15% and the runoff up to 33%. *Arola* (1999) extended this technique by applying stability corrected logarithmic profiles to compute the local wind speed, temperature and humidity at the reference level for the flux calculations, which led to further improvements in the modeling of the sensible heat flux. Conceptually their method is even more physically based than models which use the lowest atmospheric model level as reference level for the flux computations in all situation, because they explicitly estimate the blending height and use the atmospheric model layer, which is the nearest model layer below the blending height for the flux computations.

In a study by *Molod* et al. (2003) the tile approach in a GCM was extended for usage not only in the soil module, but up to the blending height. The blending height in this study is but determined depending on tile-to-tile variability. The only "tile-process", which is simulated for the atmospheric tiles, is the turbulent mixing.

The same temperature disaggregation method as in *Seth* et al. (1994) was applied in a study by *Dimri* (2009) in regional climate simulations over the Himalaya with an atmospheric grid of 60 km resolution and a 10 km mosaic surface representation. In simulations of 6 months much more variability of snow cover was obtained, due to the split up of precipitation into snowfall on the mountain tops and into rain in the valleys. Due to nonlinear processes the total snow cover increased: In snow-covered areas the albedo is higher than in the surroundings, thus less solar radiation is absorbed, leading to a cooling and thus a longer period until melting processes set in.

Giorgi et al. (2003) adopted the idea of distributed atmospheric forcing in combination with the mosaic approach in a regional climate model of 60 km grid spacing over the Alpine region, where the heterogeneity is particularly large. They employed a disaggregation based on topographic height; the temperature was downscaled using a moist adiabatic lapse rate multiplied with the elevation anomaly. Humidity was downscaled

accordingly, keeping the relative humidity constant for all subpixels, thus adjusting the specific humidity according to the temperature adjustment. Convective precipitation was distributed over one (randomly chosen) third of the subpixels. Grid scale precipitation, radiation fluxes and wind speed were not disaggregated. Using this system in simulations covering 11 months led to an improved small-scale structure and an overall better simulation of the near-surface temperature over complex terrain. Thus, the snow cover could be modelled more realistically, yielding (via feedback processes) an improved simulation of the water and energy cycle, especially during winter, and in spring during and after snow melt.

The cited studies show that considerable improvements can be achieved by taking variable atmospheric forcing into account for driving small-scale soil models. In contrast to this work, all studies addressed, however, only scales of the order of 100 km. Moreover, small-scale variability was introduced to a subset of the atmospheric forcing variables only.

Hydrological models usually operate at even higher resolutions than SVAT models, because water flow must be simulated down to the scales of individual creeks for runoff prediction. Thus downscaling of atmospheric driving fields becomes even more important (see e.g. *Seuffert* et al., 2002). A good review of effects, which can result from neglected rainfall variability, is given by *Singh* (1997). A realistic distribution of the subgrid-scale precipitation is of importance as it influences the partition into evaporation, surface runoff and subsurface runoff. Homogeneous low precipitation rates e.g. can evaporate to a large degree from the interception store, while for stronger precipitation on a smaller area more runoff is generated, because interception store and infiltration rate can be locally exceeded. The importance of an adequate representation of spatial precipitation patterns is also investigated by *Segond* et al. (2007), who studied the relation between spatial precipitation and runoff generation by using either radar data or rain gauge networks of different density to force a hydrological model. The results improved with increased sampling density of the rain events by the rain gauge networks. In a study by *Naden* (1992) spatial variability was introduced implicitly into a hygrograph for estimating flood risks by applying weights to the network-width function, which describes the spatial distribution of channels in a catchment. A more physically approach, based on a disaggregation of all forcing variables, is presented by a study by *Boé* et al. (2007). They forced a hydrological model with differently downscaled atmospheric data and compared the resulting river discharges. Downscaling was performed dynamically including a bias correction and statistically based on weather typing and conditional resampling using large-scale variables as predictors. They found the statistical approach being more efficient in reproducing the temporal and spatial autocorrelations.

4.1.4. Downscaling techniques for atmospheric parameters

A considerable amount of literature exists on statistical downscaling techniques for atmospheric variables. Some typical examples are discussed in the following; only the basic ideas and the relevant references are given.

Most techniques have been developed for climate impact studies for downscaling global climate model output to regional scales. Thus they have been designed for large scales and daily values and are usually trained on the basis of station measurements. A common assumption of all downscaling techniques is that a stable empirical relationship can be

established between atmospheric processes between different spatial (and/or temporal) scales (*Wilby* et al., 1998).

In many studies relations between variables of the free atmosphere of a GCM and local variables at the earth's surface for predicting daily mean values of several variables such as minimum and maximum temperature or precipitation rates have been exploited (*Karl* et al., 1990; *Huth*, 1999; *Schoof and Pryor*, 2001; *Huth*, 2002; *Schoof* et al., 2006). Statistical techniques which are applied for this purpose include rotated principal component analysis (PCA) for redundancy reduction, cluster analysis for synoptic circulation classification, canonical correlation analysis (CCA) for establishing simultaneous relationships between linear combinations of predictors and surface observations, and inflated regression. The studies make use of autoregression techniques, artificial neural networks, stochastic weather generators, downscaling by singular value decomposition (SVD) or multiple linear regression (MLR) techniques.

Wind speed is downscaled in a combined physical-statistical method by *de Rooy and Kok* (2004). *Pryor* et al. (2005) developed a downscaling for parameters of the monthly wind speed probability density function (Weibull parameters) as predictands based on relative vorticity and mean sea level pressure gradients as predictors.

Downscaling of humidity variables has been carried out only rarely in literature. *Huth* (2005) disaggregated surface humidity quantities from large scale fields of the higher atmosphere by multiple linear regression for single stations. Another possibility is to assume the relative humidity to be constant and thus calculate the specific humidity based on the disaggregated temperature and the constant relative humidity (*Giorgi* et al., 2003).

Precipitation downscaling is more difficult than the downscaling of other atmospheric quantities (*Maraun* et al., 2010). Difficulties arise due to the non-Gaussian distribution of precipitation, and its statistical analysis is complicated by data which are usually dominated by zeros. Not only the amount of precipitation but also the occurrence must be predicted. Moreover, no strong deterministic relationship between precipitation and surface variables, which could be exploited for disaggregation purposes, can be expected. Nevertheless, a large number of studies address the issue of precipitation downscaling, due to its central role in hydrological modeling. *Wilby* et al. (1998) compared different downscaling techniques, namely two stochastic weather generators, two methods with grid point vorticity as predictor, and neural networks with various circulation- and temperature variables as input. The weather generators performed quite well, while the neural networks failed to predict the wet-day occurrences correctly. *Bindlish and Barros* (2000) disaggregated precipitation fields from the mesoscale MM5 model on the basis of orographic effects for the use as input to a hydrological model and showed the relevance of small-scale ($1\,km^2$) variability for the reaction of runoff. *Brussolo* et al. (2008) applied a stochastic downscaling method (named RainFARM). This is a nonlinear transformation of a linearly correlated Gaussian field by extrapolation of the large-scale power spectrum to the smaller, unresolved scales. The method was applied to COSMO model output to overcome the difficulty of comparability between model output on a 7 km grid and rain-gauge measurements as point observations. *Brussolo* et al. (2009) applied this method to large-scale ECMWF ensemble predictions, to generate ensemble members for a smaller-scale ensemble, which is computationally cheaper than to generate the ensemble-members

by dynamical downscaling as usually done.

Fuzzy rule based techniques were applied by *Bardossy* et al. (2002) (circulation pattern classification based on fuzzy rules) and *Bardossy* et al. (2005) (estimating of exceedance probabilities by fuzzy rules). A simple approach was investigated by *Salathe* (2002) where the coarse-scale precipitation was multiplied by a local scaling factor on the small-scale grid, trained by observations. Another disaggregation technique is provided by the so-called analog methods, where a large historical database is searched for a similar case and the small-scale information from this case is extracted and taken as prediction for the case under consideration (e.g. *Gutierrez* et al. (2004)). *Hewitson and Crane* (2006) developed an empirical downscaling based on categories derived by self-organizing maps (SOM) for daily precipitation in South Africa. The SOMs were used to characterize the atmospheric state in the surroundings of the target domain, based on 700 hPa and surface quantities. In a next step a precipitation value is drawn from a PDF from observations associated with the respective atmospheric state. Other stochastic downscaling approaches for rainfall-disaggregation can be found in *Rebora* et al. (2006) (nonlinear filtering of the output of a linear autoregressive model) and *Früh* et al. (2006) (applying a local scaling factor derived from an observed climatology).

A comprehensive overview of many downscaling techniques can be found in *Benestad* et al. (2008).

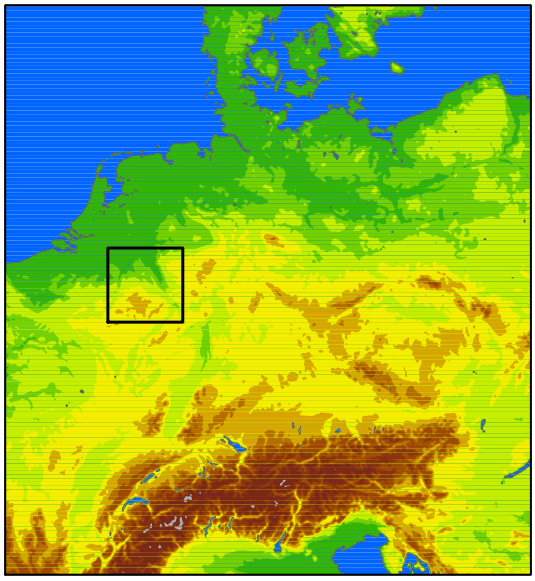

Figure 4.1.: Model domain of the standard COSMO-DE model configuration with 2.8 km grid spacing. The model domain for the small-scale model runs with 400 m grid spacing is indicated by the square.

4.2. Model setup for the 400 m COSMO simulations

The atmospheric disaggregation system has been developed based on high resolution COSMO model output with 400 m horizontal grid spacing. Since this resolution is much higher than the highest operationally used resolution of 2.8 km at DWD, an appropriate setup and a set of external parameters containing information on the surface characteristics had to be prepared. The chosen configurations and the external data sets are described in this section.

4.2.1. Model domain

The model domain (covering 168 x 168 km^2) is centred over the catchments of the two small rivers Rur and Erft in western Germany. Both rivers originate in the Eifel, a low mountain range. This region has been chosen since it is the main investigation area of the Transregio Collaborative Research Centre 32, in the framework of which most parts of this work has been carried out. Parts of Luxembourg, the Netherlands and Belgium are also covered by the model domain, which contains both mountainous regions as well as flat agricultural and urban parts. Hence a broad range of typical landscape characteristics is covered. Using 400 m resolution this area comprises 420x420 grid points, causing high computation time demands. However, for the 2.8 km resolution the number decreases to 60x60 gridpoints, which is about the minimum needed for a free model run which shall not be constrained too much by the boundary conditions. In Figure 4.1 the model domain of the driving model COSMO-DE and the area of the small-scale model runs are depicted.

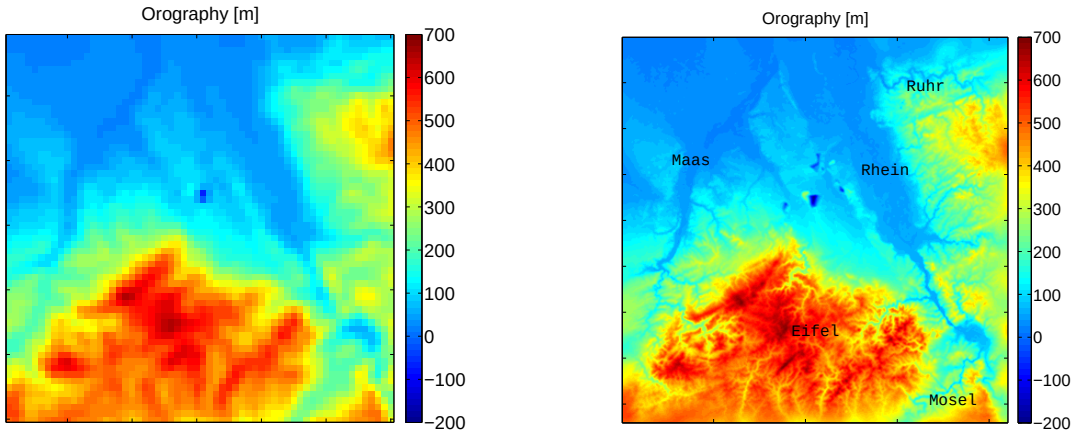

Figure 4.2.: Orographic heights for the 2.8 km (left) and 400 m (right) resolution. The depression in the centre of the domain is the opencast pit Hambach.

4.2.2. Surface parameters

The model needs a preprocessed data set of surface parameters, which contains information on the constant characteristics of the surface (see section 2.5.7). For the operationally used resolutions of 7 km or 2.8 km a data set ready to use can be obtained from the German Weather Service. For higher resolutions this data set has to be prepared. The data was transformed and rotated to the desired resolution and coordinate system respectively. Several parameters were derived from the three so-called primary data of orography, land cover and soil texture (section 2).

In the following the three primary data sets used for the derivation of the external parameters for the 400 m grid spacing are described.

Orography

For orographic height information the SRTM (Shuttle Radar Topography Mission, *Farr* et al., 2007) data are used. These are remote sensing data which have been collected in the year 2000 for the compilation of a digital terrain model. The data with a 90 m resolution were averaged to 400 m resolution. In Figure 4.2 the orographic height on the 2.8 km grid and the 400 m grid are shown. Most parts of the Eifel are covered by the model domain, as well as the foothills of the Bergisches Land in the East. In the 20 km wide boundary range at the lateral edges of the model domain the orography is slightly smoothed in order to guarantee a smooth transition to the coarse boundary forcing by matching the elevations from the surrounding coarser grid. In this work, only the inner domain is evaluated in order to avoid artificial non-realistic results near the boundaries.

Land cover

For the land use characteristics the CORINE data set (*EEA*, 2000) has been used. This data set is available on a 100 m resolution, and based on 44 land use classes. The dominating classes in the area under consideration are different kinds of forests (29%), non-irrigated arable land (22%), pastures (14%), discontinuous urban fabric (13%) and com-

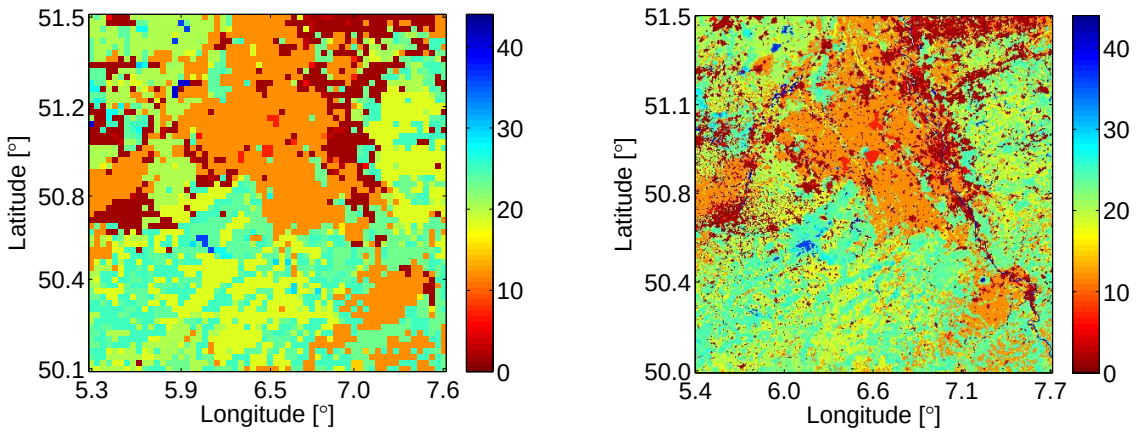

Figure 4.3.: Land use on the 2.8 km (left) and 400 m (right) resolution. The numbers correspond to the 44 different CORINE land cover classes. These are discontinuous urban fabric (dark red), non-irrigated arable land (orange), pastures and complex cultivation patterns (light green), different kinds of forests (turquoise green) and water (dark blue).

plex cultivation patterns (11%) (Figure 4.3). Vegetation characteristics such as plant cover and leaf area index have been determined by the use of lookup tables from these land use categories. The roughness length is a combination of the roughness length estimated from land use and subgrid-scale orographic information.

Soil type

Information on soil texture was obtained by merging data sets from North Rhine-Westphalia (IS BK50) and Rhineland-Palatinate (BÜK200) because in Germany such data sets are produced by the different federal lands separately. The different soil type classes in the two data sets had to be mapped onto the soil categories used in the COSMO-model. For the western parts of the model domain, which cover parts of the Netherlands, Belgium and Luxembourg, no small-scale soil information was available, thus here the coarse information used by the DWD, i.e. the FAO/UNESCO Soil Map of the World was adopted. The largest parts of the model domain can be characterized by soil class number 5 which is loam, followed by sand and sandy loam (Fig. 4.4).

Data preparation procedure

The primary data sets described above were projected onto the designated grid and transformed to model-relevant parameters. As a first step the land cover data, which was obtained in 100 m resolution, was upscaled to 400 m resolution according to the dominant land cover class. From this subgrid information, fraction of land (vs fraction of water) and fractions of evergreen and deciduous forest were calculated. The maximal and minimal values for leaf area index and fraction of plant cover and also the root depth were obtained from look-up-tables from the CORINE land use classes. Look-up-tables for the different soil texture dependent parameters such as field capacity, pore volume, plant wilting point

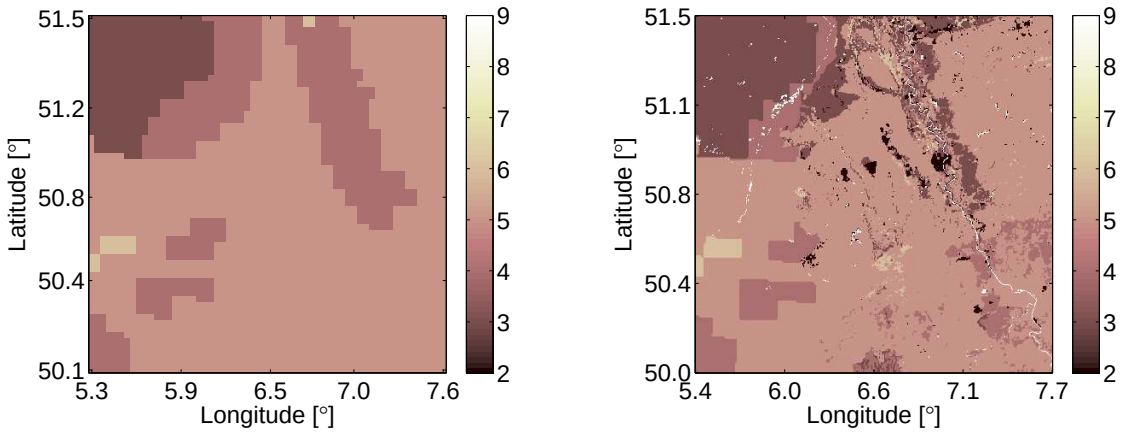

Figure 4.4.: Soil texture as operationally used from the FAO data set (left) and as merged from different data sets for the 400 m model simulations (right). The numbers correspond to the following classes: 2-rock, 3-sand, 4-sandy loam, 5-loam, 6-clay-loam, 7-clay, 8-peat, 9-water.

etc. are coded in the COSMO model. At the 400 m resolution broad rivers like the Rhine can be resolved as connected water pixels. Water pixels require the attribution of water temperature. Here the mean annual cycle of Rhine water temperatures as measured near Karlsruhe has been adopted.

4.2.3. Initialization

For the initialization and boundary forcing COSMO-DE (Δx=2.8 km) analyses are used. A broad relaxation zone at the lateral boundaries of 20 km which corresponds to 50 grid boxes has been chosen. For the majority of variables the smooth initialization state interpolated from the analysis becomes heterogeneous after some timesteps, usually in considerably less than one hour, except for soil moisture, which is a slowly changing variable. For adding variability at the 400 m grid scale, a histogram matching according to the soil type has been implemented as an intermediate step. To this end the soil moisture values belonging to a certain soil type from the coarse soil type field were matched to the new, small-scale soil type distribution. Thereby more small-scale variability is generated (see Fig. 4.5), which leads to more realistic statistics of the soil moisture, the field however is still too smooth. For soil temperature no additional steps have to be undertaken; here the small-scale structures are generated by the model in a short time range, even in deeper soil level (Figure 4.6).

4.2.4. Model configuration

For the grid scale of 400 m some default settings had to be altered. Most adaptions to the smaller scale relate to the physical parameterization settings and are described below. The vertical grid spacing has not been altered compared to the standard setup. The time step had to be adjusted from 25 to 4 seconds in order to obey the Courant-Friedrich-Levy (CFL) stability criterion for the slow dynamical processes. This high time-stepping

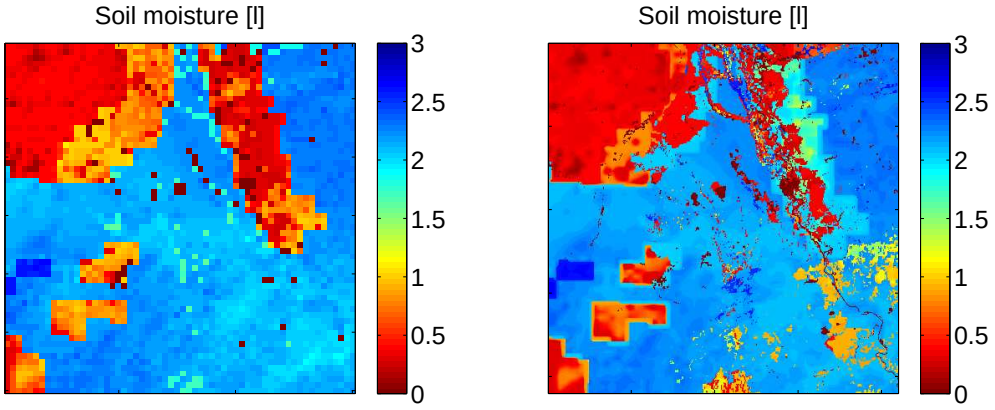

Figure 4.5.: Analysis of soil moisture, before (left) and after (right) interpolation and histogram matching depending on soil type at the 400 m grid. The coarse patterns in the western parts are due to the lack of fine-scale soil information in those regions, refer to Figure 4.4.

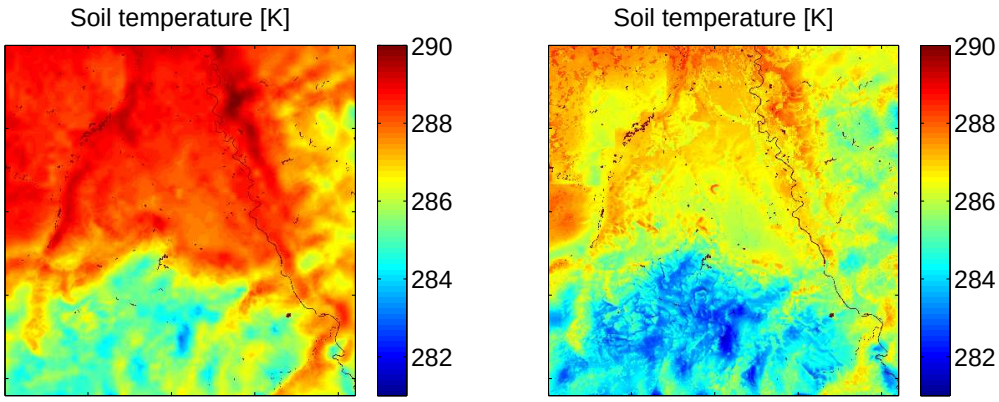

Figure 4.6.: Soil temperature of soil level four (layer between 9 and 27 cm depth) at initialization time (interpolated from coarse analysis field) and after two hours of simulation.

frequency and the large number of grid cells lead to a considerable increase in computation time. For 12 hours of forecast 8 hours computation time are needed using 48 processors of a linux cluster, whereas for a 2.8 km simulation for the same model domain only takes a few minutes.

Turbulence

The turbulence parameterization is usually developed for a certain scale and generally the underlying assumptions are not valid for application at any arbitrary scale range. Usually, the horizontal grid spacing Δx is large in comparison to the vertical grid spacing Δz, allowing the assumption that the vertical turbulent exchange is much larger than the horizontal turbulent exchange. This leads to the common simplification of neglecting the horizontal exchange coefficients. However, this approach becomes questionable at small horizontal scales of some hundred metres.

Several turbulence options are implemented in the COSMO model. The choice which one to use at the 400 m grid resolution is not straightforward. The default turbulence scheme is the prognostic TKE scheme based on a closure of order 2.5 (see section 2.5.5). Turbulent horizontal exchange is achieved by additional numerical, i.e. artificial, diffusion.

Another option is a scheme which has been developed for a very high resolution version of the COSMO model on 100 m horizontal grid spacing, the LLM (LITFASS Lokal Modell *Herzog* et al., 2002). This scheme considers also horizontal turbulent exchange by parameterizing the horizontal exchange coefficients based on the vertical coefficients, i.e. scaling the vertical coefficients by the horizontal grid spacing (see section 2.5.5).

In Figure 4.7 model results of 400 m COSMO runs with the different turbulent options (standard TKE scheme, TKE scheme with numerical diffusion and the 3D LLM scheme) are compared with temperature measurements from the meteorological tower in Jülich for August 19, 2007. Temperatures in the lowest atmospheric model layer, i.e. 10 m height, are compared with temperatures from the tower measured in 2 m and 20 m height and vertically interpolated to obtain the temperature in 10 m. From the time series no conclusion concerning the optimal turbulence option can be drawn. The autocorrelations (Fig. 4.7 bottom) are well represented by all three model configurations for time lags of less than 1.5 hours. All three schemes overestimate the temporal correlations for longer time lags, this overestimation is worst for the standard TKE scheme, and less pronounced for the 3D-turbulence scheme and the TKE-scheme with diffusion.

Based on the following pragmatic considerations the LLM-3D scheme has been chosen to be used for the 400 m model runs for building the training data set:

- The isotropic three-dimensional turbulence of the LLM-scheme with a Smagorinsky-type closure is a more physical approach for horizontal diffusion, than to employ the standard TKE scheme with numerical horizontal diffusion.

- The LLM scheme has been developed specifically for these high resolutions; the length scale is a function of the grid spacing, hence the scheme is adjusted automatically to the chosen resolution

- The TKE scheme has several tuning parameters (maximum turbulent length scale, pattern length etc.) and no specification how to adopt these for higher resolutions is available.

- There are known problems with the TKE-scheme on high resolution applications (too high vertical velocities, too high energy on small scales, bad energy conservation) while the LLM turbulence scheme performs well in these cases, with plausible spectra and vertical velocities and also a sufficient energy conservation (Ulrich Blahak (formerly IMK[2], now DWD), personal communication).

However, during the validation of the downscaling it became clear, that it is necessary to use the same turbulence scheme for the coarse model runs on 2.8 km resolution as for the small-scale model runs on 400 m resolution, which are used as reference to evaluate the performance of the downscaling and mosaic. If different turbulence schemes are used for

[2]Institut für Meteorologie und Klimaforschung Karlsruhe

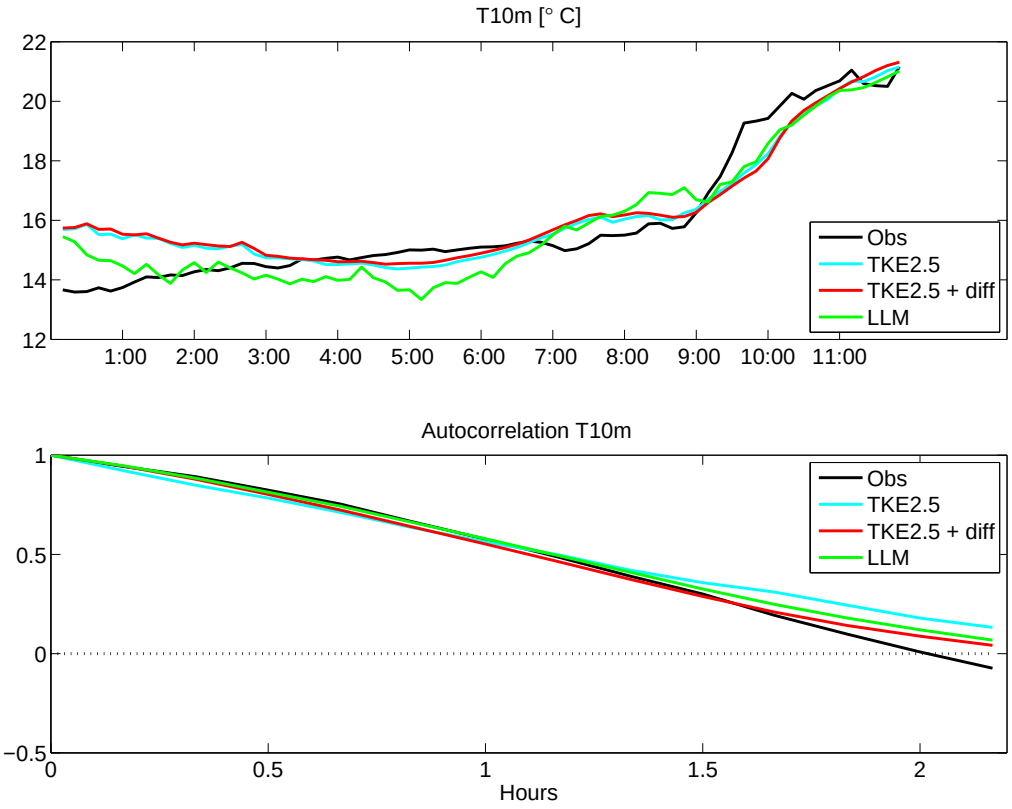

Figure 4.7.: Time series of 10 m temperatures measured and modelled with different turbulence parameterizations (top), and the corresponding autocorrelations (bottom). The measurements and the model output are both 10-minute averages.

these two different scales, the near-surface temperature during clear-sky radiation nights can have very different values. In Figure 4.8 the temperature of the lowest layer of a COSMO model run for May 12, 2008 is shown for 3:00 UTC (top) and 15:00 (bottom), respectively, for a coarse model run, the COSMO-DE analysis for the model domain, and the results for a model run on 400 m horizontal resolution. During night the temperatures are much lower for the high resolution model run with the LLM-turbulence scheme. Other variables do not show these differences (not shown). For 15:00 UTC in the afternoon the results for the different settings are comparable (Fig. 4.8, bottom).

Thus it is important to use the same turbulence schemes for the different resolutions, to avoid these large differences during clear-sky radiation nights as shown in Figure 4.8 and to be able to compare the different model simulations. However, the LLM scheme has not been developed for resolutions of the order of 1 km or more, where large parts of the turbulent motions take place on the subgrid-scale. An alternative which gives reasonable results in terms of vertical velocities and energy conservation is to use the standard TKE schemes, but with additional horizontal turbulent exchange, by using the vertical gradients also for the horizontal diffusion. In Figure 4.9 the fine-scale temperature field for 3:00 UTC for a high-resolution model run with the LLM-turbulence scheme and the TKE scheme with threedimensional turbulence is shown for direct comparison. Especially in some valleys of the Eifel low mountain range the temperatures are much lower when the

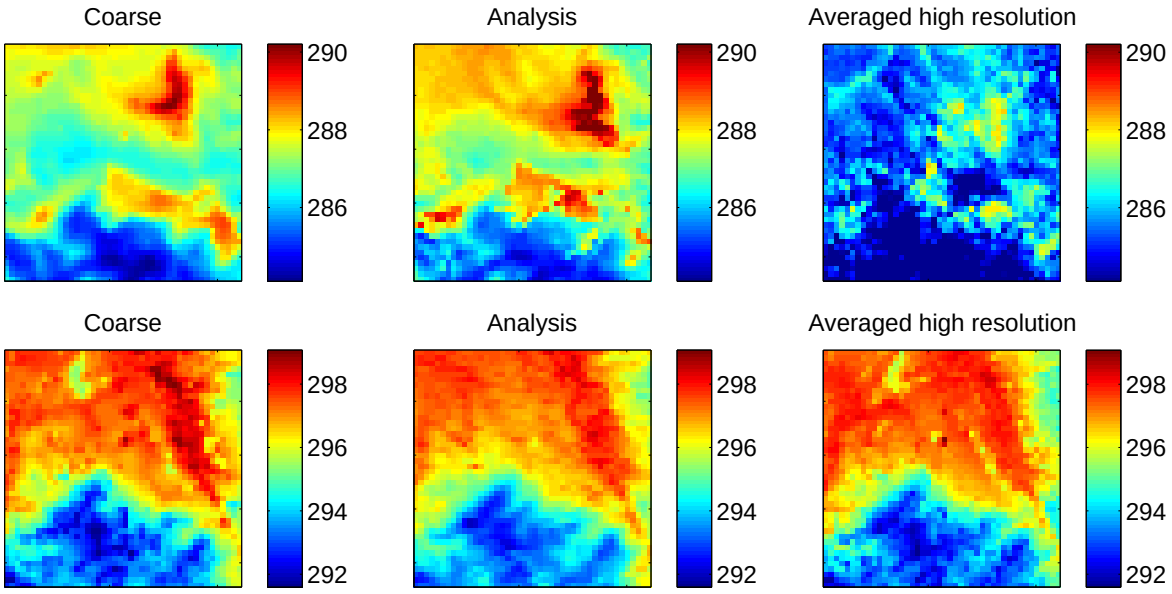

Figure 4.8.: Temperature [K] of lowest COSMO model layer, left: a 2.8 km model run with standard TKE scheme, middle: the COSMO-DE analysis, right: for a 400 m model run with the LLM-turbulence scheme, results averaged to 2.8 km. The top row shows the results for 3:00 UTC at night, the lower row depicts the same for 15:00 UTC in the afternoon. The model run was initialized at 0:00.

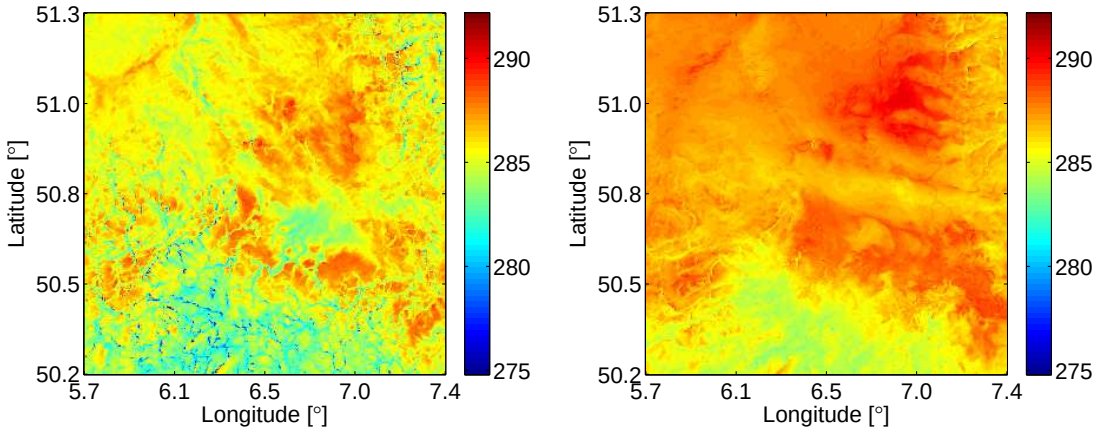

Figure 4.9.: Temperature of lowest COSMO layer for 3:00 UTC on May 12, 2008. Left: LLM turbulence option. Right: Standard TKE turbulence, but with threedimensional turbulent exchange.

LLM turbulence option is used.

In Figure 4.10 (top) the difference between the two temperature fields for the LLM scheme and the TKE scheme is depicted for 3:00 UTC (left) and 15:00 UTC (right). In the afternoon the differences are negligible, in contrast to the high differences at night. The differences are correlated with the differences in the transfer coefficient, also shown in

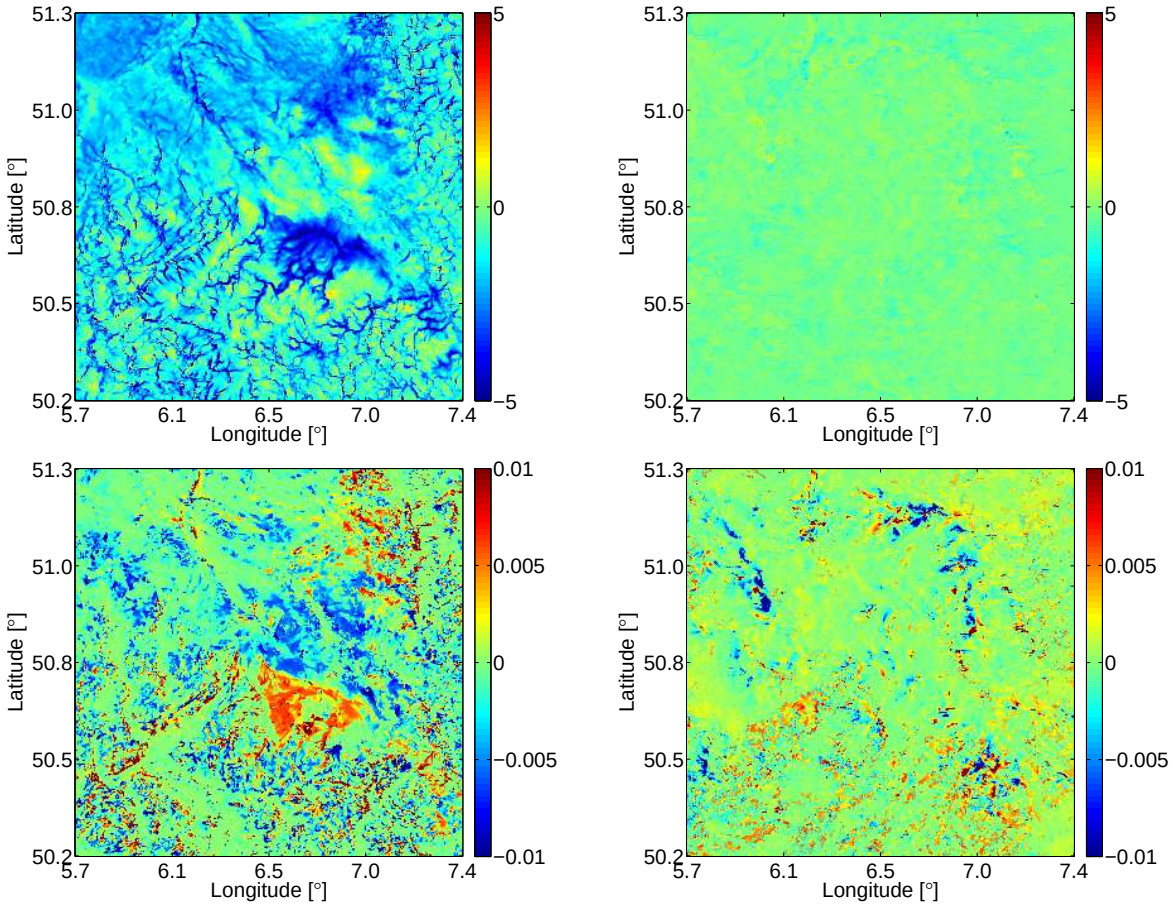

Figure 4.10.: Top: Differences in temperature for May 12, 2008, 3:00 (left) and 15:00 (right) UTC, LLM scheme minus TKE scheme. Bottom: the same for the transfer coefficient.

Figure 4.10 (bottom): in regions where the transfer coefficient is higher, the temperature is lower probably due to the stronger mixing in a stable atmosphere. The question arises, which of these two scenarios is more realistic.

A more detailed investigation of these differences should be carried out for more case studies, by making use of observations of stations located in complex terrain. Satellite measurements might provide additional information. The influence of the different tuning parameters in the TKE turbulence scheme should be analyzed by sensitivity analyses. For this work this issue could not be investigated in more detail. For the evaluation of the downscaling implemented in the COSMO model, all model runs have been carried out with the TKE turbulence scheme (with the the 3D-turbulence option, used for the high-resolution model runs) because this schemes is applicable for both scales and gives similar results. An additional argument for this scheme is, that the results resemble the analyses much more closely, which indicates a good performance, considering the analyses as “pseudo”-measurements.

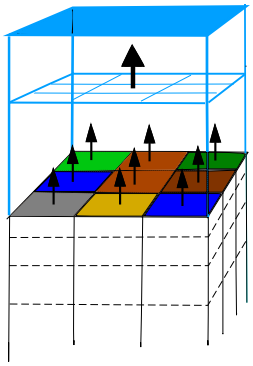

Figure 4.11.: Concept of the mosaic approach including atmospheric downscaling. The fluxes are computed separately for each subgrid pixel, and then averaged. The downscaling acts as a small-scale interface to the high-resolution SVAT model.

Radiation

Clouds can cross several 400 m grid boxes in a few minutes, thus a higher temporal frequency of radiation calculations is necessary. For consistency reasons for the development of the downscaling system, radiation computations are carried out on each atmospheric column in all COSMO simulations. No averaging as in the COSMO-DE default setup is carried out. The interval between two radiation calculations has been set to 3 minutes, which again leads to a significant increase in computation time due to the complexity of the radiation calculations.

4.2.5. The mosaic approach

In the mosaic approach (*Seth* et al., 1994), surface heterogeneities are accounted for by running the soil module, in this case TERRA, on an explicit higher resolution than the atmospheric part (Figure 4.11). The turbulent fluxes of latent and sensible heat needed by the atmospheric model on the coarser atmospheric scale are obtained by averaging. The novel disaggregation scheme of the coarse atmospheric forcing data down to the resolution of the soil module as developed in this work is described in section 4.3.

4.2.6. Data

Training data set

Eight high-resolution coupled model runs for different weather situations (Table 4.1) have been carried out to build a high-resolution data base for the downscaling scheme. The first two hours of each model run were discarded to remove spin-up effects. Days with calm, clear-sky weather, days with unstable convective situations and days with strong synoptic forcing were chosen to cover the dominant weather situations. Cases with homogeneous stratiform cloud cover are included, as well as cases with fast moving clouds under stormy conditions.

Table 4.1.: Overview of simulated days including prevailing weather situation.

Date	Weather situation
Training	
27 August 2007	varying cloud cover, no precipitation
14/15 October 2007	clear sky
3 March 2008	strong winds, variable clouds and precipitation
1/2 May 2008	clouds and precipitation
9/10 May 2008	clear sky
8 June 2008	convective clouds and precipitation
21 July 2008	synoptically driven stratiform rainfall
28 August 2008	cloudy, some rain
Validation	
12 May 2008	calm, only sparse cloud cover
15 May 2008	convective clouds, showers and thunderstorms
16 July 2008	stratiform rain
20 October 2009	cirrus clouds, no rain
21 October 2009	some clouds
26 January 2010	fog in the morning, clear sky later

Validation data: Case studies

The downscaling scheme has been validated offline by applying it to COSMO output and comparing the results to high-resolution reference output. For this purpose three days with very different weather types (see also Table 4.1) have been chosen: May 12, 2008 was characterized by very calm weather conditions. Central Europe was under the influence of a stable high pressure system for several days. Precipitation was absent and only few clouds were observed. During May 15, 2008, Central Europe was under the influence of several low pressure systems situated over the Atlantic ocean and northern Europe. The high pressure system was weakening and moved to south-eastern Europe. Under these rather unstable conditions the model domain was almost completely covered by convective clouds during the whole day, including showers and thunderstorms. On July 16, 2008 a low pressure system over the northern Atlantic influenced the weather conditions in Central Europe, with a cold front crossing Northern Germany during the day. The strong synoptical forcing led to stratiform rainfall and homogeneous cloud cover over the model domain.

For the "online" validation, i.e. the evaluation of the fully coupled mosaic-downscaling simulations, three additional days with calm weather have been simulated (the last three days in Table 4.1), because for calm days the effect of subgrid-scale heterogeneity is more visible and more important than for advective, synoptically forced days.

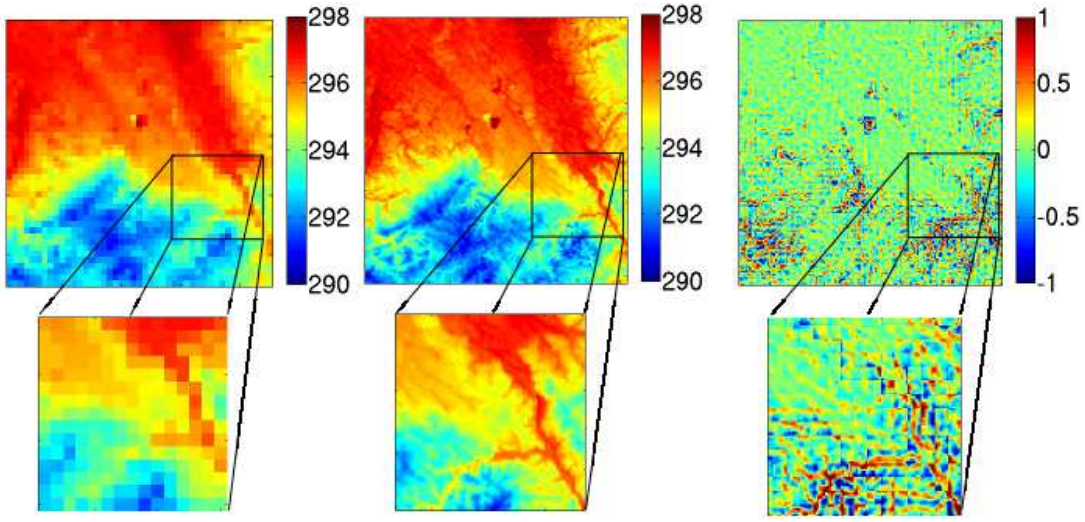

Figure 4.12.: Temperature at the lowest atmospheric model level on 9 May, 2008 at 12:00 UTC in Kelvin at 2.8 km resolution (left), 400 m resolution (middle) and the anomalies, i.e. the differences between both (right).

Table 4.2.: Downscaled variables

Variable	Abbreviation
Temperature at lowest model layer	T
Specific humidity at lowest model layer	q^v
Wind speed at lowest model layer	$\|\mathbf{v}_h\|$
Shortwave net radiation flux at surface	S_{net}
Longwave net radiation flux at surface	L_{net}
Precipitation (rain, snow, graupel)	$PREC$
Surface pressure	PS

4.3. The downscaling approach

Stepwise downscaling approach

A downscaling scheme should recover as good as possible the original fine-scale field (400 m grid spacing, for an example temperature field see Fig. 4.12, middle) from the coarse field (2.8 km grid spacing, Fig. 4.12, left). This is equivalent to predicting the anomalies (Fig. 4.12, right) based on the coarse atmosphere resolution and the high-resolution land surface information. For training and development of the downscaling scheme these anomalies were obtained by averaging the high-resolution model output to the 2.8 km scale, and subtracting these coarse values from the original 400 m model output. Downscaling is necessary for those atmospheric variables which are needed as input for a SVAT model (in our case TERRA) or hydrological models, which are usually driven by the same variables as a SVAT model (see Table 4.2).

The disaggregation system comprises three steps, which can be applied individually or subsequently, depending on the variable and the application under consideration. The

first step interpolates the coarse resolution to the fine resolution by bi-quadratic splines in x- and y-direction, while conserving mean and gradients of the coarse field. The second step exploits empirical relations between atmospheric variables and surface variables using high-resolution surface information ("deterministic" downscaling rules). The third step adds the still missing high-resolution variability by adding noise. Thus downscaling steps 1 and 2 reconstruct the high-resolution fields as accurately as possible, and step 3 replenishes the mostly too low small-scale variability up to the variability of the high-resolution simulations. Since step 3 will usually increase the error, a decision between low errors (apply only downscaling step 1 and 2) or a realistic small-scale variance (apply also step 3) has to be made. These steps are explained in detail in the following (as published in *Schomburg* et al., 2010)

4.3.1. Step 1: Spline interpolation

The average conserving bi-quadratic spline equation used in the first step

$$f(x, y) = a_1 + a_2 x + a_3 y + a_4 x^2 + a_5 y^2 \tag{4.2}$$

requires five unknown coefficients for every coarse pixel. Thus five constraints have to be formulated. Four constraints are provided by the derivatives of equation 4.2 at the edges between the coarse pixels, which are set to be equal to the derivative of the coarse field perpendicular to the edges. The conservation of the mean value serves as the fifth constraint.

4.3.2. Step 2: Deterministic downscaling rules

The second step tries to recover the difference between the spline interpolated field and the original high-resolution field with deterministic rules. For these rules high-resolution surface information is used as predictor based on linear regression.

Some variables can be downscaled by exploiting known physical relationships. By this means the surface pressure anomaly can be downscaled by using the relief height anomaly Δz in the hydrostatic equation

$$\Delta p = -\rho g \Delta z. \tag{4.3}$$

For simplicity a constant air density has been assumed, in a least-squares fit ρ=1.19 kgm^{-3} gave the best results.

The shortwave net radiation at the surface can be split up into

$$S_{net} = S_{dir}\downarrow + S_{dif}\downarrow - S_{dif}\uparrow \tag{4.4}$$

with $S_{dir}\downarrow$ the incoming direct radiation from the sun, $S_{dif}\downarrow$ the diffuse downwelling radiation and $S_{dif}\uparrow$ the reflected diffuse upwelling radiation. The downscaled diffuse upwelling radiation can be obtained from the high-resolution surface albedo for direct and diffuse light, α_{dir} and α_{dif}, via

$$S_{dif}\uparrow = \alpha_{dir} S_{dir}\downarrow + \alpha_{dif} S_{dif}\downarrow . \tag{4.5}$$

The downwelling direct and diffuse radiation are not correlated with surface variables. Both have little subgrid heterogeneity in cloud free cases (the average subgrid-scale standard deviation is 2 Wm^{-2}), while in cloudy situations their subgrid-scale variability relates to cloud cover variability on the subgrid-scale (the average subgrid-scale standard deviation is 39 Wm^{-2}). Thus, in rather homogeneous cloudfree conditions the shortwave net radiation can be disaggregated with near perfect correlation because all subgrid variability is associated with surface (albedo) variability. Under cloudy conditions the variability has to be induced by stochastic methods (in step 3).

For the remaining variables (temperature, humidity, wind speed, precipitation and longwave radiation) the situation is less intuitive. Thus the high-resolution data base was statistically evaluated for possible correlations between atmospheric and surface variables. However, usually such correlations are not generally valid, but depend on the prevailing weather conditions. Figure 4.13 depicts the spatially averaged correlation between the temperature anomalies of the lowest atmospheric model layer and the topographic height anomalies (both with respect to the 2.8 km scale) for a clear sky day. Correlations are close to minus one during the day, as one would expect for a well mixed boundary layer. The stratification leads to a simple decrease of temperature with topographic height, which can be exploited for the disaggregation of the high-resolution atmospheric near-surface temperature anomalies. During clear-sky nights, however, when outgoing longwave radiation leads to strong cooling of the ground, no or only a slightly positive correlation between temperature and elevation exists. Nighttime inversions and complex valley circulations destroy any usable statistical predictions. Thus prior to the use of the orographic high-resolution surface information as predictor for near surface temperatures, the temperature gradient of the lower atmosphere is computed and a decision made, based on its closeness to adiabatic stratification (see Fig. 4.13, bottom). For illustration the correlations without and with application of the temperature gradient as indicator are shown as scatterplots in Figure 4.14. The statistical correlation between temperature and relief anomalies is very low for the complete data base (Fig. 4.14a); using the coarse-resolution temperature gradient as pre-selection criterion, however, a strong negative correlation exists (Fig. 4.14b).

To find the most suitable predictors, indicators and thresholds, an automatic rule detection system has been developed. In this system the correlations between all possible predictors and the desired downscaled variables are calculated, based on indicators, which might allow or disallow the rule. The corresponding indicator thresholds are varied between the minimum and maximum value found in the data base for each possible indicator variable in 30 steps. For 5 predictands, 16 possible predictors, 24 possible indicators, (see Table 4.3 for a list of all provided predictors and indicators), 30 indicator-range intervals, and the whole procedure performed 2 times (testing for situations where the indicator is larger or smaller than the threshold, respectively), a total of 5*16*24*30*2=115,200 correlations were computed. The automatic rule search system is sketched in Figure 4.15. Only those rules are selected, which lead to correlation coefficients above 0.7, i.e. an explained variance of at least 50%. The final selection of a rule requires in addition, that the rule is applicable to at least 10% of the data. Table 4.4 contains all rules detected by this automatic search system. If several indicators were found describing similar situations, only the indicator applicable to the larger part of the data set is chosen. If more than

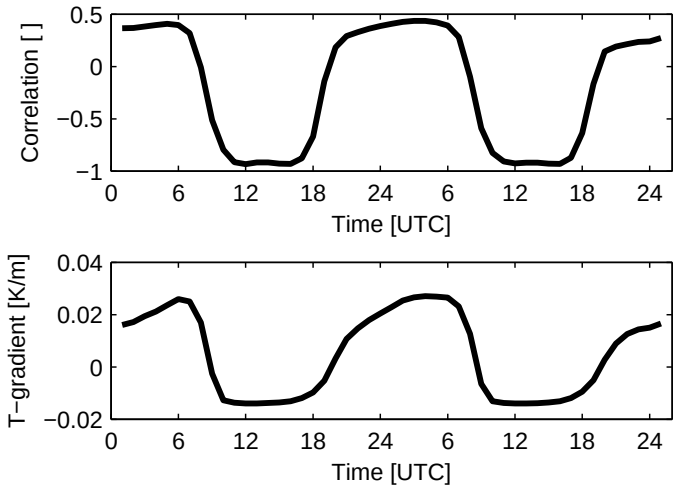

Figure 4.13.: Top: Correlations between temperature anomalies in 10 m and orographic anomalies with respect to the coarse pixel scale of 2.8 km for 9 May 2008, a clear sky radiation day. Bottom: mean coarse scale vertical temperature gradient of the lowest four model layers.

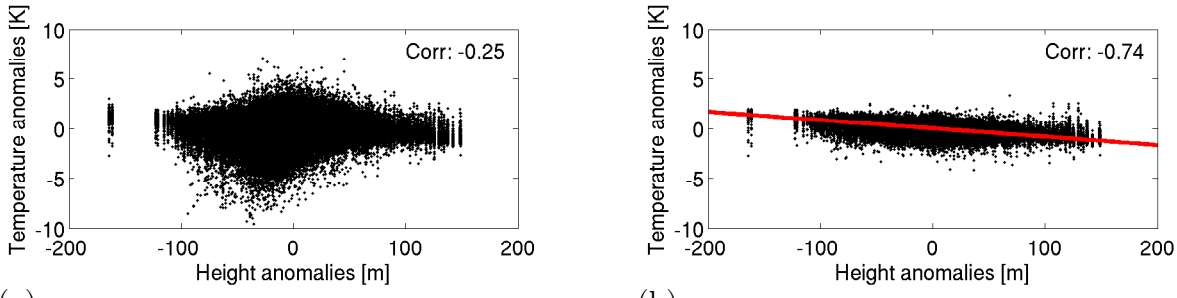

Figure 4.14.: Scatterplot of temperature anomalies versus orographic height anomalies with respect to the coarse pixel scale of 2.8 km. a) all cases. b) only where the coarse temperature gradient of the lowest 105 m is below a threshold of $0.0057\,\mathrm{Km}^{-1}$, with a linear fit.

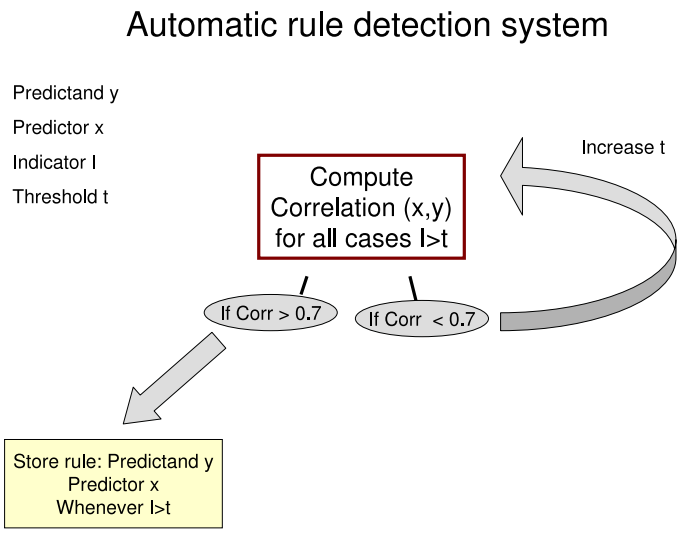

Figure 4.15.: The automatic rule search system: For all possible predictands y and predictors x the correlations for all cases in the data set larger (or smaller) than a certain threshold t of all possible indicators I are computed. If the correlation is larger than 0.7 this relationship is stored as a downscaling rule. If not the threshold is further increased (or decreased).

one predictor is found for the desired variable, its usefulness was evaluated by a stepwise regression. As a final step for each of the downscaled variables the coefficients needed for a linear regression between downscaling variable and predictors have been computed.

For the near surface temperature several rules have been found, indicating that this variable is closely related to relief height or temperature gradient multiplied with relief height, with the coarse temperature gradient as indicator. In the end only the rule using orographic information in situations indicated by the temperature gradient of the lowest 105 m was taken as a rule, because it covered the largest part of the data base (64%); using other predictors did not give substantial additional skill.

For specific humidity and wind speed no exploitable correlations with surface quantities have been found. Setting the desired correlation in the automatic search system to a lower value, i.e. 0.5 (instead of 0.7 as before), correlations between near surface humidity q^v and surface humidity q^v_{sfc} of 0.51 for 12% of the cases were found, detectable by the humidity gradient of the lowest two atmospheric layers. This rule has been discarded for the current setup due to the low correlation. Correlations between q^v and q^v_{sfc} can change strongly in short time periods, which might explain the difficulty to find useful rules for the specific humidity. In Figure 4.16 the subgrid correlations between q^v and q^v_{sfc} are shown for three consecutive hours of May 12, 2008. While at 6:00 UTC no systematic correlations are detectable, at 7.00 UTC the correlations are strongly positive on the north-western part of the model domain and anti-correlated in most regions. Only one hour later the correlations between q^v and q^v_{sfc} are close to one for almost the whole domain.

With the same criterion also a relationship between wind speed and sensible heat flux was found; this relationship was discarded, however, because of the dependency of the sensible heat flux on wind speed. Also averaging the near surface and the surface quantities over an hour did not lead to usable correlations for wind speed or specific humidity. The fields of q^v and $|\mathbf{v}_h|$ at the lowest atmospheric layer contain many transient small-

Table 4.3.: Possible predictors (available on high resolution) and indicators (coarse resolution) for the deterministic downscaling. The predictors gradients×orography are computed by using the coarse temperature gradient information (fine scale information is usually not available) and the fine scale surface information on the relief height.

Possible predictors		**Possible indicators**	
$\boldsymbol{T_G}$	Ground temperature [K]	$\boldsymbol{Tgr25}$	Temperature gradient of lowest 2 layers (25 meters) $[Km^{-1}]$
$\boldsymbol{H}$	Orography [m]	$\boldsymbol{Tgr60}$	Temperature gradient of lowest 3 layers (60 meters) $[Km^{-1}]$
$\boldsymbol{LAI}$	Leaf area index [1]	$\boldsymbol{Tgr105}$	Temperature gradient of lowest 4 layers (105 meters) $[Km^{-1}]$
$\boldsymbol{z_0}$	Roughness length [m]	$\boldsymbol{q^v gr25}$	Specific humidity gradient of lowest 2 layers (25 meters) $[m^{-1}]$
$\boldsymbol{ln(z/z_0)}$	Logarithmic roughness ratio between height of lowest model layer and roughness length [1]	$\boldsymbol{q^v gr60}$	Specific humidity gradient of lowest 3 layers (60 meters) $[m^{-1}]$
$\boldsymbol{q^v_{sfc}}$	Specific humidity at surface [kg/kg]	$\boldsymbol{q^v gr105}$	Specific humidity gradient of lowest 4 layers (105 meters) $[m^{-1}]$
$\boldsymbol{Tgr25 \times H}$	Temperature gradient of lowest 2 layers (25 meters) × orography $[K]$	$\boldsymbol{\mu}$	Cosine of solar zenith angle [1]
$\boldsymbol{Tgr60 \times H}$	Temperature gradient of lowest 3 layers (60 meters) × orography $[K]$	$\boldsymbol{LWP}$	Liquid water path $[kgm^{-2}]$
$\boldsymbol{Tgr105 \times H}$	Temperature gradient of lowest 4 layers (105 meters) × orography $[K]$	$\boldsymbol{LWP_{var}}$	LWP variance of 3x3 coarse pixels $[kg^2m^{-4}]$
$\boldsymbol{q^v gr25 \times H}$	Specific humidity gradient of lowest 2 layers (25 meters) × orography [1]	$\boldsymbol{ORO_{var}}$	Orography variance of 3x3 coarse pixels $[m^2]$
$\boldsymbol{q^v gr60 \times H}$	Specific humidity gradient of lowest 3 layers (60 meters) × orography [1]	$\boldsymbol{\lvert v_h \rvert}$	Wind speed [m/s]
$\boldsymbol{q^v gr105 \times H}$	Specific humidity gradient of lowest 4 layers (105 meters) × orography [1]	$\boldsymbol{DD}$	Wind direction [°]
$\boldsymbol{(F_h)_{sfc}}$	Sensible heat flux $[Wm^{-2}]$	$\boldsymbol{U}$	Near-surface u-wind component [m/s]
$\boldsymbol{(F_{q^v})_{sfc}}$	Latent heat flux $[Wm^{-2}]$	$\boldsymbol{V}$	Near-surface v-wind component [m/s]
$\boldsymbol{FR_{land}}$	Fraction of land [1]	$\boldsymbol{CLC}$	Cloud cover [%]
$\boldsymbol{W_{so}}$	Soil moisture of top soil layer [m H2O]	$\boldsymbol{CLC^2_{var}}$	Cloud cover variance of 3x3 coarse neighboring pixels [%]
		$\boldsymbol{q^v}$	Near-surface specific humidity [1]
		$\boldsymbol{RH}$	Near-surface relative humidity [1]
		$\boldsymbol{(q^v_{sfc})_{var}}$	Variance of 3x3 neighboring pixels of surface specific humidity [1]
		$\boldsymbol{S_{net}}$	Shortwave net radiation at surface $[Wm^{-2}]$
		$\boldsymbol{L_{net}}$	Longwave net radiation at surface $[Wm^{-2}]$
		$\boldsymbol{PS}$	Surface pressure [Pa]
		$\boldsymbol{PREC}$	Precipitation $[kgm^{-2}s^{-1}]$
		$\boldsymbol{FR_{land}}$	Fraction of land [1]

Table 4.4.: Deterministic downscaling rules found by the automatic rule search algorithm. Shown are relationships between the downscaling variables, i.e. the predictands, and possible predictors for indicators above or below a certain threshold of the indicator value. At least a correlation above 0.7 between predictor and predictand was necessary, and at least 10% of all cases of the data set needs to be covered by this rule. For abbreviations of the variables see Tables 4.2 and 4.3 and the list of symbols in the appendix B.

Predictand	**Predictor**	**Indicator with threshold**	**Correlation**	**Data coverage [%]**
$\boldsymbol{T}$	$Tgr105 * H$	$Tgr105 < 0.0022$	0.74	59
		$Tgr60 < 0.0037$	0.75	58
		$Tgr25 > 0.0065$	0.75	56
		$\lvert\mathbf{v}_h\rvert > 5.1$	0.71	12
		$LWP > 0.095$	0.71	10
		$U > 3.2$	0.71	17
		$S_{net} > 204$	0.81	29
	$Tgr60 * H$	$Tgr105 < 0.0022$	0.71	59
		$Tgr60 < 0.0037$	0.74	58
		$Tgr25 < 0.0065$	0.76	56
		$U > 3.7$	0.78	13
		$S_{net} > 204$	0.81	29
	$Tgr25 * H$	$Tgr105 < -0.0048$	0.82	47
		$Tgr60 < -0.00155$	0.78	52
		$Tgr25 < 0.0065$	0.72	56
		$S_{net} > 204$	0.78	29
	H	$Tgr105 < 0.0058$	-0.74	64
		$Tgr60 < 0.0090$	-0.73	64
		$Tgr25 > 0.0161$	-0.72	63
		$\mu > 0.82$	-0.7	17
		$\lvert\mathbf{v}_h\rvert > 4.0$	-0.76	23
		$LWP > 0.095$	-0.78	10
		$U > 3.2$	-0.78	17
		$S_{net} > 179$	-0.72	31
		$L_{net} > -15.224$	-0.7	17
$\boldsymbol{L_{net}}$	T_g	$clc < 43$	-0.72	38
		$L_{net} < -82.5$	-0.74	36

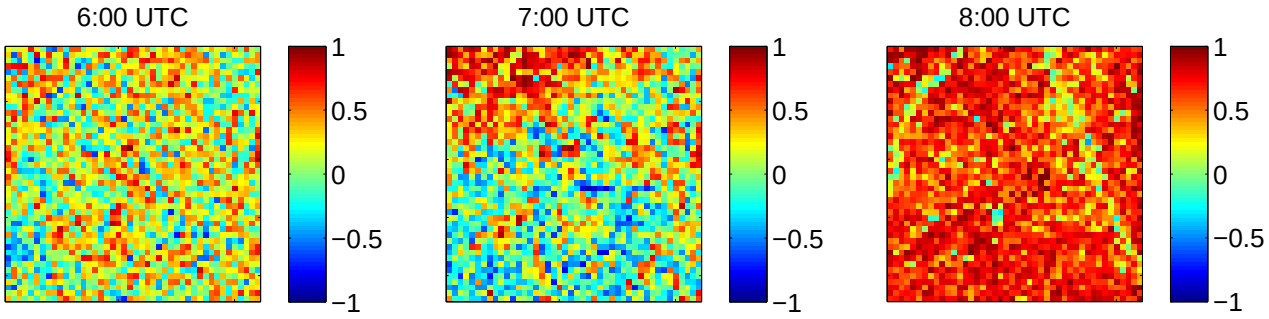

Figure 4.16.: Sub-grid-scale correlations between surface specific humidity and specific humidity of the lowest atmospheric layer for 6:00, 7:00 and 8:00 UTC on May 12, 2008.

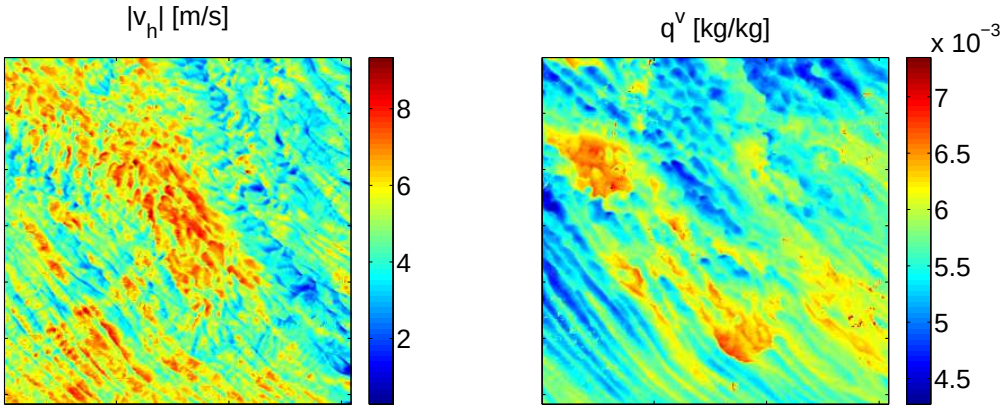

Figure 4.17.: Example field of a) wind speed and b) specific humidity of the lowest layer of the COSMO model, model output for 12:00 UTC on 9 May, 2008.

scale organized wave-like structures (for an example see Figure 4.17), indicating that these two variables are strongly dynamically driven, and thus determined by very small-scale dynamical processes. Simple statistical relationship rules with surface variables are not able to reconstruct this variability. A small cross-correlation between wind speed and specific humidity of 0.27 exists, indicating that both are partly driven by the same dynamical circulations.

The net longwave radiation L_{net} can be split up, into downward $L\downarrow$ and upward fluxes $L\uparrow$ according to

$$L_{net} = L\downarrow - L\uparrow = L\downarrow - (\alpha_{IR} L\downarrow + (1-\alpha_{IR})\sigma T_G^4) \tag{4.6}$$

with α_{IR} the infrared albedo, σ the Stefan-Boltzmann-constant and T_G the temperature of the emitting surface. We found that the ground temperature can be used to disaggregate the longwave net radiation when the cloud cover is below 43% or the longwave net radiation L_{net} is less than -82.5 Wm^{-2}. Both indicators cover about the same situations. This indicates that in cloudy cases the longwave downwelling radiation anomalies are mainly determined by clouds and less by the emitted radiation from the surface, while in cloud-

Table 4.5.: Deterministic rules with the respective regression coefficients, correlations achieved and amount of data covered.

Downscaling variable	**Predictor**	**Constraint**	**Regression coefficient**	**Correlation**	**Data coverage**
T	H	Tgr105<0.0058	-0.0084 Km^{-1}	0.74	64%
L_{net}	T_G	L_{net}<-82.5	-3.878 $Wm^{-2}K^{-1}$	0.74	36%
PS	H	-	-11.694 $Pa\,m^{-1}$	1.0	100%

free situations the longwave emission from the surface is the only source of heterogeneity.

As expected for these small scales no rules have been found for precipitation. In Table 4.5 the regression coefficients, correlation achieved and data coverage for the rules found by the automatic rule detection system are listed. The regression coefficients are based on the same data base as was used for the rule detection system (see Table 4.1).

4.3.3. Step 3: Noise generation

Except for surface pressure the downscaling steps 1 and 2 alone do not reproduce all small-scale variability contained in the simulated high-resolution fields. The full variance is, however, important for modeling the nonlinear processes at the surface. Lower variabilities can lead to biases in the computed fluxes when averaged over larger spatial and temporal scales. To avoid these biases, the yet unresolved variance is added as noise, at the expense of a higher error at the smallest scale. This third step is applied after carrying out the first two downscaling steps, or, for the variables for which no deterministic relationship can be found, directly after step 1.

Estimating the small-scale variance

In Figure 4.18 the subgrid-scale variances for temperature for different hours of the day are shown, for a clear-sky radiation day (top) and a day with stratiform homogeneous cloud cover (bottom). The subgrid variance under clear-sky conditions is larger during night than during mid-day and under stratiform synoptically driven conditions. This shows that before adding the missing small-scale variability, this missing variability first needs to be assessed, as it may vary considerably for different synoptic conditions and also for different variables.

A stepwise multiple linear regression system has been developed, which estimates the small-scale standard deviation based on the coarse-scale standard deviation of the surrounding 3x3 coarse pixels and other atmospheric variables, which serve as a measure for the atmospheric conditions. For each variable variance different predictors have been chosen by the stepwise regression (Table 4.6). For completeness the exact regression equations are given:

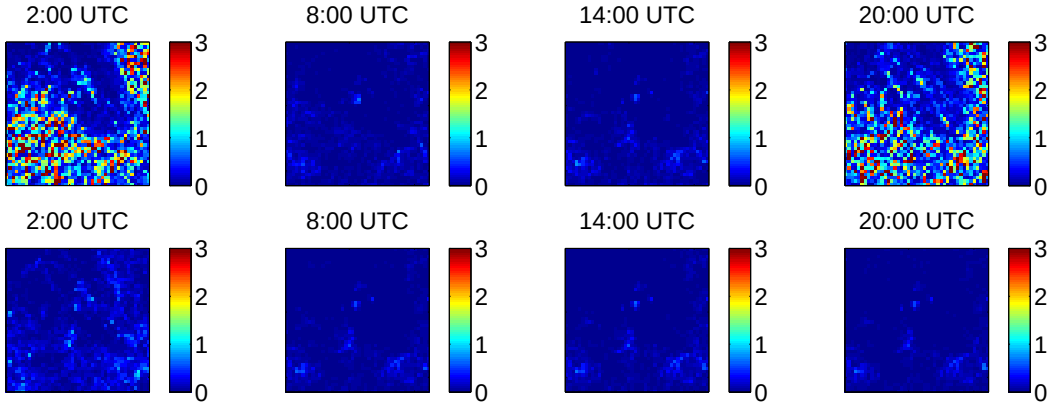

Figure 4.18.: Subgrid-scale variance for temperature (in Kelvin) per coarse pixel for a fair-weather day (9 May, 2008, top) and a day with stratiform cloud cover (21 July, 2008, bottom) for different hours of the day.

Table 4.6.: Predictors for estimating the standard deviation (stddev) at the small scale.

Downscaling variable	**Predictors**
T	Tgr25, 3x3 coarse stddev, PS
q^v	3x3 coarse stddev
$\|\mathbf{v}_h\|$	3x3 coarse stddev, PS
S_{net}	3x3 coarse stddev
L_{net}	3x3 coarse stddev, subgrid stddev of q^v_{sfc}

$$
\begin{aligned}
\sigma_T &= 4.3255 * Tgr25 + 0.5026 * \sigma_c^{3x3} - 1.5497 \cdot 10^{-5} * PS + 1.6125 \\
\sigma_{|\mathbf{v}_h|} &= 0.7762 * \sigma_c^{3x3} - 4.2692 \cdot 10^{-5} * PS + 4.5029 \\
\sigma_{q^v} &= 0.7076 * \sigma_c^{3x3} + 1.2202 \cdot 10^{-5} \\
\sigma_{S_{net}} &= 0.8882 * \sigma_c^{3x3} + 4.2606 \\
\sigma_{L_{net}} &= 0.7 * \sigma_c^{3x3} + \sigma_{qvs}.
\end{aligned}
$$

σ_c^{3x3} is the standard deviation of the respective variable of the 3x3 surrounding grid boxes, and σ_{qvs} is the subgrid-scale standard-deviation of surface specific humidity.

For variables for which downscaling step 2 has been applied, the variance generated by step 2 is subtracted from the estimated value from the regression to add only the still missing variance.

Algorithm for noise generation

The noise is modeled based on an autoregressive process, to account for its temporally correlated nature.

$$x_{new} = \phi x_{old} + \epsilon \tag{4.7}$$

where ϵ is a Gaussian noise term. The correlated noise has a zero mean value, because only the anomalies are reconstructed. To compute the intermediary autoregression noise term x_{new} with a standard deviation of unity, the standard deviation of ϵ is computed according to:

$$\sigma_\epsilon = \sqrt{1 - \phi^2}; \tag{4.8}$$

The autoregression coefficient ϕ is obtained by carrying out one or several model runs with high-resolution temporal output, and computing the autocorrelation for the desired variable and time lag. The coarse model at 2.8 km grid spacing (for the atmosphere) has a time step of 25 seconds, and the respective lag-1 autocorrelations ϕ were found to lie between 0.92 for the shortwave radiation and 0.97 for the specific humidity. The final noise field, which is added to the coarse field, is then obtained by

$$x_{noise} = \sigma_{miss} x_{new} \tag{4.9}$$

where σ_{miss} is the missing standard deviation estimated above. Spatial correlations are ignored in this step, in contrast to the first two steps. Addition of noise including the correct spatial correlations is planned for a future extension of the scheme.

For all downscaling steps the coarse mean of the grid cell is conserved by subtracting the difference between the coarse value and the mean of the downscaled values, ensuring the conservation of energy and mass. In very rare cases negative values of wind speed, shortwave radiation or precipitation result from the statistical downscaling which should not be used to force a soil model or a hydrological model. Thus, negative values are set to zero (or to the mean value for wind speed). The mean value of the coarse pixel is then conserved by multiplying the subgrid-pixel values by the fraction of the coarse means before and after setting these pixels to zero.

Precipitation

The downscaling of precipitation is treated as a special case, because additive noise could lead to negative precipitation values. Moreover Gaussian noise does not model the distribution of the anomalies well. The precipitation noise-generation algorithm consists of three steps. First, autoregressive Gaussian noise g is generated. This noise is then transformed into the following distribution, setting values below a threshold to zero and transforming the other values by a power law:

$$t = e^{(a*(g+b))} \tag{4.10}$$

The noise values t are subsequently multiplied by the coarse mean precipitation. The constants, i.e. the threshold, the fitting parameter a and b and the autoregressive constant, are optimized to fit with the distribution and the autocorrelation function of two model runs with high temporal resolution output that produced precipitation.

The different precipitation classes rain, snow and graupel are summed up and downscaled together as one precipitation class. After the downscaling they are again split up according to their original fractions.

Cross correlations

The automatic rule search algorithm described in section 4.3.2 has also been applied to search for possible cross correlations between the atmospheric downscaled variables. An overall cross correlation between wind speed and specific humidity of -0.27 (taking the whole data base into account) has been found. Shortwave and longwave radiation net fluxes are correlated by -0.52 in cloudy conditions, i.e. if $CLC > 0$. These cross-correlations have been emulated in the noise-generating process

$$\epsilon'_\psi = \sqrt{(1 - |\sigma_{cross}|)}\epsilon_\psi + \sqrt{\sigma_{cross}}\epsilon_{cross} \tag{4.11}$$

where ϵ_ψ is the noise term for a variable ψ in equation (4.7) and σ_{cross} is the respective cross correlation between two variables.

4.4. Results

In this section first the results of the different downscaling steps, applied to the various variables are shown (published in *Schomburg* et al., 2010). In section 4.4.2 offline applications of the downscaling to compute the fluxes are shown, and in section 4.4.3 the results of the downscaling implemented in the COSMO model itself and used in combination with the mosaic approach are given.

4.4.1. Disaggregation results for variables

The scheme has been tested for three case studies as described in section 4.2.6, i.e. a calm sunny day, a convective showery day and a stratiform rainy day.

The first downscaling step reduces already considerably the root mean square errors of the downscaled field for all variables, when compared to the coarse resolution field with the high-resolution model output as reference. A standard bi-linear interpolation algorithm using the four surrounding values, which has been tested for comparison only, does not lead to such a strong error reduction; here the errors are reduced only slightly, i.e. the bi-quadratic spline interpolation leads to better results, see Table 4.7 (top). Moreover, a bi-linear interpolation does not allow to conserve the coarse average to the same degree as the bi-quadratic interpolation (Tab. 4.7, bottom).

In Figure 4.19 the results of the individual downscaling steps and the final results for a temperature field of the lowest atmospheric layer are shown. The coarse field (Fig. 4.19a) is smoothed by the average conserving splines (step 1, Fig. 4.19e). After calculating the temperature anomalies, using relief height as predictor (step 2, Fig. 4.19b) and adding these to the result from the first step (Fig. 4.19f), the still missing variance is estimated and added as spatially uncorrelated noise in step 3 (Fig. 4.19c). These three steps together add up to the final field (Fig. 4.19g), which resembles closely the original fine scale field (Fig. 4.19h). In this example the deterministic downscaling yields very good results, hence the true anomalies (Fig. 4.19d) are well reproduced in downscaling step 2 (Fig. 4.19b). In contrast, in Figure 4.20 a case is shown where the deterministic downscaling has less skill. During a clear, cloudfree night, the air temperature does not decrease adiabatically with height, therefore the deterministic downscaling rule can only

Table 4.7.: Root mean square errors of the coarse field, a high-resolution field obtained by the bi-quadratic spline interpolation (downscaling step 1) and for comparison a high-resolution field generated by a standard bi-linear interpolation, spatially and temporally averaged for May 15, 2008. Top: RMSE for the small scale, bottom: RMSE for coarse scale.

Field	**T** [K]	$\|\mathbf{v_h}\|$ [m/s]	$\mathbf{q^v}$ [kg/kg]	**PS** [Pa]	$\mathbf{S_{net}}$ $[W/m^2]$	$\mathbf{L_{net}}$ $[W/m^2]$	**PREC** $[kg/m^2]$
400 m scale							
Coarse	0.26	0.42	1.62e-04	282	20.2	4.36	2.10e-04
Bi-linear	0.24	0.40	1.47e-04	260	19.5	4.15	1.98e-04
Bi-quadratic	0.23	0.38	1.33e-04	236	18.3	3.91	1.75e-04
2.8 km scale							
Coarse	0	0	0	0	0	0	0
Bi-linear	0.10	0.13	6.2e-05	109	6.75	1.40	8.8e-05
Bi-quadratic	6.2e-04	9.4e-04	4.2e-07	0.75	0.05	0.01	6.2e-07

be applied to a very small part of the model domain (Figure 4.20a). Thus the main part of the subgrid-scale variability is generated by the noise generation step (Fig. 4.20b). Since the spatial subgrid-scale correlations are not modelled, the spatial characteristics of the true anomalies (Fig. 4.20c) are not well reconstructed. In the original field cold air gathers in some of the valleys, which cannot be recovered by a simple statistical method.

Figure 4.21 shows an example for the downscaling of longwave net radiation at the surface. We start again from the coarse field (Fig. 4.21a), apply the spline interpolation (Fig. 4.21e), and add the deterministic anomaly proportional to the surface temperature anomalies, which leads to the intermediate field Fig. 4.21f. The addition of noise (step 3) finally leads to Figure 4.21g. In the original field (Fig. 4.21d and h) a small region in the northeastern part shows particular large small-scale variability. This large scatter is not reconstructed in step 2 (Fig. 4.21b), because this variability is not caused by surface heterogeneity but by some sparse clouds. The missing variance is satisfactorily replenished by step 3 (Fig. 4.21c).

The time series of the root mean square errors (RMSE) produced by the individual downscaling steps is shown in Figure 4.22 for a case study of May 12, 2008. The first step (spline interpolation) leads for all variables to a small error reduction compared to the coarse fields (here the error of the coarse field at the small scale is computed by assuming homogeneous forcing for all sub-pixels). Where applicable, i.e. for temperature, pressure and the radiation fluxes, the deterministic downscaling leads to a considerable error reduction. The error reduction for temperature (Fig. 4.22a) during the clear sky night is less distinctive than during the day. These problems do not exist during overcast nights (not shown). Adding random noise in the third step naturally increases the RMSE error for most variables (temperature at night, humidity, wind speed and the radiation fluxes in the evening, in this case); sometimes the RMSE even exceeds the RMSE of the homogeneous field.

As mentioned above, the correct subgrid-scale variability can be decisive to avoid biases for applications involving nonlinear processes. The first downscaling step introduces some variance (see Fig. 4.23). The second step leads to a another large increase of the high-

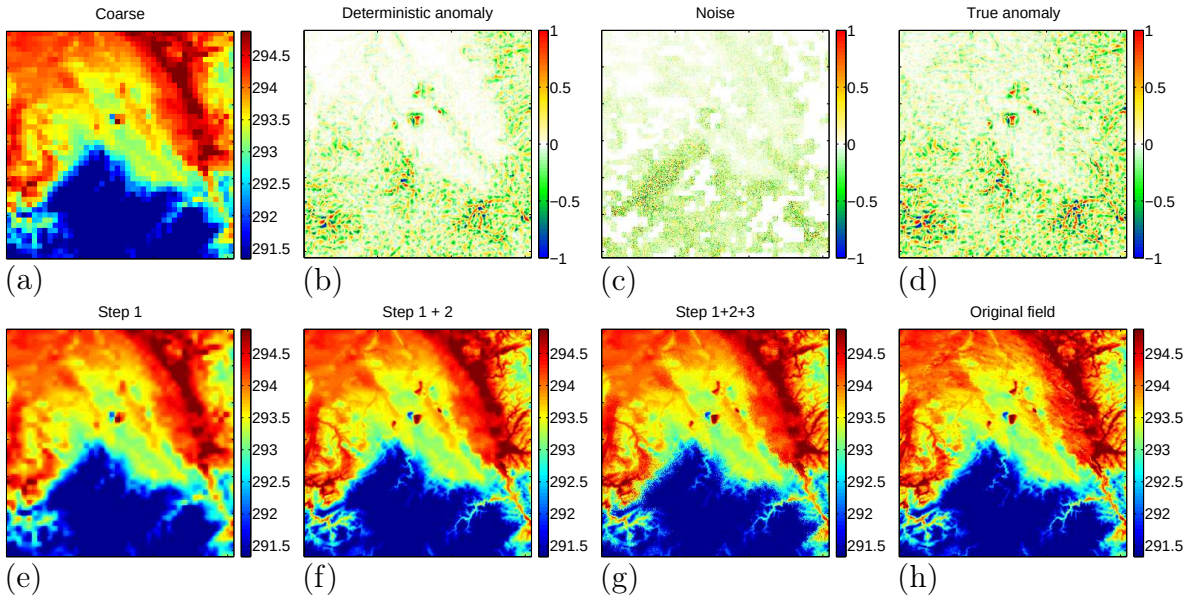

Figure 4.19.: Downscaling scheme applied to a temperature field (in Kelvin) of the lowest atmospheric model layer, 10:00 UTC, May 12th, 2008. Top: a) coarse field; b) deterministic anomaly; c) generated noise; d) true anomaly. Bottom: Temperature field after application of e) step 1 (spline interpolated); f) step 1 + 2; g) step 1 + 2 + 3 (final field, i.e. sum of all three downscaling steps); h) original fine scale field (reference).

resolution standard deviation. Even more subgrid variability is generated by step 3, in which the still missing variance is estimated and added. The subgrid heterogeneity is well parameterized, but temporary deviations from the reference do occur. For pressure the third step is not applied, because the variability generated in the second downscaling step is already sufficient (see Fig. 4.23d).

For comparison the root mean square errors and subgrid-scale standard deviations for May 15, 2008, a convective showery day, are depicted in Figure 4.24. Results are shown only for those variables which exhibit a different behaviour compared to the calm, sunny day in the previous example. Here for the radiation fluxes almost no improvements can be achieved by the second downscaling step, because the subgrid-scale variability is dominated by the heterogeneous cloud cover. The subgrid-scale standard deviation of the precipitation is reproduced well for this day (Fig. 4.24f).

The errors and subgrid-scale variabilities are averaged spatially and temporally for the three case studies and listed in Table 4.8 and 4.9. According to these results the errors are reduced slightly by the first downscaling step and strongly by the second downscaling step. The overall improvement gained for the radiation fluxes is less than for the single fair weather day shown in Fig. 4.22, because for the two other cloudy days the deterministic downscaling step has much less skill. Only under clear sky conditions the RMSE is reduced considerably by the second downscaling step, otherwise the subgrid-scale variability is not due to surface heterogeneity but to variable cloud cover. The subgrid-scale variability is enhanced slightly by downscaling step 1 and more by step 2 (where applicable) and step 3 (Tab. 4.9). For all variables the subgrid standard deviation is on average slightly too

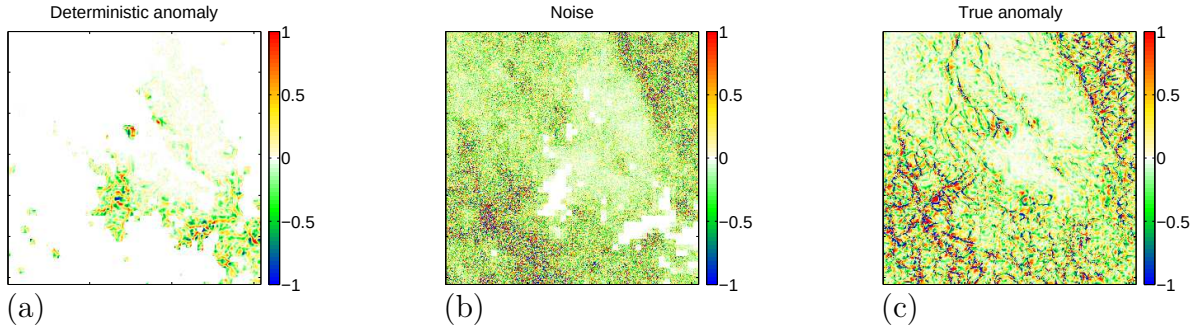

Figure 4.20.: Temperature anomalies (in Kelvin) constructed in downscaling step 2 (a) and downscaling step 3 (b) and reference anomalies for a clear-sky nighttime situation, 1:00 UTC, May 12, 2008.

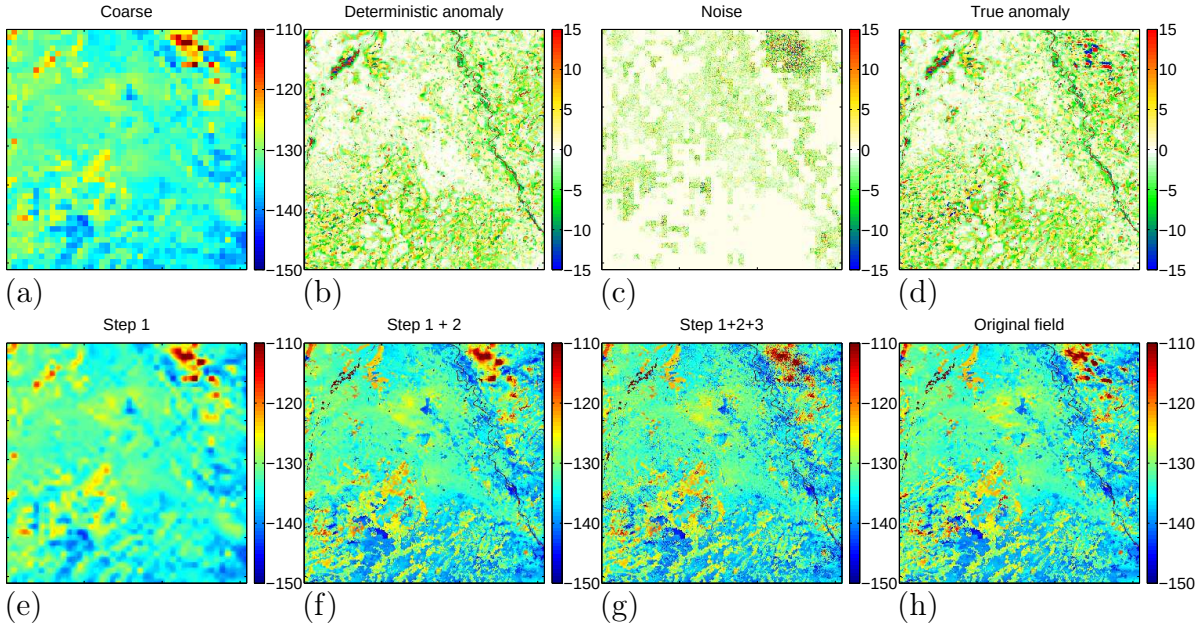

Figure 4.21.: Same as Figure 4.19, but for the longwave surface net radiation in W/m^2.

large after the last step, but only the deviations for wind speed, pressure and longwave net radiation are statistically significant. Obviously the mean statistics of these three days do not match the mean statistics of the training data set.

The temporal autocorrelations of the coarse fields are larger than those of the high-resolution reference values from the high-resolution fields (see Figure 4.25), this difference prevails after application of downscaling steps 1 and 2. Step 3 leads to a strong decrease of the autocorrelations with increasing time lags; for most variables the reference autocorrelations are now matched more closely. For precipitation the correlations are, however, too low after the third step.

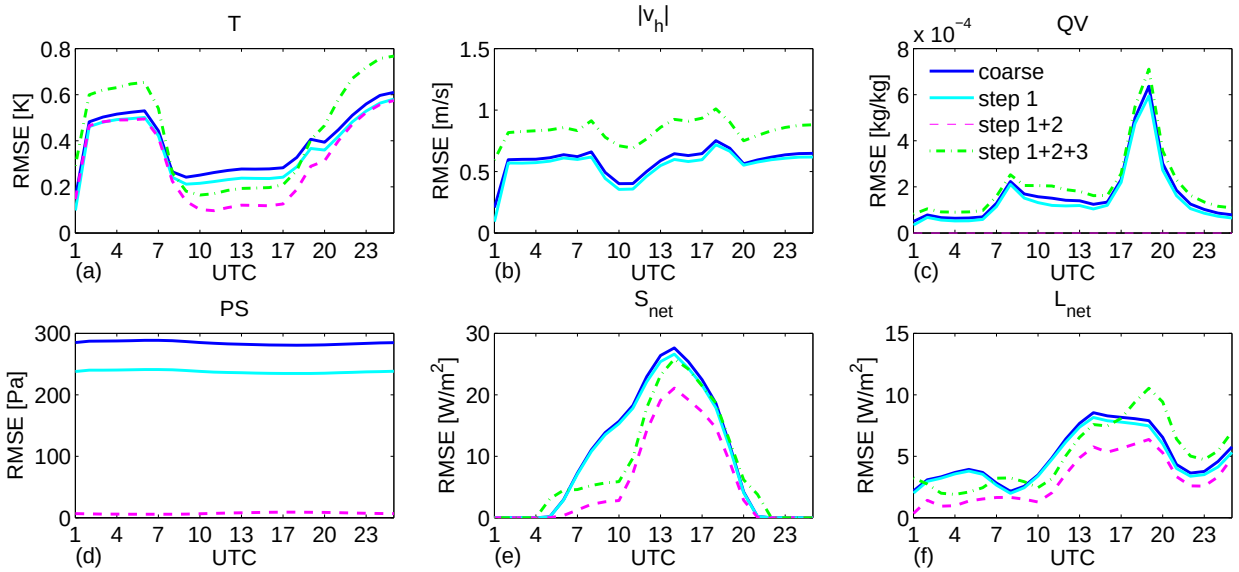

Figure 4.22.: Timeseries of root mean square error (RMSE) of the downscaling variables for the three downscaling steps for May 12, 2008: a) temperature, b) wind speed, c) specific humidity, d) surface pressure, e) shortwave net radiation, f) longwave net radiation. For wind speed, specific humidity and precipitation the deterministic step 2 is not applicable, see section 4.3.2.

Table 4.8.: Root mean square errors for the different variables for the downscaling steps averaged over the three case studies.

Disaggreg.	**T** [K]	$\|\mathbf{v_h}\|$ [m/s]	$\mathbf{q^v}$ [kg/kg]	**PS** [Pa]	$\mathbf{S_{net}}[W/m^2]$	$\mathbf{L_{net}}[W/m^2]$	**PREC** kg/m^2
no disagg	0.31	0.56	1.54e-04	285	14.73	5.09	7.75e-05
Step 1	0.27	0.52	1.34e-04	238	13.52	4.70	6.49e-05
Step 1+2	0.21	-	-	6.2	12.18	4.15	-
Step 1+2+3	0.31	0.82	1.94e-04	-	17.97	6.26	9.92e-05

Application to regional climate scale

The downscaling system was developed and tested for atmospheric variables based on 400 m grid spacing as the smaller scale and 2.8 km as the larger scale. First tests of the system for a disaggregation of the atmospheric variables from 14 km data down to 2.8 km have been conducted in order to see whether the system can also be used for regional climate simulations with the COSMO model on a 14 km grid, with surface information on a 2.8 km mosaic. Although the downscaling steps have been trained for smaller scales, the results obtained by the downscaling are very encouraging in terms of root mean square error reduction (Fig. 4.26) and subgrid-scale variance reconstruction (Fig. 4.27). This indicates that the downscaling can be applied to other scales than the development scale even without making changes to the coefficients and rules.

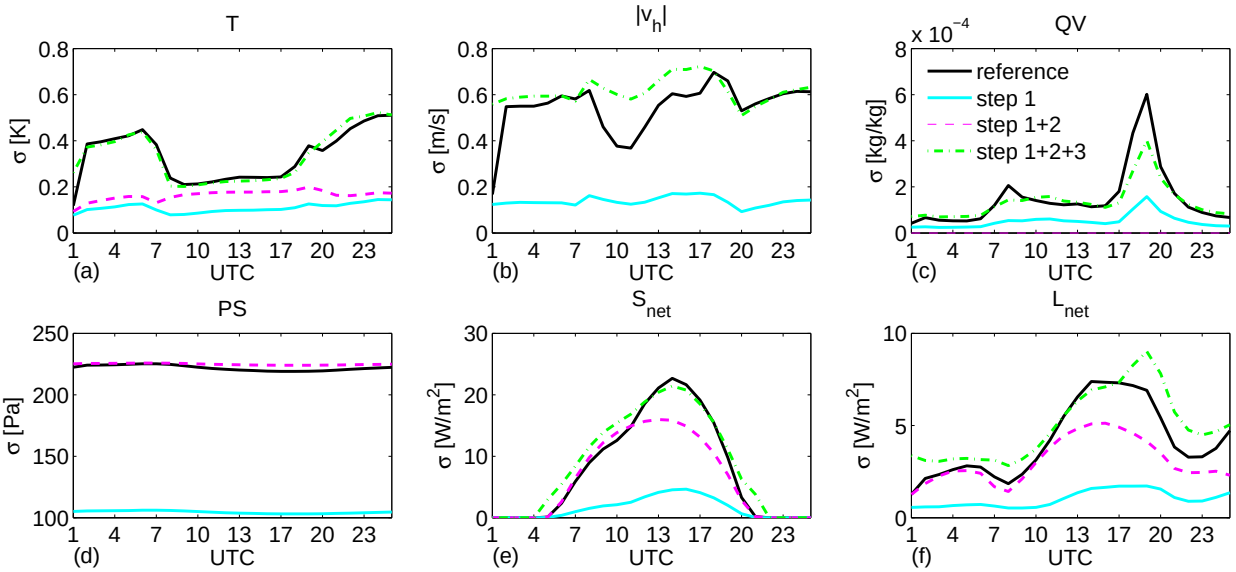

Figure 4.23.: The same as Figure 4.22 for the subgrid-scale standard deviations (σ). Here the black line denotes the reference subgrid standard deviations.

Table 4.9.: Sub-grid scale standard deviations for the different variables for the downscaling steps averaged over the three case studies.

Disaggreg.	**T** [K]	$\|\mathbf{v}_h\|$ [m/s]	$\mathbf{q^v}$ [kg/kg]	**PS** [Pa]	$\mathbf{S_{net}}[W/m^2]$	$\mathbf{L_{net}}[W/m^2]$	**PREC** kg/m^2
Step 1	0.10	0.13	5.19e-05	105	3.52	1.23	1.16e-05
Step 1+2	0.17	-	-	225	6.03	1.94	-
Step 1+2+3	0.28	0.61	1.36e-04	-	13.37	4.72	2.50e-05
Reference	0.27	0.52	1.35e-04	222	11.57	4.25	2.53e-05

4.4.2. Offline application of the downscaling system for computing the turbulent fluxes

As a first step to understand the effects of the downscaling system on the turbulent fluxes of sensible and latent heat, the fluxes have been computed in an simple offline environment by the flux equations:

$$(F_h)_{sfc} = -\rho K_h L |\mathbf{v}_h|(T - T_{sfc}). \tag{4.12}$$

$$(F_{q^v})_{sfc} = -\rho K_h c |\mathbf{v}_h|(q^v - q^v_{sfc}) \tag{4.13}$$

The transfer coefficient K_h has also been computed offline by a simple transfer scheme based on a concept by *Louis* (1979), using Monin-Obukhov similarity theory. Output of high-resolution (400 m) model runs have been used as reference. The coarse values were (as before) obtained by averaging the small-scale values to the 2.8 km scale.

Five different configurations have been compared (see Table 4.10). Two kinds of downscaling have been tested, a deterministic version applying only step one and two of the disaggregation system (i.e. spline interpolation and deterministic rules), and a stochastic version containing also step three, i.e. noise generation. These are compared with the standard mosaic approach (i.e. with homogeneous atmospheric forcing for all mosaic-

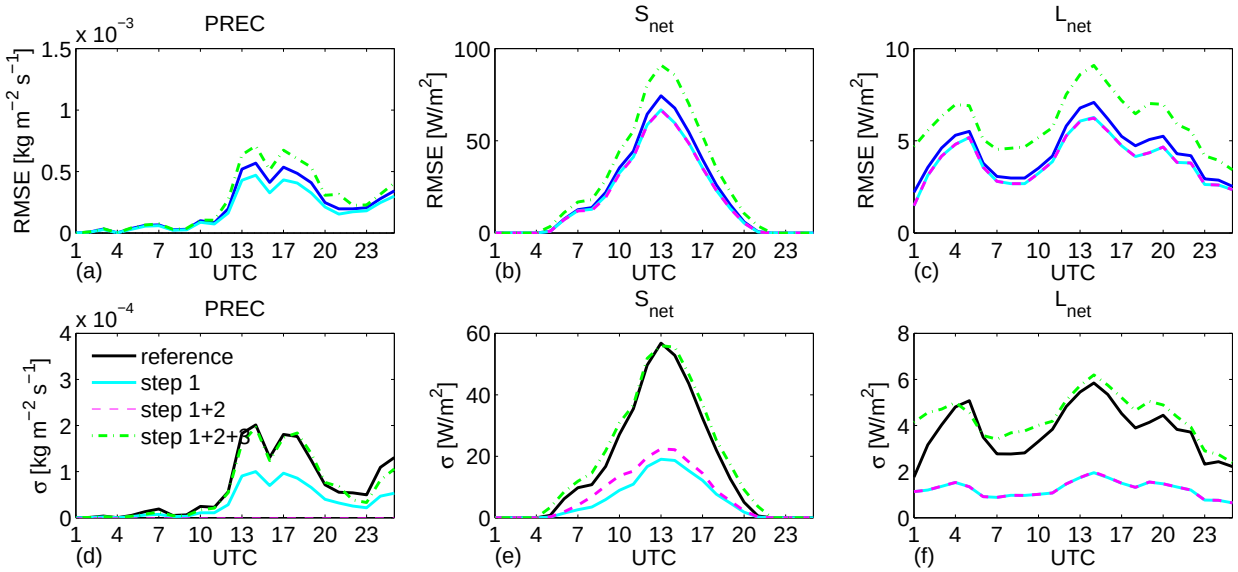

Figure 4.24.: Top: Root mean square errors for shortwave and longwave radiation fluxes and precipitation for May 15, 2008. Bottom: The respective subgrid-scale variances.

subpixels) and with the standard model grid without small scale information neither in the atmosphere nor at the surface, i.e. without any subgrid heterogeneity representation.

For the comparisons, the fluxes have been computed on the fine scale and then averaged to the coarse scale, because we are interested in the performance of the coarse fluxes, which are handed over as lower boundary condition to the atmospheric model. By this application of the disaggregation system the effects of the downscaling can be understood and isolated more easily. Most results in this chapter are from the case study of May 12, 2008, a day with only sparse clouds and no precipitation, i.e. unblocked incoming and outgoing radiation.

Diurnal characteristics

The results in terms of hourly root mean square errors (RMSE) and biases for both sensible and latent heat fluxes for May 12, 2008 are depicted in Figure 4.28. The by far largest errors are obtained for the coarse flux computations without any subgrid-scale heterogeneity, all other configurations decrease the errors substantially, especially for the

Table 4.10.: Configurations for comparisons.

Name	Atmospheric information	Surface information
Reference	exact fine scale model output	exact fine scale model output
No noise	downscaled without noise generation	exact fine scale model output
With noise	downscaled with noise generation	exact fine scale model output
Mosaic	coarse	exact fine scale model output
Coarse	coarse	coarse

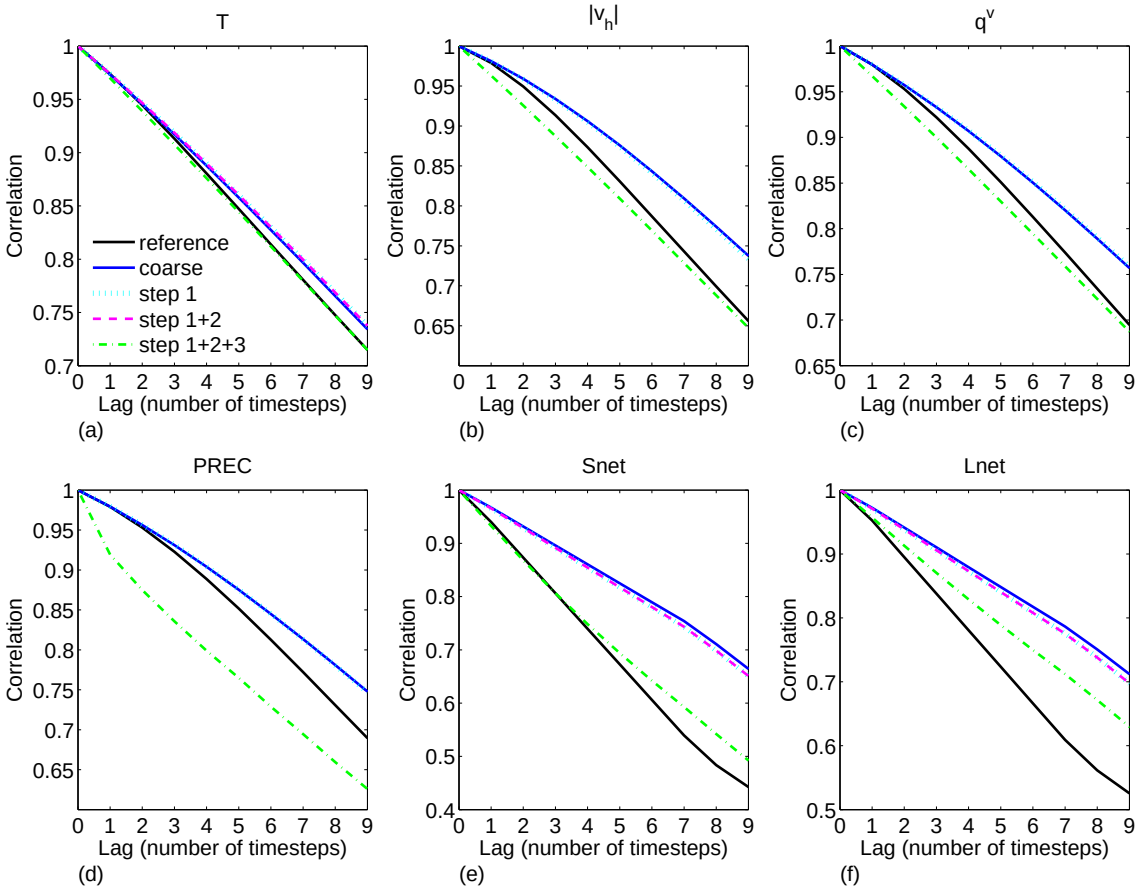

Figure 4.25.: Temporal autocorrelations for the downscaling variables for 17:00 UTC, May 15, 2008. Here one timestep is 24 seconds.

sensible heat flux. To distinguish between the different heterogeneity configurations, the RMSE are depicted again, now without the coarse results, in Figure 4.29. The lowest errors are received by applying the downscaling without noise generation, improvements of about 1 W/m^2 over the standard mosaic fluxes prevail throughout the day. Generally the fluxes computed with atmospheric downscaling based on all three downscaling steps, i.e. including the stochastic downscaling step, perform worst. Only for the sensible heat flux during night and early morning hours the full downscaling leads to the best results. In the following the causes for these results are analyzed.

The lowest errors are always obtained for that configuration, for which the mean subgrid-scale standard deviation matches the reference subgrid-scale variability most closely, see Figure 4.30. The subgrid-scale variability of the mosaic alone without downscaling is usually too high, the interpolation and deterministic downscaling helps to reduce it, whereas the application of the stochastic downscaling yields too high variabilities. The mosaic approach without any downscaling leads to too high subgrid scale variabilities, because subgrid correlations between surface variables and atmospheric variables can not be modelled. Compared to a standard model run without subgrid-heterogeneity at the surface, much additional heterogeneity is introduced. However in situations where relations e.g. between surface and air temperature exist, the imposed variability is too high,

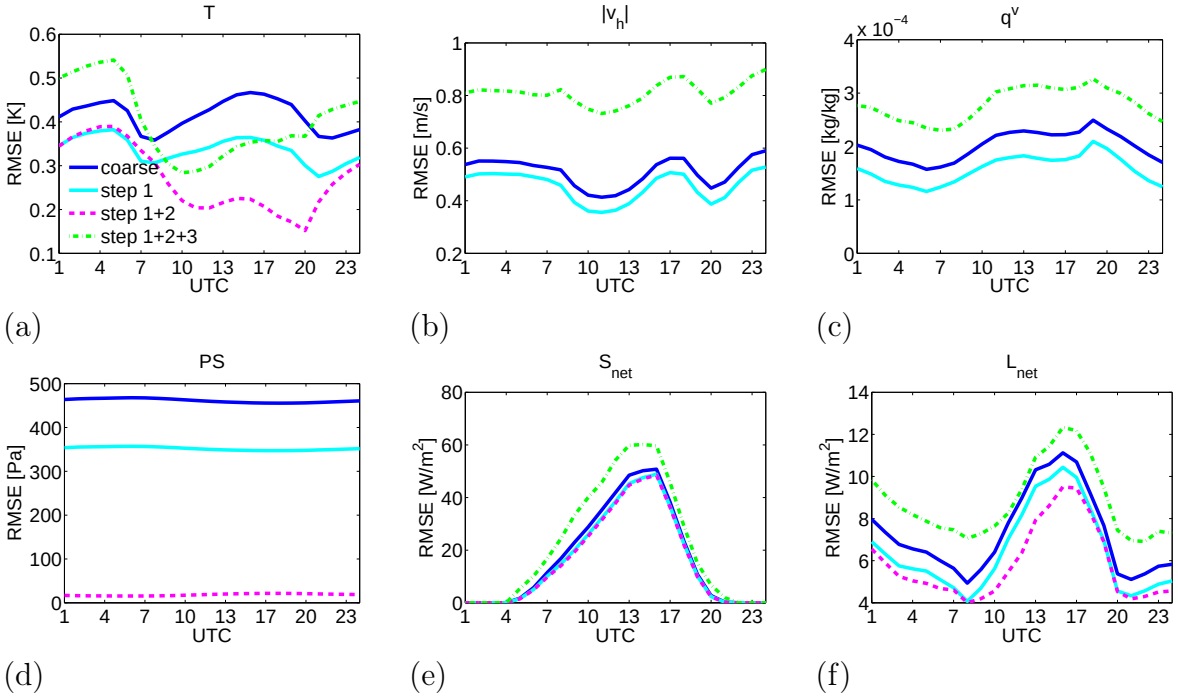

Figure 4.26.: Timeseries of root mean square error (RMSE) of the downscaling variables for the three downscaling steps for May 12, 2008: a) temperature, b) wind speed, c) specific humidity, d) surface pressure, e) shortwave net radiation, f) longwave net radiation. Downscaling from 14 km to 2.8 km.

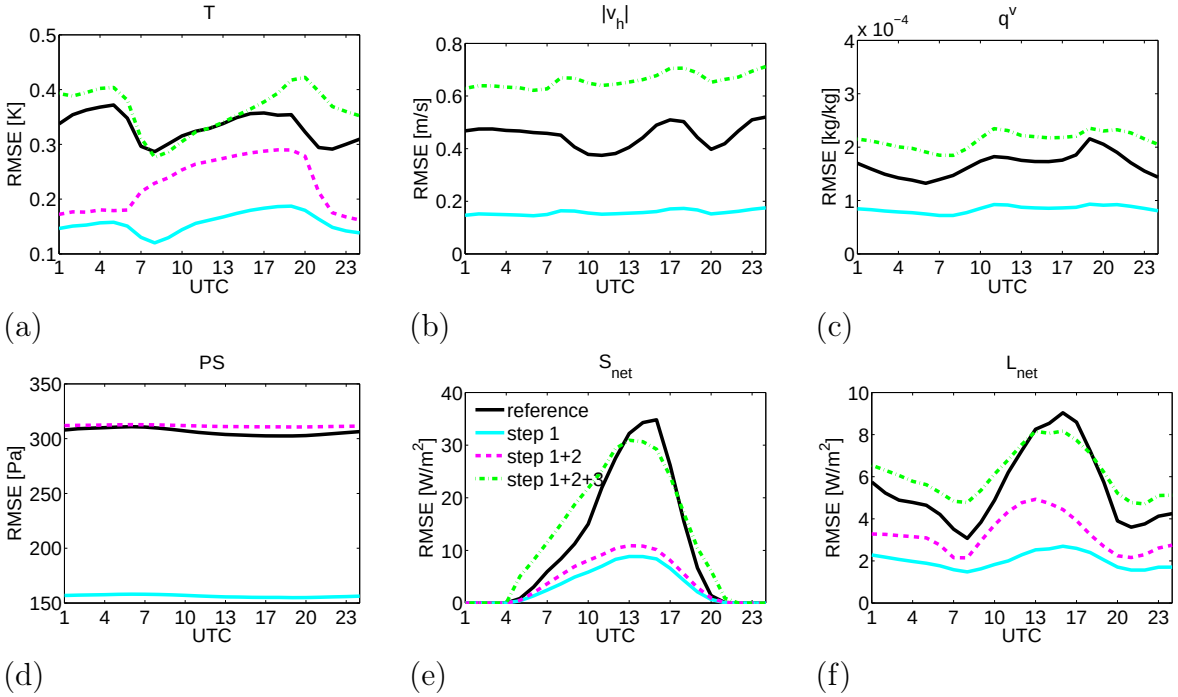

Figure 4.27.: The same as Figure 4.26 for the subgrid-scale standard deviations (σ). Here the black line denotes the reference subgrid standard deviations. Downscaling from 14 km to 2.8 km.

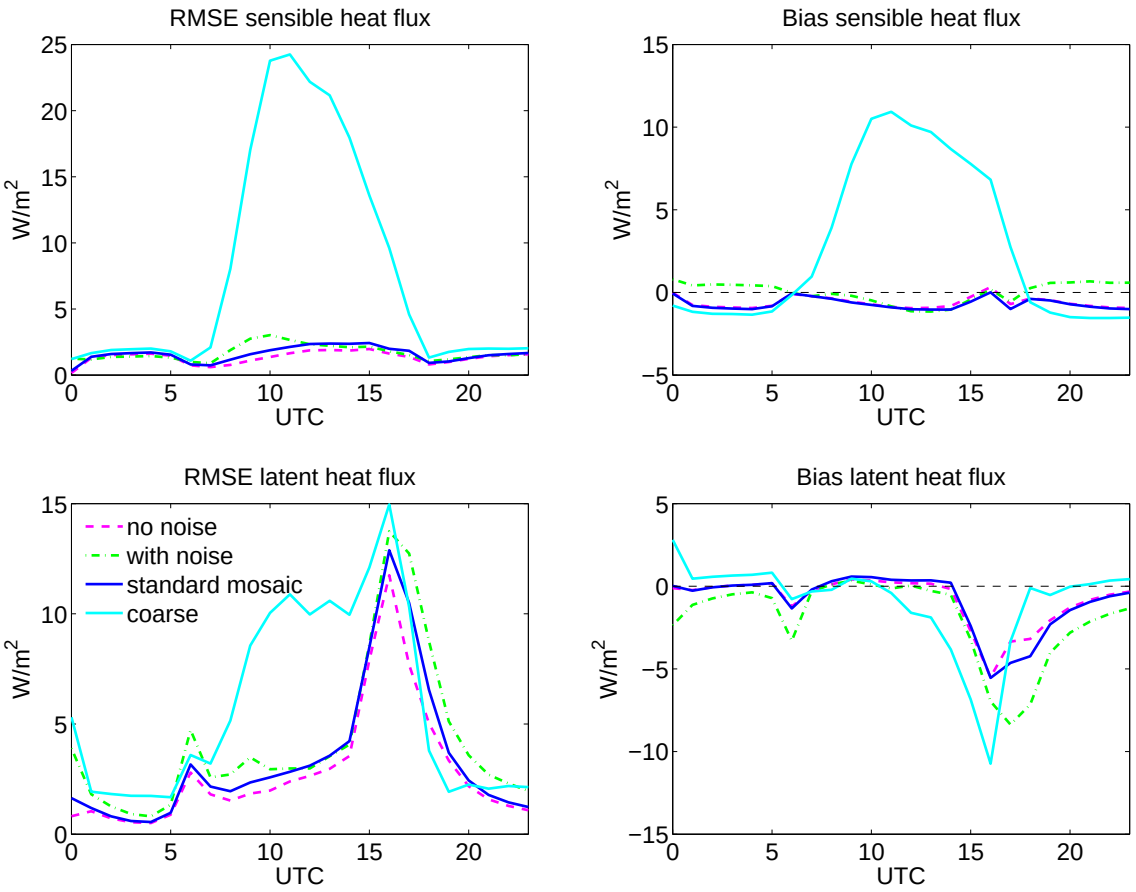

Figure 4.28.: Root mean square errors (left) and biases (right) of the sensible (top) and latent (bottom) heat flux on the coarse resolution. The fluxes have been calculated on the small scale and then averaged to 2.8 km, afterwards the errors were computed.

the gradients of temperature and specific humidity vary more than they should. Steps 1 and 2 of the downscaling approach help to re-establish these relations and thus decrease the variability down to realistic values. This hypothesis is supported by Figure 4.31, which shows the correlations between surface and near-surface temperature and specific humidity, respectively. During daytime the atmospheric temperature and the surface temperature are both strongly correlated (Fig. 4.31a) and the spatial autocorrelation in the field is high (Fig. 4.32b), the deterministic downscaling performs well in reproducing it.

A completely different behaviour can be observed for the sensible heat flux during night, which is also mainly cloudfree, where the subgrid-scale variability of sensible heat fluxes obtained by the standard mosaic is too small (Fig. 4.30). Thus, in this situation the addition of noise helps to increase the subgrid-scale variability to the correct amount, and to lower errors for the fluxes (Fig. 4.28). The subgrid-scale standard deviation of the temperature of the lowest atmospheric level is larger during the clear sky radiation night than during the day (see e.g. Fig. 4.23), because the atmospheric mixing is reduced under stable conditions. No strong relations between the surface value and the value of the lowest atmospheric layer exist (see Figure 4.31), surface and boundary layer are al-

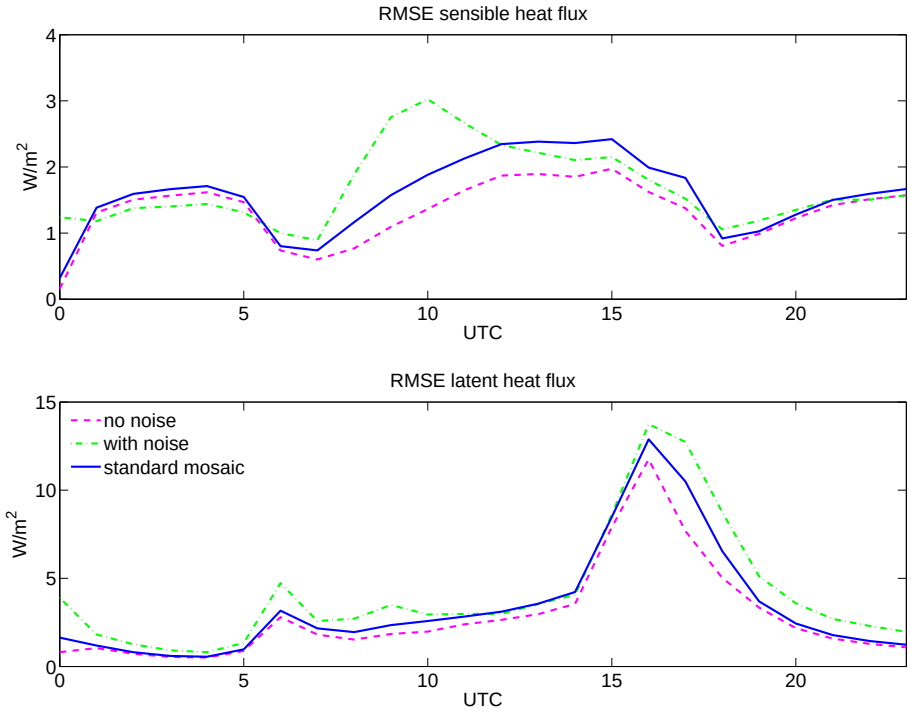

Figure 4.29.: Root mean square errors of the sensible (top) and latent (bottom) heat flux on the coarse resolution, now without the coarse results for a better illustration of the downscaling effects. The fluxes have been calculated on the small scale and then averaged to 2.8 km, afterwards the errors were computed.

most completely decoupled. The spatial correlations of the temperature field, depicted in Figure 4.32a, exemplary for 4:00 UTC during night and 12:00 UTC during day up to a lag of 10 grid boxes, are low at nighttime for the reference temperature. The spatial autocorrelations of the coarse flux, the standard mosaic approach and those of the downscaling without noise are much too high. The third downscaling step decreases the spatial correlations adequately in this situation and leads to a realistic subgrid-scale variability of the fluxes. Because correlations between atmosphere and surface are low anyhow, the random noise does not destroy any relations. For latent heat flux, the subgrid-scale variability is overestimated by all configurations throughout the day. This overestimation is most pronounced in the afternoon. Thus, also the errors are largest during the afternoon (Fig. 4.28). This can be attributed to high, not parameterized subgrid-scale correlation between q^v and q^v_{sfc} (see Figure 4.31b) in combination with high flux-values during the afternoon (not shown).

Spatial characteristics

The improvement in root mean square error has been calculated for subregions of 4x4 coarse pixels, for the mosaic versus no subgrid-heterogeneity and for the mosaic with downscaling (without noise) versus the standard mosaic, averaged over the whole day (Figure 4.33). The mosaic approach leads to the largest improvements over the flat areas

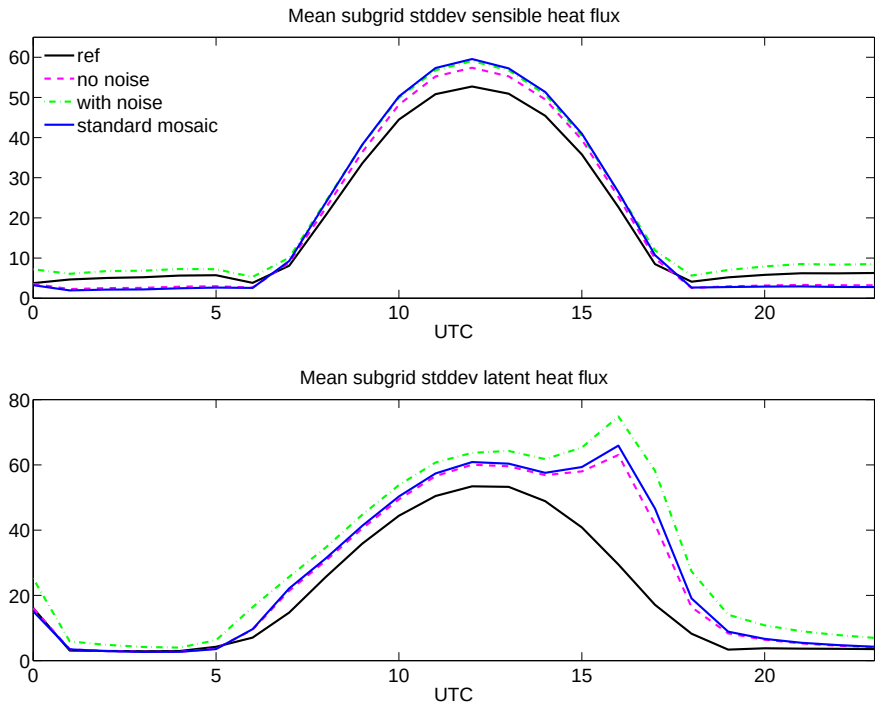

Figure 4.30.: Subgrid-scale standard deviations of the sensible (top) and latent (bottom) heat flux on the coarse 2.8 km scale.

with much heterogeneity in land cover characteristics. A huge benefit is achieved by the simulation of subgrid water pixels in the mosaic approach in contrast to the standard approach without subgrid heterogeneity representation. The downscaling is then able to improve these results further, but the effect is much smaller (Fig. 4.33, right, be aware of the different color scales). The main improvements of the atmospheric disaggregation are achieved over mountainous areas.

Summary of offline results

To ensure that these results are significant, the evaluations shown have also been carried out for a second day with a different weather situation (16th of July 2008) which was a synoptically driven overcast day with moderate winds and some precipitation. The results are very similar, only the characteristics of the clear sky night are not visible and the behaviour during night is very similar to that during daytime.

Summarizing, the mosaic approach is able to improve the simulation of the turbulent heat fluxes considerably. Under most situations, however, the mosaic without downscaling leads to excessive subgrid-scale variability, which can be reduced successfully by the downscaling steps 1 and 2 which re-establish the correlation between surface and near surface values. Downscaling with additional noise deteriorates the results by adding too much variability. Only during clear-sky radiation nights when the subgrid-scale variability of temperature is largest and inter-variable correlations low, the sensible heat flux computed based on the mosaic approach has not enough subgrid-scale variability, thus the addition of noise leads to improvements there. In conclusion, the additional improvement,

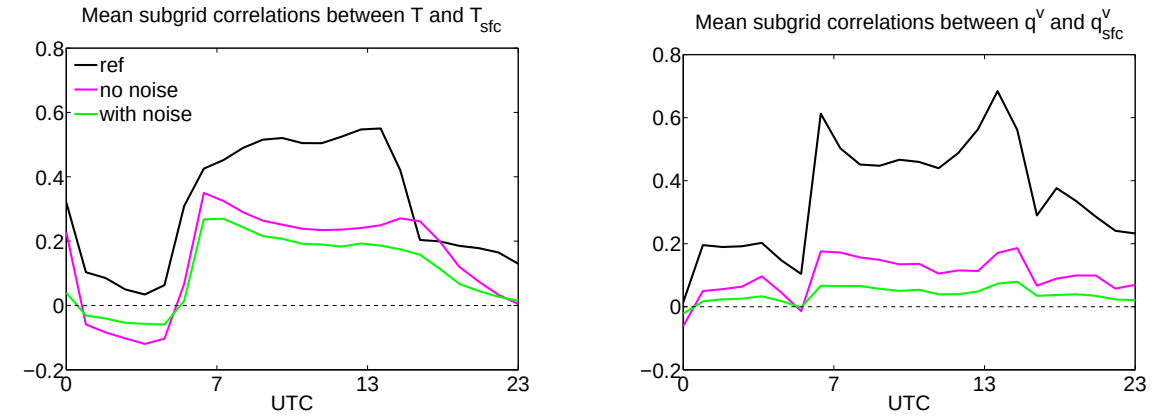

Figure 4.31.: Mean subgrid correlations between surface and near-surface temperature (top) and specific humidity (bottom) for May 12, 2008.

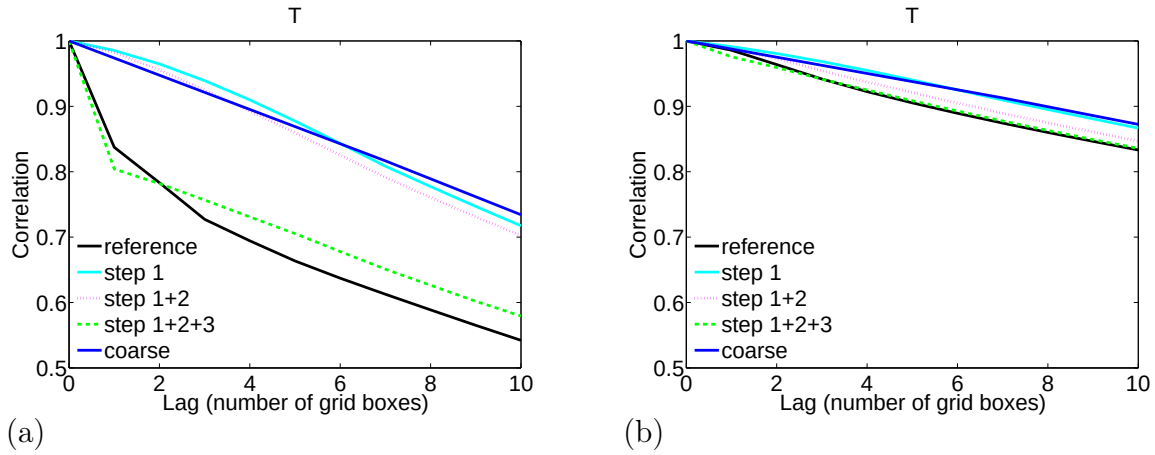

Figure 4.32.: Spatial auto-correlations for the temperature of the lowest atmospheric model layer, at 4:00 UTC (left) and 12:00 UTC (right) for the fair-weather day May 12, 2008.

which can be achieved by using the atmospheric downscaling with the mosaic approach, is much smaller than the effect of the mosaic over ignoring subgrid heterogeneities. In fully coupled applications, however, effects from the other downscaled variables, such as radiation fluxes and precipitation, can be expected. In this section only the effects of disaggregated reference-level variables temperature, specific humidity and wind speed could be considered, due to the simple setup. Moreover, the non-linear processes in the soil are not represented in this offline case study. For a more realistic and consistent analysis, the effects of mosaic and downscaling have been investigated in fully coupled COSMO model runs; details and results are given in the next section.

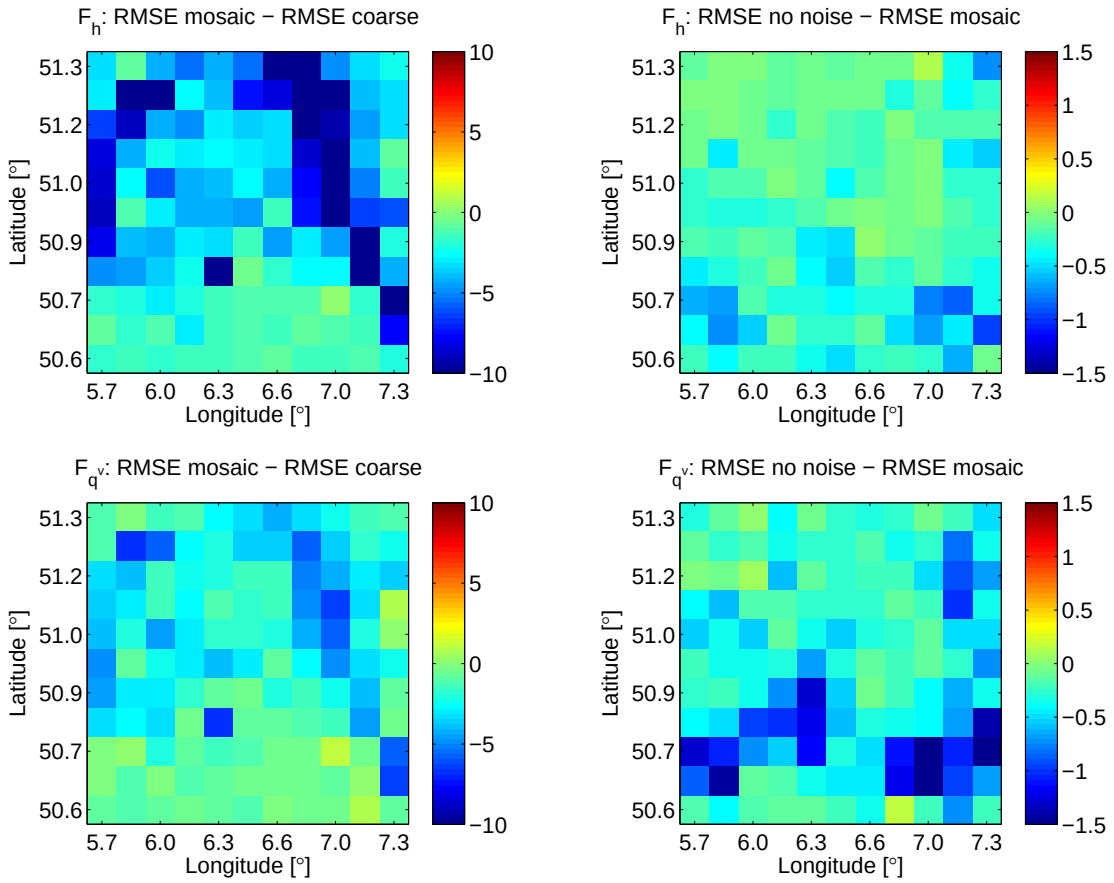

Figure 4.33.: Difference in RMSE for subregions of 4x4 coarse pixels for sensible (top) and latent (bottom) heat flux for May 12, 2008. The left figures show the difference between mosaic and a standard grid without subgrid-scale heterogeneity, the right figures the difference between downscaling (without noise) and mosaic (Note the different col or scales.). Blue colours indicate improvement of the mosaic over coarse fluxes (left) and the downscaling with mosaic versus standard mosaic (right), respectively.

4.4.3. Downscaling system in COSMO model runs

Implementation and experimental design

The downscaling of atmospheric variables has been implemented into the numerical weather prediction model COSMO, as further enhancement of the mosaic approach. For this purpose, a modified model version COSMO-SUBS (model version 4.0, modified by F. Ament at MeteoSwiss) has been used, which includes the mosaic subgrid surface representation.

The implementation has been realized in a flexible way, such that either standard coarse model runs can be carried out, or model runs with mosaic subgrid heterogeneity representation, with or without atmospheric downscaling. Furthermore, a parameter can be set to apply either the full downscaling or only downscaling step one and two.

Ament (2006) found the effect of improved soil/surface heterogeneity representation to be too small to be verified with flux measurements. The quantitative comparison

with measurements is hampered by several factors. First, the model boundary conditions (atmospheric forcing, surface characteristics, soil state etc.) have to match the reality closely, which is difficult due to imperfect knowledge of initial conditions (e.g. for soil moisture), the horizontal resolution of the model, which is generally much larger than the footprint of flux measurements, and other model related errors. Besides, also flux measurements do not reflect reality exactly, but are subject to measurement errors and non-closure of the energy-budget inherent in flux measurement techniques.

In this work, a comparison with observations is even more difficult, because the additional effect of atmospheric downscaling is expected to be smaller than the improvement gained with the mosaic versus compared to coarse standard model runs. The difference between measurements and model results is much larger than between model runs with and without the different downscaling configurations. Therefore, high-resolution model runs (400 m horizontal grid size) have been used as reference for the fully coupled online validation simulations. For online tests, this procedure, however, has the disadvantage that model runs with different configurations diverge during the model simulation. Thus, the turbulent fluxes and other variables can not be compared one-to-one, because the differences are likely to be due to different positions of the clouds, and not by different flux computations themselves. To exclude the effects of different cloud evolvement to a large degree, most case studies chosen for the online model simulations are characterized by calm weather conditions with either clear sky or rather homogeneous cloud cover (for a list of cases see Table 4.1). The comparisons with high-resolution model runs as reference can only be considered as "consistency check".

Model simulations with the same five configurations as in the previous section (Table 4.10) have been conducted, but now for each of these configurations a separate model simulation has been carried out: 1) the high resolution "reference" simulations; 2) coarse simulations without any subgrid heterogeneity representation; 3) mosaic runs without downscaling; 4) mosaic simulations with atmospheric downscaling step 1 and 2; and 5) mosaic with the full downscaling including also the third, stochastic downscaling step.

Surface energy budget

The quantitative errors measures shown in this section are obtained by averaging the results of six validation case studies, in order to obtain robust results with respect to the effects of the downscaling procedure and to alleviate effects of divergence of single model runs. The performance of the downscaling for single case studies varies to a large degree, making conclusions difficult. In Figure 4.34 the root mean square difference of the turbulent heat fluxes (on the 400 m scale) with respect to the fluxes obtained from the high-resolution model runs are depicted. It is evident, that the large errors of the coarse model runs without any subgrid scale heterogeneity representation can be substantially reduced by up to 40 W/m^2 by the mosaic runs with the different configurations. The mosaic runs without noise and without downscaling give similar results, whereas for the runs with full downscaling the errors are higher.

On the coarse grid, on which the fluxes are provided to the model dynamics, the differences between all three mosaic configurations are very small (Figure 4.35). The total averaged root mean square errors are listed in Table 4.11, the improvements by the atmospheric downscaling are marginal.

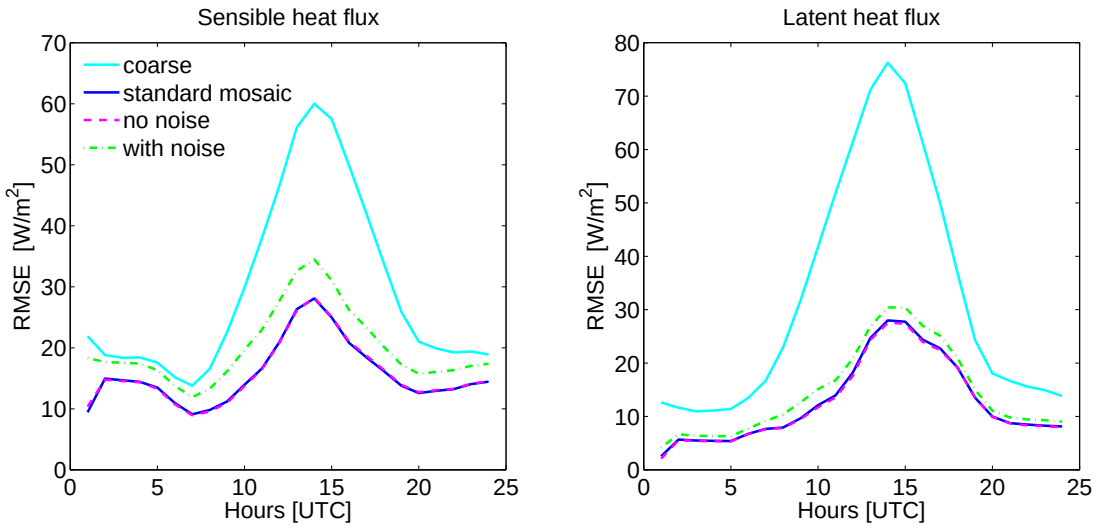

Figure 4.34.: Diurnal cycle of RMSD of turbulent heat fluxes, averaged over the six validation case studies, computed on the 400 m scale.

Table 4.11.: Stochastic (RMSD) and systematic (bias) errors of the turbulent heat fluxes and radiation net fluxes, for coarse surface and atmosphere, mosaic and mosaic plus downscaling steps 1 and 2 or full downscaling, averaged over six case studies.

	RMSD $[W/m^2]$				Bias $[W/m^2]$			
	coa	mos	no noise	with noise	coa	mos	no noise	with noise
Sensible heat	19.31	11.02	10.98	10.97	1.42	1.77	1.65	1.48
Latent heat	20.72	7.96	7.91	7.94	0.19	-0.26	-0.04	0.35
SW radiation	14.44	13.47	13.47	13.47	-0.98	-0.80	-0.80	-0.81
LW radiation	6.94	6.17	6.18	6.18	0.47	-0.03	-0.05	-0.11

The behaviour of the bias is less systematic, no clear conclusion can be drawn. The values are low for all configurations, and the model runs with the best performance alternate during the day (Figure 4.36). For all simulations the sensible heat flux systematic error is positive throughout the day, approaching zero during sunrise and sunset. The totally averaged flux biases (Table 4.11) although small are further reduced by the downscaling. Downscaling steps 1 and 2 are always beneficial, the third, stochastic downscaling step leads to an increase of the bias of the latent heat flux. Generally, small improvements are possible for fair-weather days, while for the days with clouds and rain, where the turbulent fluxes are less determined by local surface characteristics, hardly any differences can be detected (not shown).

For the radiation fluxes (Table 4.11) the differences of the mosaic with and without downscaling are low, the reason being that also in the standard mosaic a disaggregation of the surface radiation net fluxes is applied, similar to the disaggregation in the downscaling system.

Besides good results for the mean fluxes, a good parameterization of the second moments, i.e. the subgrid-scale variability, is important for nonlinear processes. In Table 4.12

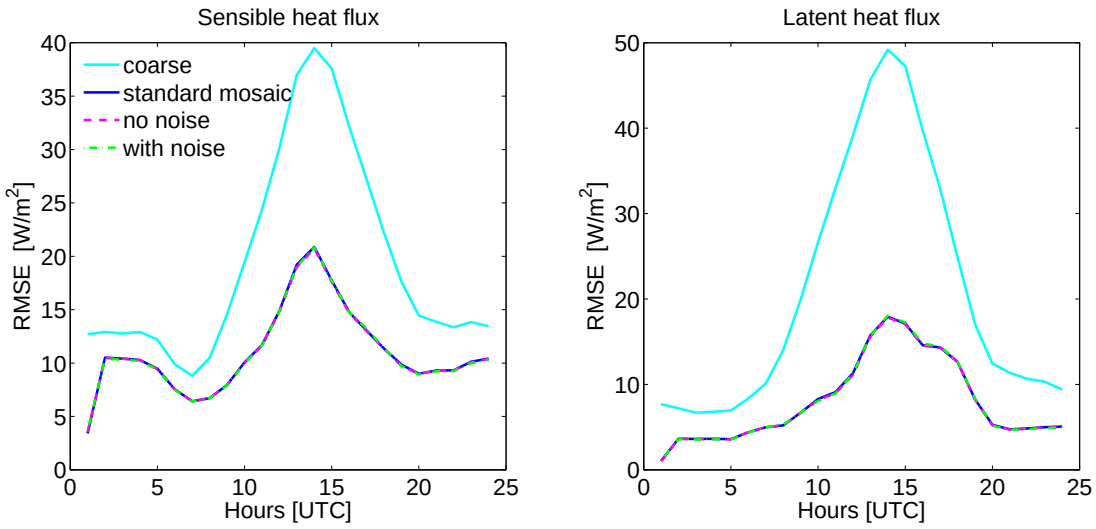

Figure 4.35.: As Fig. 4.34, but computed on the 2.8 km scale.

Table 4.12.: Mean subgrid-scale standard deviations [W m^{-2}], averaged over all six validation case studies.

	coa	mos	no noise	with noise	ref
Sensible heat	0	12.50	13.30	16.11	13.44
Latent heat	0	14.97	14.81	15.65	14.68
SW radiation	0	1.85	2.33	5.60	4.96
LW radiation	0	2.38	1.64	3.01	2.87

the mean subgrid-scale standard deviations per coarse pixel are listed. For the sensible heat flux the subgrid scale variability of the mosaic alone is too small, and is increased to a value closer to the reference if atmospheric downscaling without noise is applied. The heterogeneity of the latent heat flux is too large for the standard mosaic, and can be reduced by the downscaling steps 1 and 2. The full downscaling again leads to excessive variabilities for both fluxes, probably due to inter-variable relationships not accounted for adequately by the stochastic noise generation. For the radiation fluxes, however, the full downscaling gives the best results, because it is trained to parameterize also the effect of subgrid-scale variabilities of clouds, while mosaic and mosaic with downscaling step 1 and 2 can only account for surface heterogeneities.

Error analysis

In this section the results are analyzed in some more detail, for a better understanding why the effect of the downscaling is rather small, even smaller than for the offline test case in section 4.4.2. Figure 4.37 depicts the root mean square errors for the atmospheric and surface temperature and specific humidity respectively, computed on the 400 m scale. The downscaling without noise leads to improved atmospheric temperature of the lowest atmospheric layer (keep in mind that these disaggregated temperatures are only used

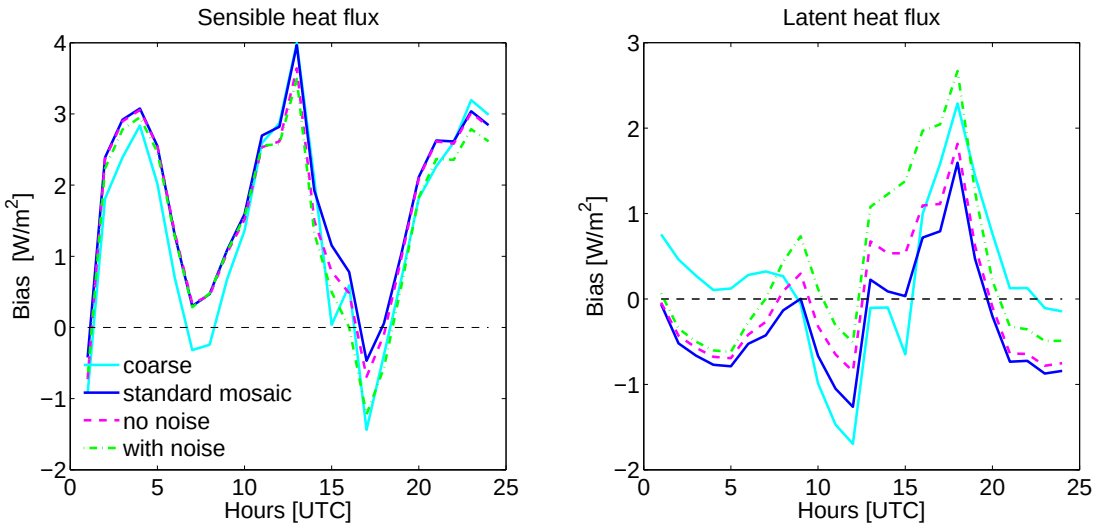

Figure 4.36.: Diurnal cycle of biases of turbulent heat fluxes, averaged over the six validation case studies.

as input for the SVAT module and for the flux computations, not in the dynamics of the model). Improvements are also visible in the surface temperature (note the different scale), these improvements are obtained through indirect effects, because no downscaling is applied to the surface temperatures, as they are explicitly calculated on the small scale. Hence, by forcing the soil model with disaggregated atmospheric quantities a beneficial effect also on the soil variables can be achieved. For the specific humidity hardly any difference is visible with downscaling without noise, because no deterministic downscaling step is applied. For the full downscaling the stochastic noise leads naturally to an increase of errors on this 400 m scale.

Despite improvements of downscaling steps 1+2 for the state variables at the surface and at the lowest atmospheric model layer, which enter the turbulent flux computations as vertical gradient, no improvements for the gradients themselves can be achieved (Figure 4.38).

The reason, why the improvements on the state variables are almost completely lost for the gradients, can be found in the correlations between the errors of atmospheric and surface values, for temperature and specific humidity, see Figure 4.39. For all mosaic simulations these correlations are large, in contrast to the standard model run without subgrid heterogeneity. The largest correlations, are, however, obtained for the standard mosaic without downscaling. This positive correlation of the errors of the surface and atmospheric variables leads to a cancelling of the errors when the gradient is computed and thus also for the fluxes. If atmospheric and surface temperatures are too high by about the same degree, the gradient will still have about the correct value. The question is why the errors of the standard mosaic are that strongly correlated. An indication is given by Figure 4.40, which shows an exemplary two-dimensional field of the errors for atmospheric and surface temperature of the standard mosaic and mosaic with downscaling steps 1 and 2. The explanation for the strong correlations between these error fields is, that the error structures in the atmospheric and the surface variables resemble each other closely, they

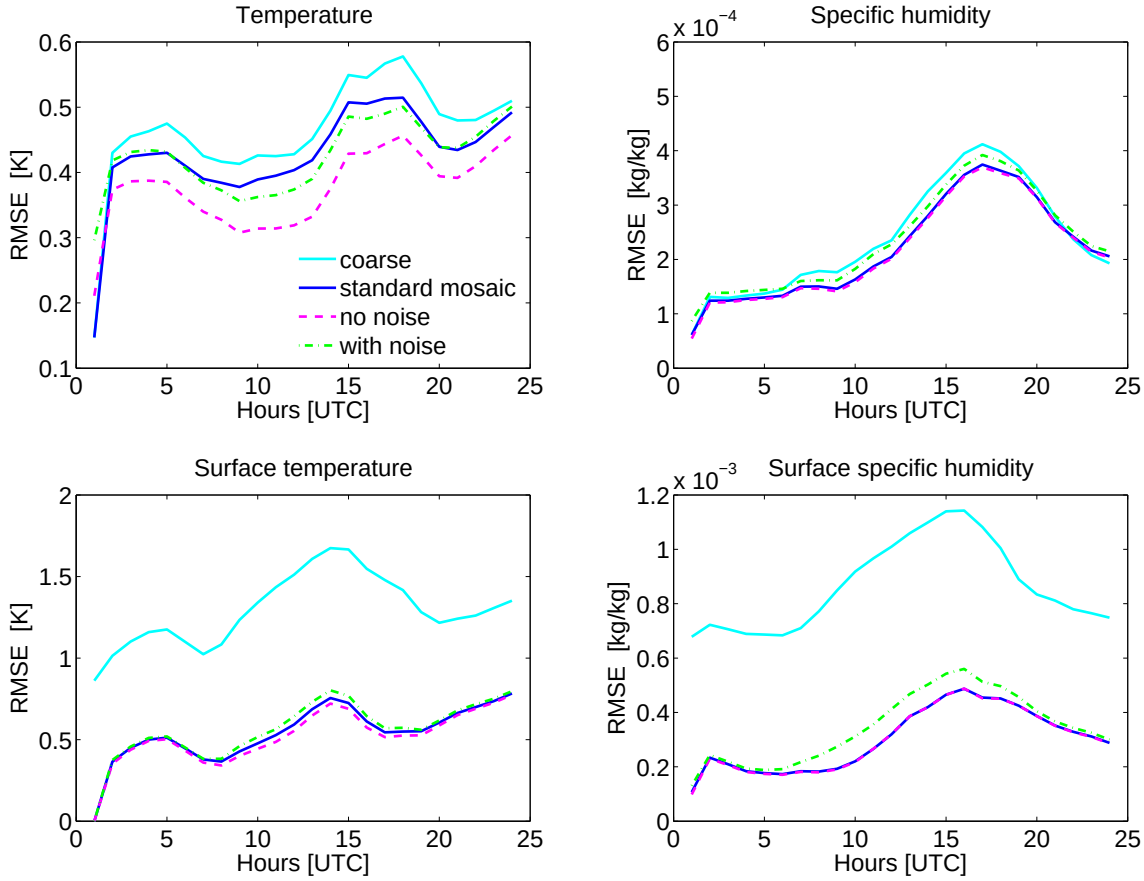

Figure 4.37.: Root mean square differences for atmospheric (top) and surface (bottom) temperature (left) and specific humidity (right), averaged over all case studies.

are both caused by the coarse atmospheric forcing in the standard mosaic approach. Over- or underestimations due to unresolved valleys, gradients, or other characteristics are visible in the atmospheric as well as in the surface temperature field. Some small-scale surface temperature structures are captured due to resolved land cover characteristics, however, the edges of the coarse pixels are still visible (see Fig. 4.41). The valleys are too cold, the ridges too warm, which is not the case in the model simulations with disaggregation of the atmospheric forcing variables.

Thus, despite the lower and less structured errors achieved by the downscaling (Fig. 4.40 right), this beneficial behaviour does not lead to improvements in the gradients, and therefore only a marginally better performance is obtained for the fluxes. Contrary to the offline results, where the subgrid-scale variability of the standard mosaic fluxes is too large, here the reference subgrid-scale standard deviations are matched closely by the standard mosaic approach or are even slightly too low (see Fig. 4.42). Downscaling without noise leads to a small increase of this variability, which is beneficial during night and for the latent heat flux, but not during day for the sensible heat flux. Full downscaling leads generally to excessive subgrid-scale variabilities.

A perfect downscaling would still lead to smaller improvements of the mosaic approach

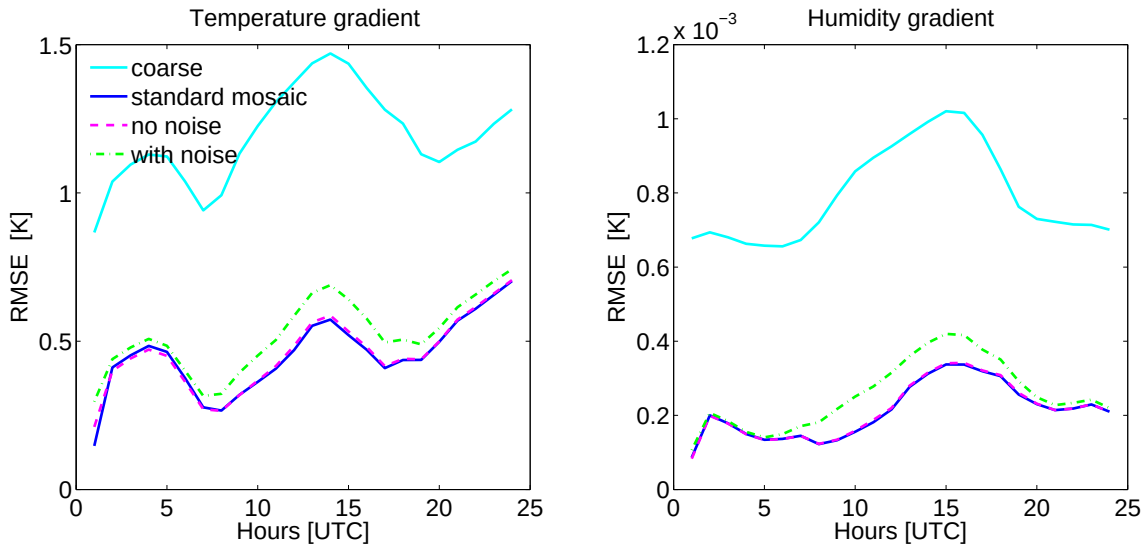

Figure 4.38.: Root mean square differences for temperature (left) and specific humidity (right) gradients between surface and lower atmosphere.

compared to a standard coarse simulation without subgrid-scale heterogeneities. A general estimate of the effect that can be expected if subgrid heterogeneities on a 400 m grid with 2.8 km as coarse grid are taken into account can be derived from Figure 4.43. The subgrid scale standard deviations at the surface and in the atmosphere are depicted, at night and during mid-day, for different days with varying weather conditions (for a description of the weather situations see Table 4.1), obtained from 400 m model simulations. For specific humidity the small-scale variability in the atmosphere is always much lower than at the surface. For temperature in some nights also large variability is visible in the lower boundary layer, especially for 14 October 2007 and 9 May 2008, both clear nights without clouds. During daytime, however, the atmosphere is well mixed, thus subgrid-scale variability is small due to smoothing.

Table 4.13 lists the mean difference between the spatial correlation length of the heat fluxes and the correlation length of the reference 400 m simulations. As expected the correlation length of the coarse model simulations without subgrid-scale heterogeneity is on average too large. For the standard mosaic the correlation length is strongly reduced, and atmospheric downscaling steps one and two further improve the results. The stochastic downscaling step, however, reduces the spatial autocorrelations too strongly, due to the neglection of spatial correlations.

Effect on model dynamics

The effect on the model dynamics in terms of divergence from the reference has been investigated. In Figure 4.44 the divergence from the high-resolution simulations is shown exemplary for 15 May 2008, for surface pressure, precipitation sum since initialization and 2 m temperature, normalized with the respective "reference" standard deviation, to exclude the diurnal cycle. The deviations of the coarse simulation is largest, the three mosaic configurations are closely together, and show a lower divergence from the 400 m

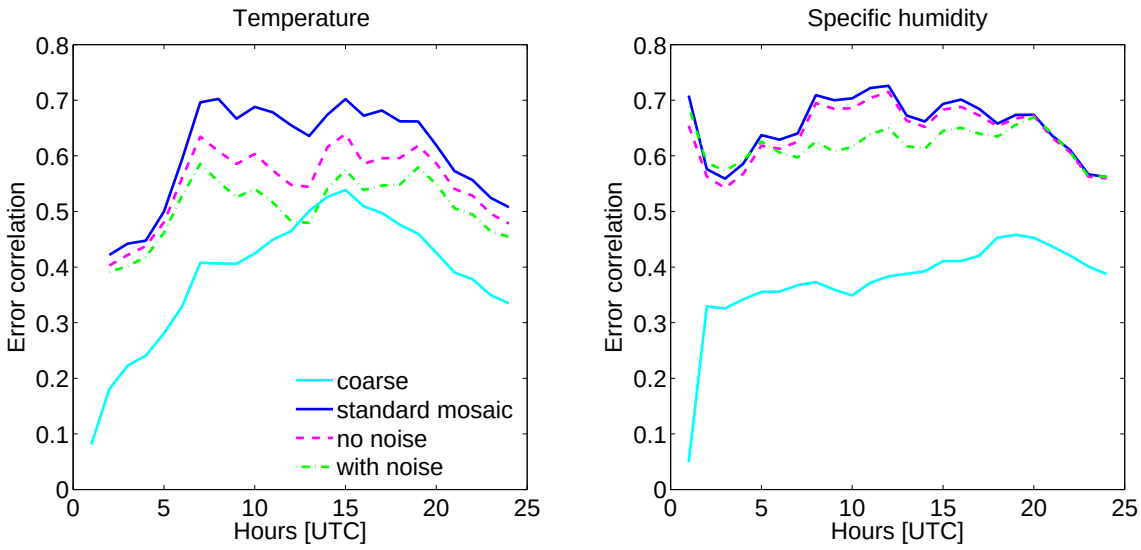

Figure 4.39.: Correlations of errors of surface and atmospheric temperature (left) and specific humidity (right).

]bt[

Table 4.13.: Mean difference of correlation length of sensible and latent heat flux to the correlation length of the high-resolution model run. Averaged spatially and temporally, for all validation case studies, in [m].

	coarse	mosaic	no noise	with noise
Sensible heat flux	178.5	36.5	-0.5	-129.0
Latent heat flux	156.3	18.10	15.2	-33.9

simulation. The effect of the downscaling, is again rather small.

4.5. Discussion

Interpretation of the results

The performance of the atmospheric downscaling scheme has first been evaluated by applying it to lowest model layer variables of the COSMO model for three case studies. The first two downscaling steps considerably reduce the errors compared to the homogeneous coarse scale values. All steps increase subgrid-scale variance towards the reference small-scale variability. The first step leads to a small error reduction and a small increase of the subgrid scale variability. The second step, wherever applicable, largely reduces the errors and improves variability. Since step 2 is weather dependent, also the performance of the disaggregation is dependent on the atmospheric conditions. The third step achieves a good reproduction of the subgrid scale variability, however, at the expense of an increased root mean square error.

The question remains whether the weak correlations of near surface wind speed and

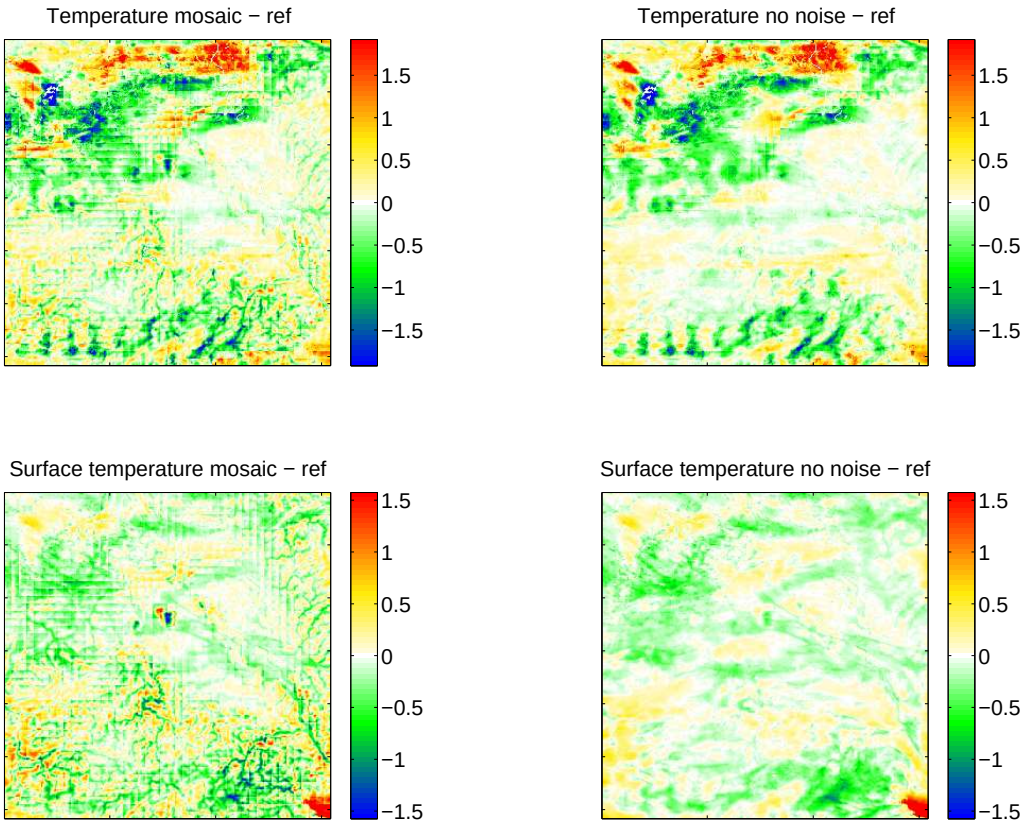

Figure 4.40.: Temperature (top) and surface temperature (bottom) difference field (with respect to the high resolution reference) for 12:00 UTC on 16 July 2008 for model run with pure mosaic (left) and mosaic plus downscaling step 1 and 2 (right).

specific humidity with surface variables is a model-specific behaviour, or whether this is real. *Bertoldi* et al. (2008) for example coupled a large-eddy simulation (LES) model to a surface energy balance scheme and found strong correlations of the near-surface atmospheric properties with surface variables. In their study near-surface atmospheric temperature was strongly correlated with the sensible heat flux, specific humidity with the latent heat flux, and the wind speed with surface roughness. They analyzed scales of L=10 to L=1000 m, which are similar to the scales considered in this study. They found the strongest correlations between surface and atmospheric quantities to be one pixel downwind the respective surface pixel. Spatial lags have not been considered in this work. Another difference is the vertical resolution, the lowest atmospheric model level in the LES used by *Bertoldi* et al. (2008) is in 2.5 m height, compared to 10 m in this work. The different correlations found may be due to different transfer parameterizations for the turbulent exchange fluxes in their coupling and in the COSMO model.

Besides the performance of the downscaling for the atmospheric variables, also the effects on the turbulent fluxes have been analyzed. To this end the downscaling has been applied to coarsened fine-resolution model output from 400 m COSMO runs, and compared to fluxes which have been computed based on the standard mosaic approach,

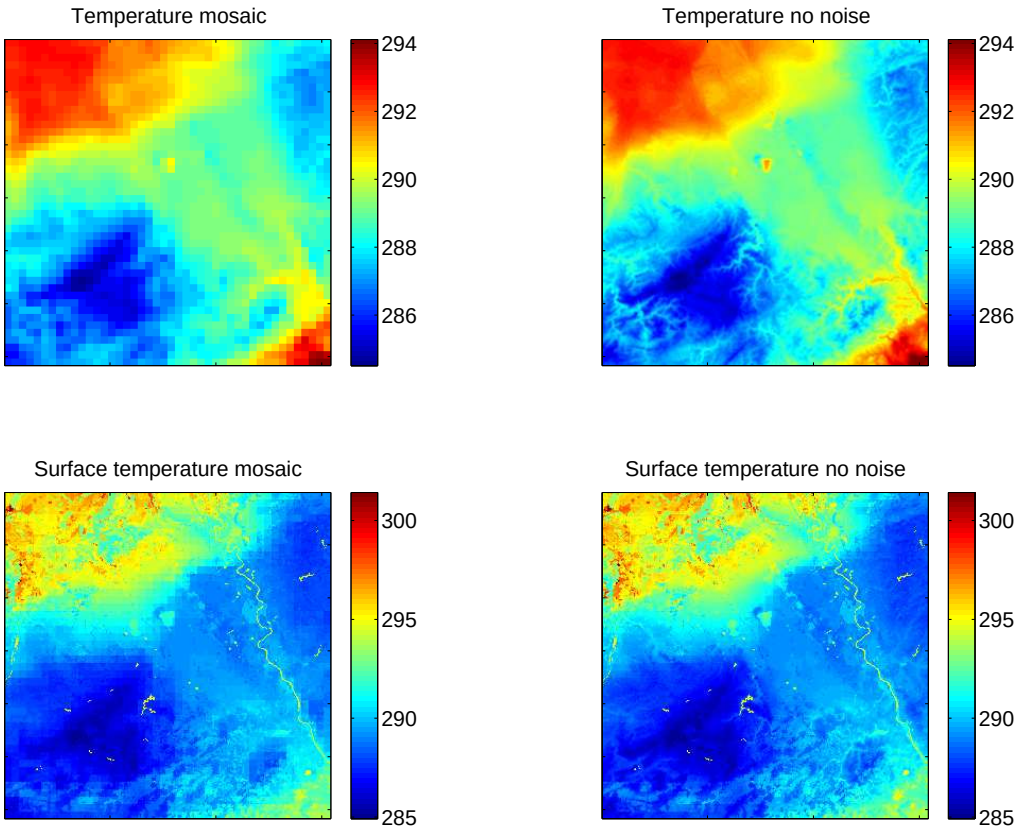

Figure 4.41.: Temperature (top) and surface temperature (bottom) field for 12:00 UTC on 16 July 2008 for model run with pure mosaic (left) and mosaic plus downscaling step 1 and 2 (right).

i.e. with a fine surface but coarse atmosphere. The results indicate that improvements of about 1 W/m^2 can be gained by employing the downscaled atmospheric reference level quantities for the computation of the fluxes, if only downscaling steps 1+2 are carried out. Only during clear-sky radiation nights, with heterogeneous near-surface atmospheres the full downscaling gives the best results for the sensible heat flux. Contrary to the situation during daytime, the small-scale variability of the sensible heat flux is too small without downscaling in these situations. The mosaic approach leads to improvements mainly over areas with strong heterogeneity in land use and soil characteristics, whereas the largest positive effects attributed to the downscaling are on average found over mountainous regions.

Finally, the disaggregation scheme has been implemented into a COSMO model version with mosaic surface heterogeneity representation. Comparisons of model output from simulations with and without mosaic and downscaling (either steps 1+2 or steps 1+2+3) were carried out. Summarizing, the model simulations with mosaic approach gave overall notably better results than model simulations without any surface variability representation. Root mean square errors of sensible and latent heat fluxes were reduced by about 9 W/m^2 and 13 W/m^2, respectively (averaged over six case studies).

The new atmospheric downscaling scheme, however, leads to only marginal further

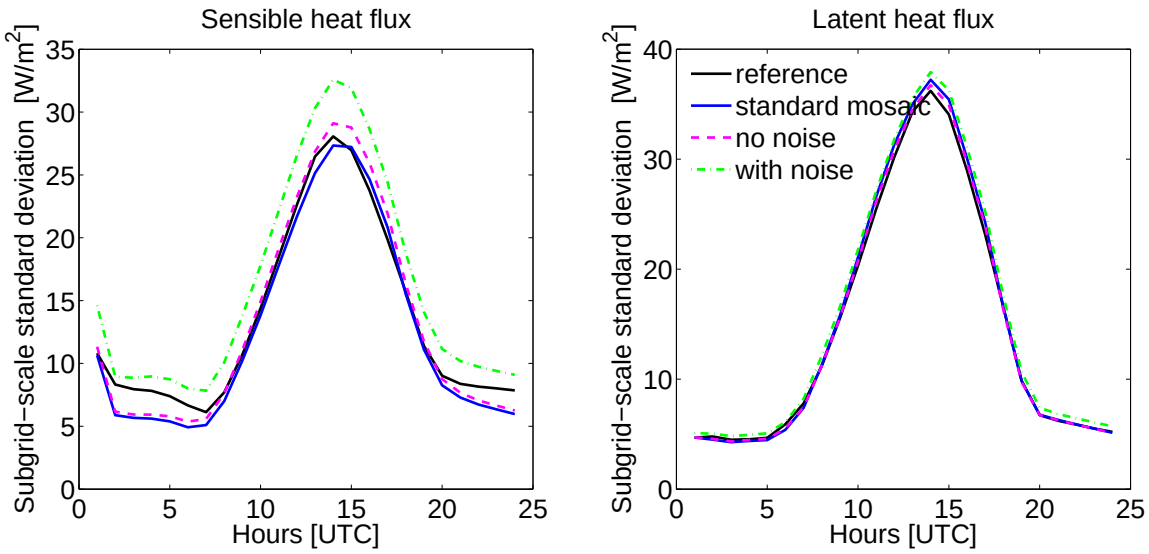

Figure 4.42.: Mean subgrid-scale standard deviation of the sensible (left) and latent (right) heat flux, averaged over the six online validation case studies.

improvements. At first glance, this result is unexpected, because the results for the single terms in the flux equations mainly show a positive impact. But the gradients and thus the fluxes do not benefit from this effect. The cause for this behaviour can be found in the characteristics of the errors. For the standard mosaic the errors of surface and atmospheric temperature (and also to some degree for specific humidity) are stronger correlated. Thus, if the temperature at the atmospheric reference level is too high, in general also the surface is too warm. This leads to a cancelling of errors of the fluxes in the standard mosaic approach. Thus, although the structure of the surface variables is more realistic due to the distributed atmospheric forcing, the overall benefits are marginal.

In the offline computation of the fluxes this effect is not visible, because the surface fields in the offline tests were the same for the standard mosaic offline flux as well as for the mosaic with atmospheric downscaling, namely high-resolution model output. The simple setup does not allow the simulation of feedback processes, hence it can only reveal part of the behaviour of the fully coupled model system. The offline evaluation can however be regarded as proof of concept for applications of the disaggregation for stand-alone soil model applications.

To outperform the standard mosaic approach an option would be to downscale the gradients directly, instead of the screen-level parameters. This, however, is much more difficult, because clear physical relations with surface quantities do not exist.

Generally the stochastic downscaling step, does not improve the results. Although the added small-scale variability has about the right value for each of the downscaled variables, the variability for the fluxes is too large, indicating more not-captured cross-correlations between the relevant variables.

The additional effects, which can be expected due to the disaggregation of the atmospheric forcing variables, are much smaller than those of the mosaic approach versus model simulations without surface heterogeneity representation, because the surface is much more heterogeneous than the atmosphere. Only during clear-sky nights the near-

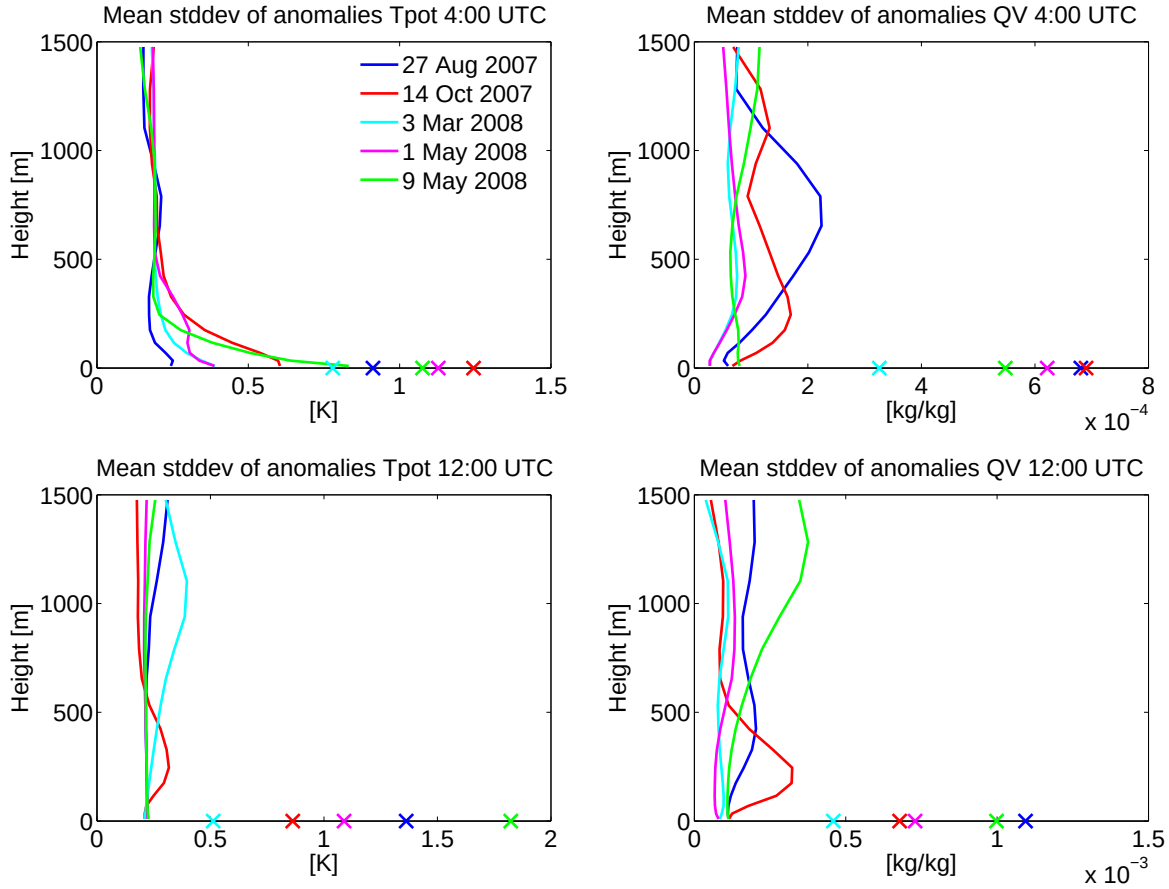

Figure 4.43.: Subgrid-scale standard deviations for potential temperature (left) and specific humidity (right) for 4:00 (top) and 12:00 UTC (bottom) in the atmosphere and at the surface (marked by crosses).

surface atmospheric temperature variability is comparably large, but still only half as large as the mean surface heterogeneity.

Surface heterogeneity representation in general is most important in calm weather situations. In synoptically driven weather conditions with strong advection, or large-scale rainfall or cloud cover, the surface characteristics have less impact on the surface fluxes and lower boundary layer. It is believed that the coupling strength (i.e. the degree to which anomalies in land-surface state can affect rainfall generation and other atmospheric processes; *Koster* et al., 2006) between surface and atmosphere is strongest in summer, when the evapotranspiration rates are high.

Scales

There are a few studies where atmospheric disaggregation in combination with the mosaic approach has been applied (e.g. *Seth* et al., 1994; *Giorgi* et al., 2003; *Dimri*, 2009, for an overview refer to section 4.1). In these studies positive effects due to e.g. temperature downscaling have been demonstrated. Their simulations however were conducted on scales of about 50-100 km for several months or even years, and over highly structured terrain

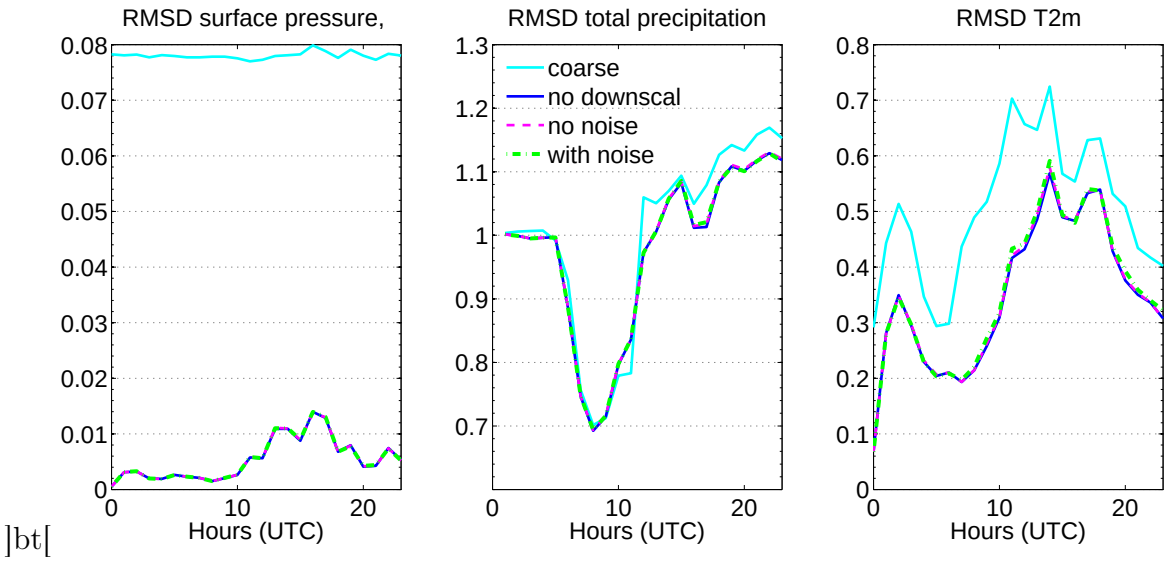

Figure 4.44.: Root mean square difference (normalized with reference standard deviation) of pressure, total precipitation (sum since model initialization) and 2 m temperature with respect to high-resolution model run for 15 May 2008.

such as the Alps or the Himalaya. Positive effects were e.g. achieved for the hydrological cycle due to a better representation of snow cover in winter.

In this work a downscaling system for atmospheric variables based on 400 m grid spacing as the smaller scale and 2.8 km as the larger scale has been developed and tested. First tests of the system for a downscaling from 14 km data down to 2.8 km have been conducted to analyze whether the system can also be used for regional climate simulations with the COSMO model on a 14 km grid, with surface information on a 2.8 km mosaic subgrid. Although the downscaling steps have been trained for smaller scales, the results obtained by the downscaling are very encouraging in terms of root mean square error reduction and subgrid-scale variance reconstruction for the atmospheric variables. These results indicate that the approach could also be employed for climate modeling without changes to the scheme or parameters. In larger-scale simulations larger beneficial effects due the downscaling may be expected, because more subgrid-scale variability in atmospheric quantities than on the meso-γ-scale is neglected. The summation of positive effects of a more realistic representation of precipitation, snow cover or runoff processes should lead to positive impacts on the overall hydrological cycle in longer simulations.

Surface-heterogeneity representation

The downscaling system is applicable whenever a mosaic approach is used in an atmospheric model. In the so-called tile approach (see for example *Avissar and Pielke*, 1989; *Avissar*, 1991; *Heinemann and Kerschgens*, 2005; *Ament and Simmer*, 2006) the soil processes are modelled separately for different land use classes, available at the subgrid-scale, and the resulting fluxes are averaged according to the fractional coverage of these land use classes. Hence, in the tile approach only one source of subgrid heterogeneity is accounted for; this is usually land use, while topographic or soil texture variability is not considered.

The approach presented here cannot be applied without modifications to a tiled surface, because high-resolution surface information of different surface properties is necessary, for example of topographic height, albedo and surface temperature. This usually is available in a consistent way only in the explicit subgrid mosaic approach.

A general drawback of both mosaic and tile approach is the neglect of horizontal fluxes and advective effects between patches within a grid box. If for example a cool water body is situated upwind of an agricultural sub-pixel, in reality the atmospheric conditions at the downstream pixels would be affected by advection of cool or moist air, and thus also the turbulent fluxes.

Soil moisture

A general issue, which has not been discussed in this study, is soil moisture initialization. Many studies show the strong dependence of simulated fluxes on the soil moisture representation (e.g. *Chow* et al., 2006; *Maxwell* et al., 2007; *Schmidli* et al., 2009), at least under calm weather conditions. In this work the soil moisture has been initialized by interpolating soil moisture from COSMO-DE analyses, also for the 400 m model simulations. Inadequately represented soil moisture fields can lead to a biased partitioning of the available energy into sensible and latent heat. For the development of the atmospheric downscaling system, however, the accurate soil moisture representation was not crucial, because for that purpose a close representation of "real" conditions was not important, only the consistent modeling of the inter-variable relations. In an operational employment of the mosaic approach, high-resolution soil initialization information would be available, stored on the subgrid from the previous model runs. Generally, the application of the mosaic in a continuous data-assimilation-forecast system is preferred over the single case studies carried out in this work, because then spin-up effects due to coarse soil-initialization would cease to exist.

Potential applications

Possible applications of the downscaling scheme are the generation of high-resolution input for SVAT models and hydrological models, based on low-resolution atmospheric model output. This can be useful for either stand-alone applications, or for fully coupled simulations, where the soil is resolved on a finer grid than the atmosphere. A large beneficial effect of a mosaic in combination with the atmospheric disaggregation should be expected for applications in highly structured terrain, for example in the Alpine region, due to a more realistic partitioning of precipitation in rain and snow dependent on elevation leading to indirect positive impacts due to more realistic patterns of high and low surface albedo over snow-covered and snow-free subpixels.

Another application would be the modeling of fog. The simulation of fog-formation requires an accurate simulation of the feedbacks between surface and atmosphere. Both temperature and specific humidity in the lower boundary need to be captured accurately. Such a setup would allow running a fog model on the higher mosaic resolution.

Since COSMO model version 3.18, a lake parameterization (FLake, *Mironov* et al., 2010) is available (although not operationally used) in the COSMO model. This module is a bulk model capable of predicting the vertical temperature structure and mixing conditions

at various depth of inland water bodies, and thus to represent the effects of lakes on numerical weather prediction models. The implementation could be modified to allow a subgrid application of this FLake model in the mosaic with atmospheric disaggregation. That way also effects of lakes smaller than the horizontal grid resolution could be taken into account.

Neunhäuserer et al. (2007) simulated urban heat island effects with COSMO on a 1.1 km grid for Helsinki by introducing urban external surface parameters and an anthropogenic heat source (introduced into the surface heat budget equation). A mosaic representation could take into account the effects of small cities in model simulations with coarser mesh sizes.

The downscaling scheme should be tested in combination to hydrological models by providing high-resolution atmospheric input for these models. Using atmospheric model output directly to drive hydrological models can lead to too low precipitation intensities, attributed to the generally too low spatial resolution of atmospheric models, compared to hydrological models. Too low precipitation rates can give rise to unrealistic low runoff (see, e.g., *Segond* et al., 2007).

Possible improvements

In the future, attempts should be made to conserve also spatial correlations in downscaling step 3, i.e. to generate spatially red noise instead of white noise. This would be especially important for distributed hydrological models, which are usually three-dimensional models and simulate lateral exchange.

The mosaic approach in the version implemented in the COSMO-SUBS model version contains the subgrid approach only for the turbulent fluxes of sensible and latent heat, whereas the momentum flux is still calculated on the coarse scale. The reason for this inconsistent treatment is that in COSMO the roughness length z_0 contains not only the roughness of the land cover characteristics, but also a second term for gravity wave drag for the momentum flux computations. The latter part can not be readily disaggregated in the current implementation. In a newer COSMO model version, a new, separate parameterization of this gravity wave drag, after Lott and Miller (1997), has been implemented. For application of the mosaic in a more recent COSMO model version, a mosaic-type implementation also for the momentum flux should be developed.

Another important topic is validation. The offline computation of the fluxes does not represent the effects in a coupled model system, and can thus only help to understand the effects of the system. Online validation by comparing the different mosaic and downscaling configurations with high-resolution reference model simulations, however, is hampered by divergence of the model simulations. The high-resolution simulations can only be used as consistency check and proof of concept, not as the "true" atmospheric state. As a compromise between these two test environments a test with a stand-alone SVAT module would provide another testbed, for example TERRA stand-alone. That way the soil module could be run on high resolution, to emulate the mosaic approach, and could be driven by either high-resolution (as reference), coarse (as standard mosaic), or disaggregated (as test of the downscaling) atmospheric information. Thus, the effects of the downscaling could be isolated more easily, effects of different cloud positions for example could be excluded. Furthermore, longer simulations would be possible. However,

also in such a setting no feedbacks between the soil-vegetation system and atmosphere can be considered and conclusions concerning effects of the scale-consistent soil-vegetation-atmosphere coupling on the atmospheric model evolution would not be possible.

5. Concluding remarks

A detailed discussion of the two presented approaches have been given at the end of the respective chapters. In this chapter more general conclusions with respect to both introduced schemes are drawn and possible future research topics are sketched.

Novelty and goals of the proposed techniques

In this work two approaches have been presented, which aim at an adequate and efficient representation of small-scale heterogeneities in numerical weather prediction models. Heterogeneity in the atmosphere is accounted for with respect to radiative transfer by a computationally efficient approach that is able to track small fast moving clouds. Heterogeneity at the surface is accounted for by computing the soil-surface-vegetation processes on a higher horizontal resolution, including a novel downscaling scheme to generate spatially distributed small-scale atmospheric forcing.

The appropriate consideration of heterogeneities becomes more important with decreasing grid sizes of the atmospheric models, because the processes are less Gaussian on small scales and inherent nonlinearities hamper the use of averaged and effective parameters. The available computer time is, however, always a constraining factor. This leads to the practise to use spatial and temporal sampling and averaging techniques for the computation of physical processes in operational meteorological models. The two approaches introduced in this work provide solutions to overcome these neglections of small-scale variability and thus represent patterns in the soil-vegetation-atmosphere system more adequately.

Both, a better representation of radiative effects and a scale-consistent coupling of land-surface and atmosphere, lead to an improved energy budget at the earth surface, which is crucial as the lower boundary for the atmospheric model and has a large impact on boundary layer development.

A new aspect is the explicit estimation and generation of subgrid-scale variability by adding random noise, which has been introduced in the downscaling scheme. In the past, parameterizations have typically been used to predict the evolution of grid-mean quantities due to unresolved subgrid-scale processes. In recent years, however, the field of stochastic modeling (*Palmer and Williams*, 2009) has evolved, which moves away from bulk formula parameterizations towards the incorporation of stochastic terms in climate and weather forecast models, in order to account for the uncertainty inherent in the subgrid-scale processes. Such stochastic representations of subgrid-scale processes are also valuable to account for model error in ensemble systems, (see e.g. *Buizza* et al., 1999) and the stochastic step in the downscaling scheme can be considered as an application of this theory.

Critical assessment of the results

Both schemes, the adaptive radiation scheme and the atmospheric downscaling in combination with the mosaic approach, have been implemented into the COSMO model and test cases have been simulated for the COSMO-DE configuration on a horizontal grid resolution of 2.8 km.

By employing the adaptive radiative transfer parameterization error reductions by 15-25 % for the radiation surface net fluxes compared to the COSMO-DE default radiation setup were achieved. Model consistency was improved by a more realistic simulation of the relation of cloud characteristics and radiation. Furthermore, it was demonstrated that model runs with the adaptive radiation diverge less from the reference model run.

The improvements gained by the combination of the mosaic approach with atmospheric disaggregation have to be considered more differentiated. It has been proven that the incorporation of surface heterogeneity into the COSMO model has a large positive impact (as shown before by *Ament and Simmer*, 2006), reducing the root mean square differences of the fluxes to reference high-resolution simulations by about 50%. The additional introduction of subgrid-scale atmospheric forcing for the sub-pixels by statistical downscaling, however, led only to marginal additional improvements, although the downscaling itself works well. The rather small effect can be explained by two factors: First, it has been shown that the atmosphere is less heterogeneous, especially on theses small scales, compared to the soil surface. Second, in the standard mosaic approach with homogeneous atmospheric forcing, errors for the surface and atmospheric variables are strongly positively correlated, i.e. overestimations in e.g. atmospheric temperature coincides with overestimation in surface temperature (and vice versa), which leads to a cancellation of errors. Thus, although the downscaling leads to more realistic fields of surface and near-surface variables, the net effect on the turbulent fluxes is less pronounced. This, however, is due to the rather simple parameterization of the exchange fluxes in current atmospheric models. In future applications, especially on smaller scales, non-local effects may become more important, and thus the fluxes will likely be parameterized by other, less simple concepts than after Monin-Obukhov. Then a realistic representation of the fields will probably prove valuable.

In conclusion, the operational application of the adaptive radiation parameterization can be recommended, because it has a large positive impact and does not lead to an increase in computation time. The mosaic approach itself also leads to a considerable improvement for the representation of the turbulent heat fluxes, and the whole dynamical model development. Thus, an operational employment of the mosaic approach should also be considered, although the higher resolution of the soil module lead to higher computational demands, depending on the subgrid resolution. In this work a subgrid resolution of 7x7, i.e. of 49 sub-pixels per coarse pixel, has been used. A sensitivity study changing the number of sub-pixels and evaluating the tradeoff between lower errors versus increased computing time should be carried out, to find an optimal compromise for an operational application. Due to the small overall effect of the atmospheric disaggregation on the model simulation an operational application can not necessarily be recommended. The disaggregation approach, however, is computationally cheap, and does thus not increase computation time noticeably. And although the effects for meteorological models are rather small in the current setup, a positive impact can be expected if hydrologi-

cal models are driven with distributed atmospheric forcing generated by the atmospheric downscaling scheme. A more realistic structure of precipitation and the other atmospheric driving variables will lead to an improved soil moisture distribution. Also a positive effect on runoff can be expected, especially in convective situations with heterogeneous precipitation patterns.

Other aspects of physical parameterizations in numerical atmospheric models would be more worthwhile to invest in, because larger beneficial effects could be expected. For example, *Ament* (2006) showed that a measurement driven soil moisture analysis and improvements in the SVAT scheme TERRA such as using enhanced stomatal resistance parameters, had a larger positive effect than the representation of subgrid-scale heterogeneities. Another topic neglected in most atmospheric models is ground water depth. *Maxwell* et al. (2007) and *Kollet and Maxwell* (2008) showed that the effects of variations in ground water depth on latent heat flux may be as large as effects due to variations in soil type and land use, if the groundwater level is in the range of a critical depth, i.e. not too far away from the surface, but also not too shallow. Especially under calm conditions the development of the atmospheric boundary layer is strongly influenced by the available soil water. Thus, the efforts in improving the description of the soil surface state should not be constrained to constant parameters such as land cover representation. Advancements in soil moisture assimilation and parameterization techniques are highly desirable, though challenging. Optimal would be a representation of lateral surface and subsurface flow, to simulate e.g. topographic effects on soil ground water and soil water availability adequately.

A drawback of both introduced methods in this work is that they both contain several empirically and statistically derived parameters, for example the search algorithm in the adaptive radiation scheme, and the regression coefficients in the regression based downscaling rules. Generally, parameterizations, which are mainly based on physical equations and less on tunable parameters, are desirable, as they are more easily transferable to other scales, climates or other applications than the special application for which they were trained. This, however, is a general problem of parameterizations which provide an estimate of the effect of subgrid-scale processes on grid-scale variables.

Possible aspects of future work

Both schemes should be tested on other scales than the meso-γ-scale. The adaptive radiation scheme has already been proven to yield good results for the COSMO-EU configuration with a horizontal grid mesh size of 7 km (section 3.4.2). For small scales an adequate sampling of fast developing and advection clouds is more important, than on larger scales on which the cloud cover is more homogeneous. Nevertheless benefits due to a more frequent sampling than the infrequent calls to the radiation scheme, as usually performed in global models, are possible. In section 4.4.1 it has been shown that the downscaling gives also satisfactory results for disaggregating the atmospheric variables from a 14 km horizontal grid size to 2.8 km, which would be a possible application of the mosaic in regional climate simulations. However, online tests of this setting have not yet been carried out. On that scale, possibly larger effects than in this work could be expected, because more subgrid-scale heterogeneity is neglected on the regional climate scale. According to the same arguments, also an employment in global models would be

advisable, though computational resources have to be taken into consideration.

A general issue is the evaluation of the model simulations including one or both of the presented techniques. In this work validation has been limited to comparisons with either higher resolution model simulations (for the mosaic/downscaling model runs), more as a consistency check, or simulations with high-frequent radiation computations (for the adaptive radiation parameterization validation). For a profound validation, a large number of simulations, ideally in a continuous data-assimilation-forecast-cycle should be carried out and detailed comparisons should be made in an operational verification framework, to be able to draw final conclusions about the performance in operational numerical weather prediction systems.

In this work the two new techniques with respect to radiation and soil/surface parameterizations have been tested separately. As a next step an combined implementation of these two schemes into the actual COSMO model version and test cases with application of both, the adaptive radiation scheme and better resolved soil module including downscaling, could be evaluated. One application for which a combination of both techniques would be beneficial, is the consideration of topographical effects in the radiation module. During sunrise and sunset, shading and increased solar insolation absorption to slope inclination is important, as it strongly influences the local surface heat budget. Thermal surface contrasts resulting from slope orientation can have a large impact on turbulent fluxes and local flow (*Seth* et al., 1994), because the orientation of the terrain with respect to the sun is a critical parameter for capturing the right amount of solar insulation at the surface (*Avissar and Pielke*, 1989). *Chow* et al. (2006) for example demonstrated that the consideration of topographic shading in the radiation module can delay the breakup of the morning inversion layer by about half an hour and impact the valley and slope wind patterns strongly. The adaptive radiation parameterization leads to a better representation of the surface radiation net fluxes during sunrise and sunset due to a better sampling and due to the correction of the fluxes according to actual solar zenith angle. Spatial variability in direct solar insulation due to terrain slope, aspect and shading could be captured adequately on the high surface resolution in the mosaic approach, thus here a combination of the adaptive radiation and scale-consistent land surface modeling may result in a large positive impact. The option for topographical corrections in the radiation scheme is available in the COSMO model since model version 3.23. Thus, such a study would be straightforward in principle, however the respective external parameters would have to have be prepared first.

Another promising idea would be the development of an adaptive framework for other parts of the model physics. A possible extension could be the coupling of the existing model system with a hydrological model, where the hydrological model is called in only a fraction of time or space with an intelligent sampling and with a generalization to the rest of the field in other timesteps.

A. List of Abbreviations

Acronym	**Explanation**
CCA	Canonical Correlation Analysis
CFL	Courant-Friedrichs-Levi
CLM	Community Land Model
CORINE	CoORdination of INformation on the Environment
COSMO	COnsortium for SMall-scale MOdeling
COSMO-DE	COSMO-model DEutschland
COSMO-EU	COSMO-model EUrope
DEM	Digital Elevation Model
DWD	German Weather Service (Deutscher Wetterdienst)
ECMWF	European Centre of Medium-range Weather Forecasts
FAO	Food and Agriculture Organization of the United Nations
GCM	Global Circulation Model
GME	Global model of the DWD
IFS	Integrated Forecasting System
LAI	Leaf area index
LES	Large Eddy Simulation
LITFASS	Lindenberg Inhomogeneous Terrain - Fluxes between Atmosphere and Surface - a long term Study
LM	Lokal-Modell (former name of COSMO model)
LLM	LITFASS-Lokal-Modell
LMK	Lokal-Modell Kürzestfrist
LW	Longwave
LWP	Liquid Water Path
MODIS	MODerate-resolution Imaging Spectroradiometer
PCA	Principal Component Analysis
PDF	Probability Density Function
SRTM	Shuttle Radar Topography Mission
SVAT	Soil Vegetation Atmosphere Transfer
SW	Shortwave
TKE	Turbulent kinetic energy
UNESCO	United Nations Educational, Scientific and Cultural Organization
UTC	Universal Time Coordinated

B. List of Symbols

Symbol	Definition
c	specific heat capacity
CLC	cloud cover
CLC^2_{var}	cloud cover variance of 3x3 coarse neighboring pixels
DD	wind direction
D_w	hydraulic diffusivity
E_b	evaporation of bare soil
E_i	evaporation from interception store
E_{pot}	potential evaporation
E_{snow}	evaporation from snow store
$(F_{q^v})_{sfc}$	surface flux of water vapor
$(F_h)_{sfc}$	sensible heat flux
FR_{land}	fraction of land
F_{w_l}	flux of soil water ψ
F_ψ	flux of variable ψ
f_i	fractional coverage of grid box by interception water
f_{plnt}	fraction of grid box covered by vegetation
f_{snow}	snow covered fraction of grid box
f_ψ	forcing term due to slow processes
G_P	heat flux of freezing rain and melting snowfall
$G_{snow,melt}$	heat flux of melting surface snow
G_ψ	nudging coefficient
G_{sfc}	soil heat flux at surface
H	orography
$\underline{K}_\psi$	threedimensional turbulence coefficient of variable ψ
K_h	transfer coefficient for heat
K_w	hydraulic conductivity
k	vertical index
ke_{soil}	number of vertical soil layers
LAI	leaf area index
L	latent heat of vaporization
L_{net}	longwave net radiation flux at surface
LWP	liquid water path
$PREC$	precipitation (rain, snow, graupel)
PS	surface pressure
P_ψ	all dynamic and physical processes of the model
$Q_{rad,net}$	net radiation at the surface

Q^v	saturation specific humidity
q^c	cloud water
q^i	cloud ice
q^g	graupel
q^r	rain water
q^s	specific snow water content
q^v	specific humidity
$q^v gr25$	specific humidity gradient of lowest 2 layers (25 meters)
$q^v gr60$	specific humidity gradient of lowest 3 layers (60 meters)
$q^v gr105$	specific humidity gradient of lowest 4 layers (105 meters)
q^v_{sfc}	specific humidity at surface
$(q^v_{sfc})_{var}$	variance of 3x3 neighboring pixels of surface specific humidity
RH	near-surface relative humidity
S_{net}	shortwave net radiation flux at surface
s_ψ	source terms due to fast processes (sound and gravity waves)
T	temperature
T_G	ground temperature
$Tgr25$	temperature gradient of lowest 2 layers (25 meters)
$Tgr60$	temperature gradient of lowest 3 layers (60 meters)
$Tgr105$	temperature gradient of lowest 4 layers (105 meters)
T_{sfc}	surface temperature
T_{so}	soil temperature
Tr	transpiration
U	near-surface u-wind component
V	near-surface v-wind component
W_{so}	soil moisture of top soil layer
$\mathbf{v}_h$	horizontal wind vector
W_k	weight in nudging system between 0 and 1
w_l	liquid water fraction: liquid water content per layer of thickness Δz
z	vertical coordinate
z_0	roughness length
α_{so}	solar albedo
α_{IR}	infrared albedo
ζ	vertical orography following coordinate
λ	heat conductivity
ρ	air density
ρ_w	water density
ψ	arbitrary atmospheric variable
σ	Stefan-Boltzmann-constant
Θ	solar zenith angle

Bibliography

Ament, F., *Energy and moisture exchange processes over heterogeneous land-surfaces in a weather prediction model*, Ph.D. thesis, Rheinische Friedrich-Wilhelms-Universität Bonn, 2006.

Ament, F. and C. Simmer, Improved representation of land-surface heterogeneity in a non-hydrostatic numerical weather prediction model, *Bound. Layer Meteorol.*, 121, 1, 153–174, 2006.

Arola, A., Parameterization of turbulent and mesoscale fluxes for heterogeneous surfaces, *J. Atmos. Sci.*, 56, 584–598, 1999.

Avissar, R., A statistical-dynamical approach to parameterize subgrid-scale land-surface heterogeneity in climate models, *Surv. Geophys.*, 12, 155–178, 1991.

Avissar, R., Conceptual aspects of a statistical-dynamical approach to represent landscape subgrid-scale heterogeneities in atmospheric models, *J. Geophys. Res.*, 97, 2729–2741, 1992.

Avissar, R., Which type of soil-vegetation-atmosphere transfer scheme is needed for general circulation models: a proposal for a higher-order scheme, *J. Hydrology*, 212-213, 136–154, 1998.

Avissar, R. and R. A. Pielke, A parameterization of heterogeneous land surfaces for atmospheric numerical models and its impact on regional meteorology, *Mon. Wea. Rev.*, 117, 2113–2136, 1989.

Avissar, R. and T. Schmidt, An evaluation of the scale at which ground-surface heat flux patchiness affects the convective boundary layer using large-eddy simulations, *J. Atmos. Sci.*, 55, 2666–2689, 1998.

Baldauf, M., J. Förstner, S. Klink, T. Reinhardt, C. Schraff, A. Seifert, and K. Stephan, Kurze Beschreibung des Lokal-Modells Kürzestfrist COSMO-DE (LMK) und seiner Datenbanken auf dem Datenserver des DWD, Deutscher Wetterdienst, Geschäftsbereich Forschung und Entwicklung, Offenbach, Germany, http://www.cosmo-model.org, 2009.

Bardossy, A., I. Bogardy, and I. Matyasovszky, Fuzzy rule-based downscaling of precipitation, *Theor. Appl. Climatol.*, 23, 11–22, 2005.

Bardossy, A., J. Stehlik, and H.-J. Caspary, Automated objective classification of daily circulation pattens for precipitation and temperature downscaling based on optimized fuzzy rules, *Climate Res.*, 23, 11–22, 2002.

Barker, H. W., G. L. Stephens, and Q. Fu, The sensitivity of domain-averaged solar fluxes to assumptions about cloud geometry, *Q. J. R. Meteorol. Soc.*, 125, 2127–2152, 1999.

Benestad, R. E., I. Hanssen-Bauer, and D. Chen, *Empirical-Statistical Downscaling*, World Scientific Publishing Co. Pte. Ltd., 2008.

Bertoldi, G., W. P. Kustas, and J. D. Albertson, Estimating spatial variability in atmospheric properties over remotely sensed land surface conditions, *J. Appl. Meteor. Climatol.*, 47, 2147–2165, 2008.

Beyrich, F., J. Leps, M. Mauder, J. Bange, T. Foken, S. Huneke, H. Lohse, A. Lüdi, W. Meijninger, D. Mironov, U. Wesensee, and P. Zittel, Area-averaged surface fluxes over the LITFASS region based on eddy-coveriance measurements, *Bound. Layer Meteorol.*, 121, 33–65, 2006.

Beyrich, F. and H.-T. Mengelkamp, Evaporation over a heterogeneous land surface: EVA_GRIPS and the LITFASS-experiment - an overview, *Bound. Layer Meteorol.*, 121, 5–32, 2006.

Bindlish, R. and A. P. Barros, Disaggregation of rainfall for one-way coupling of atmospheric and hydrological models in regions of complex terrain, *Global and Planetary Change*, 25, 111–132, 2000.

Boé, J., L. Terray, F. Habets, and E. Martin, Statistical and dynamical downscaling of the Seine basin climate for hydro-meteorological studies, *Int. J. Clim.*, 27, 1643–1655, 2007.

Bonan, G. B., D. Pollard, and S. L. Thompson, Influence of Subgrid-Scale Heterogeneity in Leaf Area Index, Stomatal Resistance, and Soil Moisture on Grid-Scale Land-Atmosphere Interactions, *J. Climate*, 6, 1882–1896, 1993.

Brussolo, E., J. von Hardenberg, L. Ferraris, N. Rebora, and A. Provenzale, Verification of Quantitative Precipitation Forecasts via Stochastic Downscaling, *J. Hydrometeo.*, 9, 1084–1094, 2008.

Brussolo, E., J. von Hardenberg, and N. Rebora, Stochastic versus Dynamical Downscaling of Ensemble Precipitation Forecasts, *J. Hydrometeo.*, 10, 1051–1061, 2009.

Buizza, R., M. Miller, and T. N. Palmer, Stochastic representation of model uncertainties in the ECMWF ensemble prediction system, *Q. J. R. Meteorol. Soc.*, 125, 2887–2908, 1999.

Chevallier, F., F. Chéruy, N. A. Scott, and A. Chédin, A neural network approach for a fast and accurate computation of a longwave radiative budget, *J. Appl. Meteorol.*, 37, 1385–1397, 1998.

Chevallier, F., J.-J. Morcrette, F. Chéruy, and N. A. Scott, Use of a neural-network-based long-wave radiative-transfer scheme in the ECMWF atmospheric model, *Q. J. R. Meteorol. Soc.*, 126, 761–776, 2000.

Chow, F., A. Weigel, R. Street, M. Rotach, and M. Xue, High-resolution large-eddy simulations of flow in a steep Alpine valley. part i: Methodology, verification, and sensitivity experiments, *J. Appl. Meteor. Climatol.*, 45, 63–86, 2006.

Claussen, M., Estimation of areally-averaged surface fluxes, *Bound. Layer Meteorol.*, 54, 387–410, 1991.

Claussen, M., Flux aggregation at large scales: on the limits of validity of the concept of blending height, *J. Hydrology*, 166, 371–382, 1995.

Clough, S., M. Shephard, E. Mlawer, J. Delamere, M. Iacono, K. Cady-Pereira, S. Boukabara, and P. Brown, Atmospheric radiative transfer modeling: A summary of the AER codes, *J. Quant. Spectrosc. Radiat. Transfer*, 91, 233–244, 2005.

Cox, P., R. Betts, C. Bunton, R. Essery, P. Rowntree, and J. Smith, The impact of new land surface physics on the GCM simulation of climate and climate sensitivity, *Climate Dyn.*, 15, 183–203, 1999.

de Rooy, W. C. and K. Kok, A combined physical-statistical approach for the downscaling of model wind speed, *Wea. Forecasting*, 19, 485–495, 2004.

Dickinson, R., Modeling evapotranspiration for three-dimensional global climate models: Climate processes and climate sensitivity, *Geophysical Monograph 29*, 5, 58–72, 1984.

Dickinson, R., A. Henderson-Sellers, and P. Kennedy, Biosphere atmosphere transfer scheme (BATS) version 1e as coupled to the NCAR Communtiy Climate Model, NCAR Tech. Note NCAR/TN-387-STR, Natl. Cent. for Atmos. Res. Boulder Colorado, 1993.

Dimri, A., Impact of subgrid scale scheme on topography and landuse for better regional scale simulation of meteorological variables over the western himalayas, *Clim. Dyn.*, 32, 565–574, 2009.

Doms, G., J. Förstner, E. Heise, H.-J. Herzog, M. Raschendorfer, T. Reinhardt, B. Ritter, R. Schrodin, J.-P. Schulz, and G. Vogel, *A description of the nonhydrostatic regional model LM, Part II: Physical parameterization*, Deutscher Wetterdienst, P.O. Box 100465, 63004 Offenbach, Germany, 2007.

EEA, *Corine Land Cover (CLC90)*, European Environment Agency, Copenhagen DK, 2000, http://dataservice.eea.eu.int/dataservice/.

Essery, R., M. Best, R. Betts, and P. Cox, Explicit representation of subgrid heterogeneity in a GCM land surface scheme, *J. Hydrometeo.*, 4, 530–543, 2003.

Farr, T. G., P. A. Rosen, E. Caro, R. Crippen, R. Duren, S. Hensley, M. Kobrick, M. Paller, E. Rodriguez, L. Roth, D. Seal, S. Shaffer, J. Shimada, J. Umland, M. Werner, M. Oskin, D. Burbank, and D. Alsdorf, The shuttle radar topography mission, *Rev. Geophys.*, 45, 2007, doi: 10.1029/2005RG000183.

Früh, B., J. Schipper, A. Pfeiffer, and V. Wirth, A pragmatic approach for downscaling precipitation in alpine-scale complex terrain, *Meteorol. Z.*, 15, No. 6, 631–646, 2006.

Gao, Y., F. Chen, M. Barlage, W. Liu, G. Cheng, X. Li, Y. Yu, Y. Ran, H. Li, H. Peng, and M. Ma, Enhancement of land surface information and its impact on atmospheric modeling in the heihe river basin, northwest china, *J. Geophys. Res.*, 113, D20S90, 2008.

Giorgi, F. and R. Avissar, Representation of heterogeneity effects in earth system modeling: Experience from land surface modeling, *Rev. Geophys.*, 4, 413–438, 1997.

Giorgi, F., R. Francisco, and J. Pal, Effects of a subgrid-scale topography and land use scheme on the simulation of surface climate and hydrology. Part I: Effects of temperature and water vapor disaggregation, *J. Hydrology*, 4, Part 2, 317–333, 2003.

Gutierrez, J., A. Cofino, R. Cano, and M. Rodriguez, Clustering methods for statistical downscaling in short-range weather forecasts, *Mon. Wea. Rev.*, 132, 2169–2183, 2004.

Heinemann, G. and M. Kerschgens, Comparison of methods for area-averaging surface energy fluxes over heterogeneous land surfaces using high-resolution non-hydrostatic simulations, *Int. J. Clim.*, 25, 379–403, 2005.

Heinemann, G. and M. Kerschgens, Simulation of surface energy fluxes using high-resolution non-hydrostatic simulations and comparisons with measurements for the litfass-2003 experiment, *Bound. Layer Meteorol.*, 121, 195–220, 2006.

Henderson-Sellers, A. and A. J. Pitman, Land-surface schemes for future climate models: Specification, aggregation, and heterogeneity, *J. Geophys. Res.*, 97, 2687–2696, 1992.

Herzog, H.-J., U. Schubert, G. Vogel, A. Fiedler, and R. Kirchner, LLM - the high-resolving nonhydrostatic simulation model in the DWD-project LITFASS. Part I: Modelling technique and simulation method. COSMO Technical Report No. 4, Technical report, Deutscher Wetterdienst, 2002.

Hess, R., Assimilation of screen-level observations by variational soil moisture analysis, *Meteorology and Atmospheric Physics*, 77, 145–154, 2001.

Hewitson, B. and R. G. Crane, Consensus between GCM climate change projections with empirical downscaling: Precipitation downscaling over South Arfrica, *ijc*, 26, 1315–1337, 2006.

Hu, Z. and S. Islam, Effects of subgrid-scale heterogeneity of soil wetness and temperature on grid-scale evaporation and its parameterization, *Int. J. Clim.*, 18, 49–63, 1998.

Huth, R., Statistical downscaling in central Europe: evaluation of methods and potential predictors, *Climate Res.*, 13, 91–101, 1999.

Huth, R., Statistical downscaling of daily temperature in central Europe, *J. Climate*, 15, 1731–1742, 2002.

Huth, R., Downscaling of humidity variables: a search for suitable predictors and predictands, *Int. J. Clim.*, 25, 243–250, 2005.

Jacobsen, I. and E. Heise, A new economic method for the computation of the surface temperature in numerical models, *Contributions to Atmospheric Physics*, 55, 128–141, 1982.

Karl, T., W.-C. Wang, M. E. Schlesinger, R. W. Knight, and D. Portman, A method of relating general circulation model simulated climate to the observed local climate. Part I: Seasonal statistics, *J. Climate*, 3, 1053–1079, 1990.

Kessler, E., On the distribution and continuity of water substance in atmospheric circulations, in *Volume 32 of Meteorological Monographs*, volume 10, Boston, USA, Am. Meteorol. Soc., 1969.

Klemp, J. B. and R. B. Wilhelmson, The simulation of three-dimensional convective storm dynamics, *J. Atmos. Sci.*, 35, 1070–1096, 1978.

Kollet, S. and R. Maxwell, Capturing the influence of groundwater dynamics on land surface processes using an integrated, distributed watershed model, *Water Resour. Res.*, 44, W02402, 2008.

Koster, R. D., Z. Guo, P. Dirmeyer, G. Bonan, E. Chan, P. Cox, H. Davies, C. Gordon, S. Kanae, E. Kowalczyk, D. Lawrence, P. Liu, C.-H. Lu, S. Malyshev, B. McAvaney, K. Mitchell, D. Mocko, T. Oki, K. W. Oleson, A. Pitman, Y. Sud, C. Taylor, D. Verseghy, R. Vasic, Y. Xue, and T. Yamada, GLACE: the global land-atmosphere coupling experiment. part i: Overview, *J. Hydrometeo.*, 7, 590–610, 2006.

Koster, R. D. and M. J. Suarez, Modeling the land surface boundary in climate models as a composite of independent vegetation stands, *J. Geophys. Res.*, 97, 2697–2715, 1992.

Krasnopolski, V. M., M. S. Fox-Rabinovitz, and D. V. Chalikov, New approach to calculation of atmospheric model physics: Accurate and fast neural network emulation of longwave radiation in a climate model, *Mon. Wea. Rev.*, 133, 1370–1383, 2005.

Krasnopolski, V. M., M. S. Fox-Rabinovitz, Y. T. Hou, S. J. Lord, and A. A. Belochitski, Accurate and fast neural network emulations of model radiation for the NCEP coupled climate forecast system: climate simulations and seasonal predictions, *Mon. Wea. Rev.*, 138, 1822–1842, 2010.

Louis, J.-F., A parametric model of vertical eddy fluxes in the atmophere, *Bound. Layer Meteorology*, 17, 187–202, 1979.

Manners, J., J.-C. Thelen, J.Petch, P.Hill, and J. Edwards, Two fast radiative transfer methods to improve the temporal sampling of clouds in numerical weather prediction and climate models, *Q. J. R. Meteorol. Soc.*, 135, 457–468, 2009.

Maraun, D., F. Wetterhall, A. Ireson, E. R.E. Chandler, M. Widmann, S. Brienen, H. Rust, T. Sauter, M. Themeßl, V.K.C.Venema, K. Chun, C. Goodess, R. Jones, C. Onof, M. Vrac, and I. Thiele-Eich, Precipitation downscaling under climate change: Recent developments to bridge the gap between dynamical models and the end user, *Rev. Geophys.*, 48, RG3003, 2010.

Marsigli, C., F. Boccanera, A. Montani, and T. Paccagnella, The COSMO-LEPS mesoscale ensemble system: validation of the methodology and verification, *Nonlinear Processes Geophys.*, 12, 527–536, 2005.

Maxwell, R. M., F. K. Chow, and S. J. Kollet, The groundwater-land-surface-atmosphere connection: Soil moisture effects on the atmospheric boundary layer in fully-coupled simulations, *Adv. Water Resour.*, 30, 2447–2466, 2007.

Mironov, D., E. Heise, E. Kourzeneva, B. Ritter, N. Schneider, and A. Terzhevik, Implementation of the lake parameterisation scheme FLake into the numerical weather prediction model COSMO, *Boreal Env. Res.*, 15, 218–230, 2010.

Mlawer, E., S. Taubman, P. Brown, M. Iacono, and S. Clough, Radiative transfer for inhomogeneous atmospheres: Rrtm, a validated correlated-k model for the longwave, *J. Geophys. Res.*, 102, 16663–16682, 1997.

Molod, A., H. Salmun, and D. W. Waugh, A new look at modeling surface heterogeneity: Extending its influence in the vertical, *J. Hydrology*, 4, 810–825, 2003.

Molteni, F., R. Buizza, T. N. Palmer, and T. Petroliagis, The ECMWF ensemble prediction system: Methodology and validation, *Q. J. R. Meteorol. Soc.*, 122, 73–119, 1996.

Morcrette, J.-J., On the effects of the temporal and spatial sampling of radiation fields on the ECMWF forecasts and analyses, *Mon. Wea. Rev.*, 128, 876–887, 2000.

Morcrette, J.-J., H. Barker, J. Cole, M. Iacono, and R. Pincus, Impact of a new radiation package, McRad, in the ECMWF integrated forecasting system, *Mon. Wea. Rev.*, 136, 4773–4798, 2008.

Naden, P. S., Spatial variability in flood estimation for large catchments: the exploitation of channel network structure, *Hydrol. Sci.*, 37, 1, 53–71, 1992.

Neunhäuserer, L., B. Fay, and M. Raschendorfer, Towards urbanisation of the non-hydrostatic numerical weather prediction model Lokalmodell (LM), *Bound. Layer Meteorol.*, 124, 81–97, 2007.

Oleson, K., Y. Dai, G. Bonan, M. Bosilovich, R. Dickinson, P. Dirmeyer, F. Hoffman, P. Houser, S. Levis, G.-Y. Niu, P. Thornton, M. Vertenstein, Z.-L. Yang, and X. Zeng, *Technical description of the community land model (CLM)*, National Center for atmospheric research, Boulder Colorado, 2004.

Palmer, T. and P. Williams, editors, *Stochastic Physics and Climate Modelling*, Cambridge University Press, 2009.

Pielke, R., T. Matsui, G. Leoncini, and T. Nobis, A new paradigm for parameterizations in numerical weather prediction and other atmospheric models, *National Weather Digest*, 30, 93–99, 2005.

Pincus, R., H. Barker, and J.-J. Morcrette, A fast, flexible, approximate technique for computing radiative transfer in inhomogeneous clouds, *J. Geophys. Res.*, 108D, 4376, 2003.

Pryor, S., J. Schoof, and R. Barthelmie, Empirical downscaling of wind speed probability distributions, *J. Geophys. Res.*, 110 Issue D19, D19109, 2005.

Rebora, N., L. Ferraris, J. v. Hardenberg, and A. Provenzale, RainFARM: Rainfall downscaling by a filtered autoregressive model, *J. Hydrometeo.*, 7, 724–738, 2006.

Ritter, B. and J.-F. Geleyn, A comprehensive radiation scheme for numerical weather prediction models with potential applications in climate simulations, *Mon. Wea. Rev.*, 120, 303–325, 1992.

Salathe, E., Comparison of various precipitation downscaling methods for the simulation of streamflow in a rainshadow river basin, *Int. J. Clim.*, 23 No. 8, 887–901, 2002.

Schättler, U., G. Doms, and C. Schraff, *Description of the Nonhydrostatic Regional Model LM. Part VII: User's Guide*, COSMO-Consortium for Small-Scale Modelling, 2005.

Schlünzen, K. H. and J. J. Katzfey, Relevance of sub-grid-scale land-use effects for mesoscale models, *Tellus*, 55, No. 3, 232–246, 2003.

Schmidli, J., G. Poulus, M. Daniels, and F. Chow, External influences on nocturnal thermally driven flows in a deep valley, *J. Appl. Meteor. Climatol.*, 48, 3–23, 2009.

Schomburg, A., V. Venema, F. Ament, and C. Simmer, Application of an adaptive radiative transfer parameterisation in a mesoscale numerical weather prediction model, *Q. J. R. Meteorol. Soc.*, 2011, in press.

Schomburg, A., V. Venema, R. Lindau, F. Ament, and C. Simmer, A downscaling scheme for atmospheric variables to drive soil-vegetation-atmosphere transfer models, *Tellus*, 62B, 242–258, 2010.

Schoof, J. and S. Pryor, Downscaling temperature and precipitation: a comparison of regression-based methods and artificial neural networks, *Int. J. Clim.*, 21, 773–790, 2001.

Schoof, J., S. Pryor, and S. M. Robeson, Downscaling daily maximum and minimum temperatures in the midwestern USA: a hybrid empirical approach, *Int. J. Clim.*, 27, 439–454, 2006.

Schraff, C. and R. Hess, Datenassimilation für das LM, *Promet*, 27, 156–164, 2002.

Segond, M.-L., H. S. Wheater, and C. Onof, The significance of spatial rainfall representation for flood runoff estimation: A numerical evaluation based on the lee catchment UK, *J. Hydrology*, 347, 116–131, 2007.

Seth, A., F. Giorgi, and R. Dickinson, Simulating fluxes from heterogeneous land surfaces: Explicit subgrid method employing the biosphere-atmosphere transfer scheme (BATS), *J. Geophys. Res.*, 99, No. D9, 18,651–18,667, 1994.

Seuffert, G., P. Gross, and C. S. an E.F. Wood, The influence of hydrologic modeling on the predicted local weather: two-way coupling of a mesoscale weather prediction model and a land surface hydrologic model, *J. Hydrometeo.*, 3, Issue 5, 505–523, 2002.

Singh, V. P., Effect of spatial and temporal variability in rainfall and watershed characteristics on stream flow hydrograph, *Hydrol. Process.*, 11, 1649–1669, 1997.

Smagorinsky, J., General circulation experiments with the primitive equations: 1. The basic experiment., *Mon. Wea. Rev.*, 91, 99–164, 1963.

Stephens, G. L., The parameterization of radiation for numerical weather prediction and climate models, *Mon. Wea. Rev.*, 112, 826–867, 1984.

Steppeler, J., G. Doms, and G. Adrian, Das Lokal-Modell LM, *Promet*, 27, 123–128, 2002.

Steppeler, J., G. Doms, U. Schättler, H. Bitzer, A. Gassmann, and U. Damrath, Meso-gamma scale forecasts using the nonhydrostatic model LM, *Meteor. Atmos. Phys.*, 82, 75–96, 2003.

Stull, R. B., *An Introduction to Boundary Layer Meteorology*, Kluwe Academic Publishers, 1988.

Tiedtke, M., A comprehensive mass flux scheme for cumulus parameterisation in large-scale models, *Mon. Wea. Rev.*, 117, 1779–1799, 1989.

Venema, V., S. G. Garcia, and C. Simmer, A new algorithm for the downscaling of 3-dimensional cloud fields, *Q. J. R. Meteorol. Soc.*, 136, 91–106, 2010.

Venema, V., A. Schomburg, F. Ament, and C. Simmer, Two adaptive radiative transfer schemes for numerical weather prediction models, *Atmos Chem Phys*, 7, 5659–5674, 2007.

Weigel, A., F. Chow, M. Rotach, R. Street, and M. Xue, High-resolution large-eddy simulations of flow in a steep alpine valley. Part II: Flow structure and heat budgets, *J. Appl. Meteor. Climatol.*, 45, 87–107, 2006.

Wilby, R. L., T. M. L. Wigley, D. Conway, P. D. Jones, B. C. Hewitson, J.Main, and D. S. Wilks, Statistical downscaling of general circulation model output: A comparison of methods, *Water Resour. Res.*, 34, No. 11, 2995–3008, 1998.